A quantitative structural activity relationship modelling study on HDAC3 inhibitors: Unveiling important structural features for potent activity

Submitted by

Mr. Rahul Jana

Exam Roll No.: **M4PHC23025**

Class Roll No.: **002111402042**

Reg. No.: **160267** of **2021-22**

Under The Guidance Of

Prof. Tarun Jha

Natural Science Laboratory
Department Of Pharmaceutical Technology
Jadavpur University, Kolkata-700032

Thesis submitted in partial fulfilment of the requirements for the Degree of Master of Pharmacy

Department of Pharmaceutical Technology

Faulty of Engineering and Technology

Jadavpur University, Kolkata

2023

Jadavpur University

Jadavpur, Kolkata-700032, India

CERTIFICATE OF APPROVAL

This is to certify that **Rahul Jana** (Exam Roll No. **M4PHC23025** , Reg. No.-**160267** of **2021-2022**) has sincerely carried out the research work on the subject entitled **"Structural exploration of diverse HDAC3 inhibitors: An in-silico approach to identify key attributes for potent HDAC3 inhibition"** under the supervision of **Prof. Tarun Jha**, Natural Science Laboratory, Department of Pharmaceutical Technology of Jadavpur University. He has incorporated his research in this thesis, which he submitted to Jadavpur University as a partial fulfilment of the requirements for the degree of **Master in Pharmacy** (Pharmaceutical Technology). He has carried out the research work independently and sincerely with proper care and attention to our entire satisfaction.

27.9.23

Head of the Department
Department of Pharmaceutical technology
Jadavpur University
Kolkata 700032, India

HEAD
DEPT. OF PHARMACEUTICAL TECHNOLOGY
JADAVPUR UNIVERSITY, KOLKATA, INDIA

Tarun Jha 29.9.23

Prof. Tarun Jha
Department of Pharmaceutical technology
Jadavpur University
Kolkata 700032, India

Saswati Majumdar 29.9.23

Dean
Department of Pharmaceutical technology
Jadavpur University
Kolkata 700032, India

DEAN
Faculty of Engineering & Technology
JADAVPUR UNIVERSITY
KOLKATA-700 032

Jadavpur University

Jadavpur, Kolkata-700032, India

CERTIFICATE OF APPROVAL

This is to certify that **Rahul Jana** (Exam Roll No. - **M4PHC23025**, Reg. No.- **160267** of **2021-2022**) has sincerely carried out the research work on the subject entitled "**A quantitative structural activity relationship modelling study on HDAC3 inhibitors: Unveiling important structural features for potent activity**" under the supervision of **Prof. Tarun Jha**, Natural Science Laboratory, Department of Pharmaceutical Technology of Jadavpur University. He has incorporated his research in this thesis, which he submitted to Jadavpur University as a partial fulfilment of the requirements for the degree of **Master in Pharmacy** (Pharmaceutical Technology). He has carried out the research work independently and sincerely with proper care and attention to our entire satisfaction.

Head of the Department
Department of Pharmaceutical technology
Jadavpur University
Kolkata 700032, India

Prof. Tarun Jha
Department of Pharmaceutical technology
Jadavpur University
Kolkata 700032, India

Dean
Department of Pharmaceutical technology
Jadavpur University
Kolkata 700032, India

Acknowledgement

The final outcome of this thesis required a lot of guidance and assistance from many people. I am extremely fortunate to have these all along the completion of my work. I would not forget to thank them because what I have accomplished has only been possible because of their advice and support. I am highly obliged and like to express my deep gratitude and profoundness to my reverend mentor **Prof. Tarun Jha** of Department of Pharmaceutical Technology, Jadavpur University, Kolkata for his excellent and constant guidance and help, endless encouragement, thoughtful and freedom and stupendous co-operation throughout the term paper till its successful completion. I am greatly indebted to his motivation, fruitful suggestions and inspirations. I owe my deep respect to **Dr. Amalesh Samanta**, Head of the Department, Department of Pharmaceutical Technology, Jadavpur University, Kolkata for all the necessary help and encouragement. I would like to convey my sincere gratitude to AICTE and Jadavpur University for their financial and equipmental support for my **M. Pharm** course. I am extremely honored and grateful to **Dr. Nilanjan Adhikari**, **Dr. Shovanlal Gayen, Mr. Sandip Kr. Baidya**, **Mr. Sk. Abdul Amin**, **Mr. Sanjib Das**, **Mr. Suvankar Banerjee** for their priceless guidance and support which assisted me to gather knowledge about the different aspects of this work. Finally, I would like to express my deep respect to my father and mother and my friends and relatives for their continuous help, love, encouragement and moral support throughout the period of my work.

[Rahul Jana]

Date:

Place: Department of Pharmacy, Jadavpur University, Kolkata

Declaration of Originality and Compliance of Academic Ethics

I hereby declare that this thesis contains literature survey and original research work performed by me (**Rahul Jana**) as a part of my Master of Pharmacy studies. All the information in this document have been obtained and presented in accordance with academic rules and ethical conduct.

I also declare that, as required by these rules and conduct, I have cited and referenced the materials and results that are not original to this work.

Name: **Rahul Jana**

Exam Roll Number: **M4PHC23025**

Class Roll Number: **002111402042**

Registration Number: **160267 of 2021-2022**

Thesis Title: "**A quantitative structural analysis relationship modelling study on HDAC3 inhibitors: Unveiling important structural features for potent activity**".

(Rahul Jana)

Signature with Date

Dedicated to My Parents

Table of Contents

Preface

In recent, scientists or researchers have been particularly interested in metalloenzymes like HDAC for several reasons. Metalloenzymes play crucial roles in various diseases. HDAC3, for instance, is a zinc-dependent enzyme involved in epigenetic regulation. It plays a pivotal role in gene expression. Understanding metalloenzymes like HDAC3 is crucial for unraveling biological mechanisms. Metalloenzymes are often associated with several diseases and health conditions. Dysregulation of HDAC3 has been implicated in cancer, neurodegenerative disease, cardiovascular disease, kidney disease, etc. So HDAC3 is a promising target to treat these diseases. Investigating the structural and functional aspects of HDAC3 helps in designing more effective drugs with fewer side effects. However, this thesis endeavors these critical features through a series of classifications and regression-based QSAR modeling studies. This thesis is organized into several chapters, each designed to elucidate a specific aspect of HDAC3 inhibitors, from their molecular structure to their mechanisms of action. ***Chapter 1*** provides outlines of cancer and other diseases with their possible mechanism connected with HDAC3. In addition, this chapter also covers the basic introduction of HDAC and their classification with their domain organization and structure of HDAC3. ***Chapter 2*** mainly deals with several HDAC3 inhibitors such as hydroxamate, benzamide, Hydrazide, Thiol based HDAC3 inhibitors. Additionally, discussed several QSAR modeling performed on HDAC3 in previous. Herein newer category of HDAC3 inhibitors have also been proposed as potential HDAC3 inhibitors. ***Chapter 3*** mainly discussed with importance of study on HDAC3. ***Chapter 4*** deals with procedures and methods performed on HDAC3 inhibitors to reach final outcomes. ***Chapter 5*** describes the result and discussion related to my work. In this section, we discussed how our model is statically significant or robust to get an idea about some important structural features and fingerprints for designing crucial HDAC3 inhibitors in the future. ***Chapter 6*** concludes the overall result that we get. Hydroxamate and benzamide-based HDAC3 inhibitors might be beneficial for the development of potent HDAC3 inhibitors. The significance of HDAC3 inhibitors in the field of drug development cannot be overstated, as they hold immense promise in the treatment of various diseases, including cancer and neurodegenerative disorders. It is this potential that sparked my fascination with this subject and fueled my determination to delve deeper into understanding the structural elements that underlie their potency.

It is my hope that this work will contribute to the advancement of our knowledge in this field and pave the way for more effective drug development strategies.

As I look back on the challenges faced and the lessons learned throughout this research, I am filled with gratitude for the opportunity to embark on this academic journey. I am excited to share my findings with the academic community and anticipate the positive impact they may have on the development of new therapeutic agents.

.....

[Rahul Jana]

Chapter 1: Introduction

1.1. Cancer

Cancer is the second leading cause of death worldwide. This accounting for nearly 10 million deaths in 2020 or nearly one out of six deaths [1,2]. The common cancers found in 2020 are colon and rectum cancer (1.93M cases), breast cancer (2.26M cases), lung cancer (2.21M cases), and prostate cancer (1.41M cases) [1]. Thus, the development of anticancer drugs is one of the major advances in the field of medicine. The major disadvantage of existing drugs is the narrow therapeutic range and several adverse effects because they cannot differentiate between normal cells and cancerous cells thereby resulting in negative side effects and toxic effects consequences. A target-specific drug must be needed immediately to overcome limitation of chemotherapeutic drugs. There are so many reasons to develop cancer cells such as consumption of tobacco, alcohol, high body mass, and lack of physical activity. Additionally, genetic and epigenetic changes are also playing a crucial role to develop cancer cells. Genetic changes can lead to developing cancer cells if they alter the way of cell develop and spread. These risk factors [3] may either directly or indirectly encourage the growth of cancer. Cancer prevention may be defined as to reducing the chance of developing cancer [4]. This might entail maintaining a healthy lifestyle, keeping away from substances known to cause cancer (carcinogen), and receiving cancer-prevention therapies or vaccinations. As a result, the internal and external elements stated above may be used to reduce the risk or possibility of developing cancer. Other approaches to cancer treatment may be used, such as surgery, radiation therapy, biological therapy, gene therapy, and chemotherapy using anticancer medications [5-9]. The main five cancer types are (a) carcinoma, (b) sarcoma, (c) melanoma, (d) lymphoma, and (e) leukemia. Carcinoma mainly originated in the lungs, breast, skin, pancreas, glands, and others organs. Sarcomas often develop in the body's soft or connective tissues such as blood vessels, cartilage, bone muscle and fat. Melanomas are malignancies that start in the melanocytes, which regulate the skin's color. Leukemia is a blood cancer, whereas lymphomas are lymphocyte malignancies. Typically, leukemia does not become solid tumors.

1.2. Histone deacetylases (HDACs)

Gene expression is affected by inheritable and reversible epigenetic changes [10]. It is well known that epigenetic alterations, notably DNA methylation and histone modifications are widely documented to have a significance role in the emergence of cancer [11]. Acetylation, methylation, and phosphorylation are just a few examples of the histone modifications that have been found to control gene expression. Acetylation state is one of these alterations that is recognized to be crucial in the development and spread of cancer. Histone deacetylases

(HDACs) and histone acetyltransferases (HATs) are two categories of enzymes that play major roles in determining the acetylation state of histone proteins. The HATs transfer acetyl groups to the lysine residue of the N-terminal tails of histones and HDACs remove the acetyl groups from histones. This chemical modification increases or decrease the transcriptional activity. The HAT neutralizes the positive charge of histone tails by acetylating the lysine residues, which decreases the attraction of the histones for the negatively charged DNA backbone. Therefore, increases the transcription of tumor suppressor genes (e.g., CDKN2A) [12-13] (**Figure 1.1**). The equilibrium between histone acetylation and deacetylation is maintained by these two families of enzymes (HDACs and HATs), which have opposing roles [14]. Cell proliferation, apoptosis, and cell-cycle control are all regulated by this equilibrium. If it is upset, it can result in the emergence of various malignancies/cancers [15].

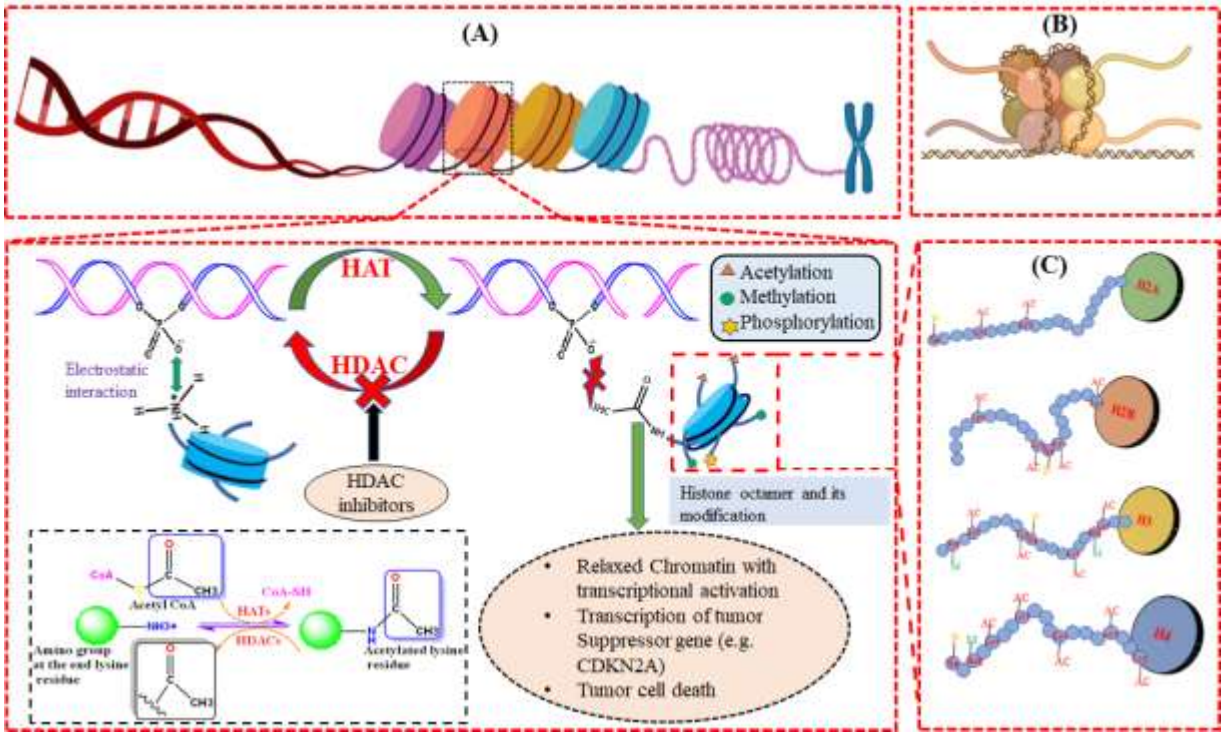

Figure 1.1: (A) Histone acetylation and deacetylation process with chemical modification. (B) Structure of histone. (C) Histone modification of each globular domain.

HDACs remove the acetyl group from the lysine residue of histones and thus increase the positive charge of octamers of linker histone (H1 or H5) and four highly basic histones (H3, H4, H2A, and H2B) that interact with the negatively charged DNA via electrostatic bonds. The linker histone such as H1 and H5 are responsible for the stabilization of chromosomes, promoting the formation of the higher order structures. Each histone octamer is tightly coiled by 147 base pairs of DNAs (**Figure 1.1**) [16]. This will result in more compact DNA and gene silencing.

1.3. Classification of HDACs

HDAC is a member of the either histone deacetylase family (Zn^{+2} metalloenzymes: requires Zn^{+2} for their enzymatic activity) or the Sir2 family (metal free sirtuins: requires NAD^{+} as a cofactor for enzymatic activity). In humans, HDACs are divided into distinct groups known as class-based sequence similarities, and a detailed analysis was given in **Figure 1.2**. According to several structural and functional characteristics as well as domain organization, mammalian HDACs are now divided into four classes (class I, II, III, and IV) [17]. Class I include HDAC1, 2, 3, and 8 that are located in the nucleus and contain a unique deacetylase domain, and are homologous to the *Rpd3* gene [18]. Class II is split into two subclasses, class IIA (HDAC4, 5, and 7) and class IIB (HDAC6 and 10); these HDACs are similar to yeast Hda1 and are found in the nucleus and cytoplasm [19]. However, Hos1, Hos2, and Hos3 from *Saccharomyces Cerevisiae* share 35% - 49% identity with *Rpd3* and 21% - 28% identity with Hda1. Hence, class I and II HDACs are also related to the yeast Hos proteins [20]. On the other hand, Class IV is restricted to the nucleus and comprises solely HDAC 11. These three classes are all reliant on Zn+2. In contrast, class III sirtuins (SIRT1-7) are NAD+ dependent [21]. In addition, SIRT1, 2, 6, and 7 are located in the nucleus and SIRT3-5 are located in the mitochondria [22]. The classification, cellular localization, and physiological roles of HDACs are given in **Table 1.1**.

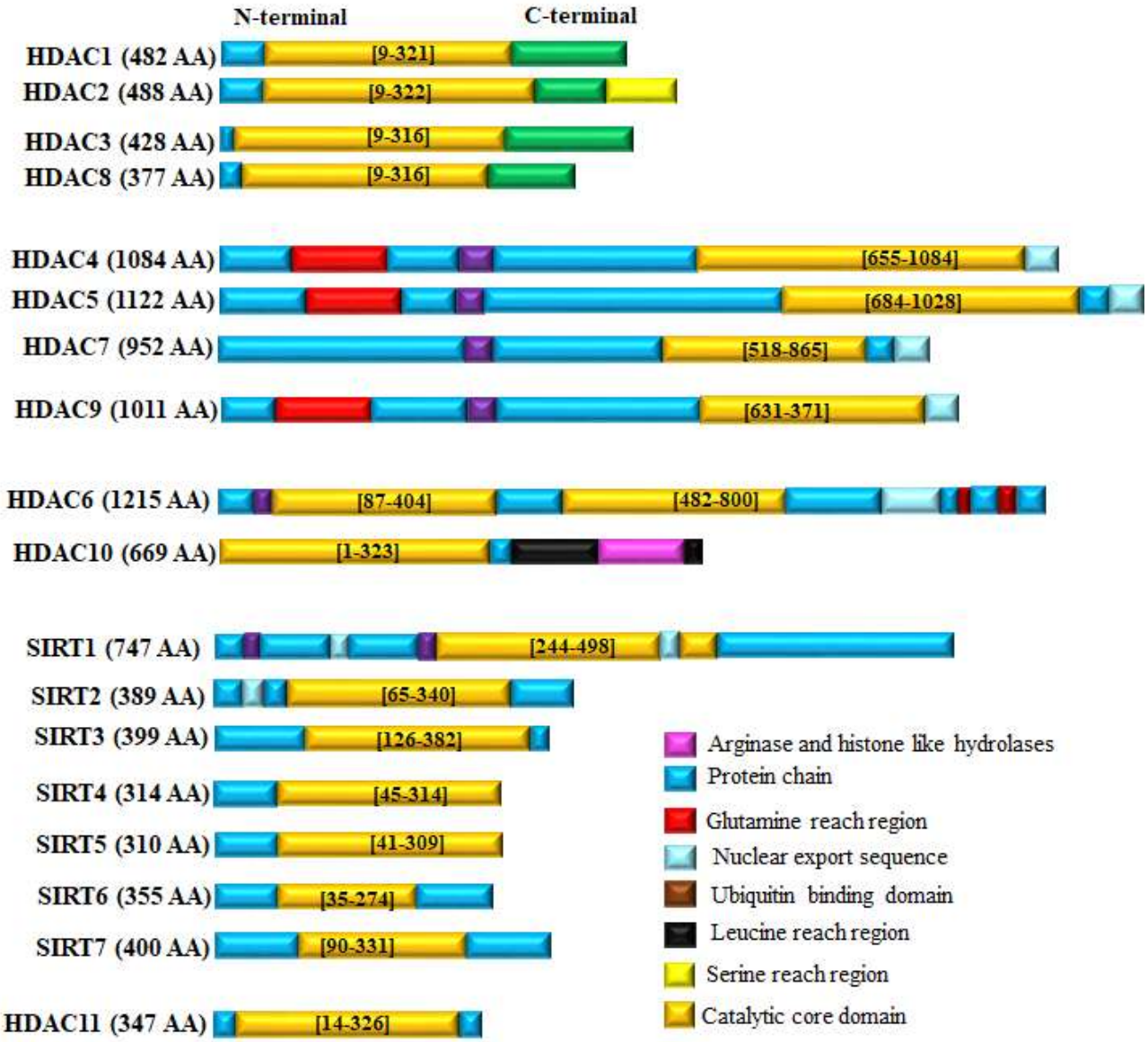

Figure 1.2: Different classes of HDAC and domain organization of different HDACs with total number of amino acids.

Table 1.1: A detail description of HDACs.

Class	HDAC isoform	No. of Amino acid	Cellular location	Tissue distribution	Sequence homology	Catalytic domain	Pathophysiological implications	Ref.
I	HDAC 1	482	Nucleus	Ubiquitous	Yeast Rpd3 protein [35%-49% sequence similarity to the three proteins (Hos1, Hos2, and Hos3) of Saccharomyces cerevisiae]	1	Cancer, neurodegenerative diseases, cardiovascular diseases, inflammation, anti-fungal	[20], [23], [24], [25], [26], [27]
	HDAC 2	488	Nucleus			1		
	HDAC 3	428	Nucleus			1		
	HDAC 8	377	Nucleus/cytoplasm			1		
IIa	HDAC 4	1084	Nucleus/cytoplasm	Heart, brain, skeletal muscle	Yeast Hda 1 [21% - 28% sequence similarity to the three proteins (Hos1, Hos2, and Hos3) of Saccharomyces cerevisiae]	1	Muscle development and regeneration, cardiac hypertrophy, cancer, neurodegenerative diseases	[19], [28], [20], [29]
	HDAC 5	1122	Nucleus/cytoplasm			1		
	HDAC 7	952	Nucleus/cytoplasm/mitochondria	Heart, skeletal muscle, pancreas		1		
	HDAC 9	1011	Nucleus/cytoplasm	Skeletal muscle, brain		1		
IIb	HDAC 6	1215	Cytoplasm	Heart, liver, kidney, placenta		2	Neurodegenerative diseases, cancer, immune disorders	
	HDAC 10	669	Cytoplasm			1		
III	SIRT 1	747	Nucleus/cytoplasm		Yeast Sir 2 protein	1	Aging, metabolism, cancer,	[30], [31], [32], [33]
	SIRT 2	389	Cytoplasm			1		
	SIRT 3	399	Mitochondria			1		

	SIRT 4	314	Mitochondria			1	neurodegeneration, apoptosis, stress resistance	
	SIRT 5	310	Mitochondria			1		
	SIRT 6	355	Nucleus			1		
	SIRT 7	400	Nucleus			1		
IV	HDAC 11	347	Nucleus/cytoplasm	Brain, skeletal muscle, heart, kidney	Sequence similarity for both class I and class II	2	T-cell development, immune response, cancer	[34], [35], [36]

1.4. A Short trip of HDAC3

HDAC3, one of the crucial classes I HDACs has paramount importance in the regulation of cancers as well as apoptosis. The HDAC3 is a member of the class I HDACs and exhibits abnormal expression in a variety of malignancies, contributing significantly to the development of cancer and several other human disorders [37]. Micro-RNA and HDAC are the most prominent target for cancer treatment. There is a complex relationship between HDACs and miRNA which is not fully understood yet. Some literature showed that overexpression of HDAC3 has been attributed to the downregulation of several tumor suppressor genes include micro-RNAs, including miR-495-3p, miR-296-3p, and miR-451 in melanoma, colorectal and prostate cancer, respectively [38-40]. It was observed that TRAF5 inhibition could prevent melanoma cells from proliferating while causing them to undergo apoptosis. TRAF5 is a family member of tumor necrosis factor-associated factor family members (TRAFs) and plays an essential role in cell biological processes via binding to their cognate cellular receptors [41]. Moreover, high expression of HDAC3 is linked to the brain cancer and tumorigenesis. Some authors suggest that the elevation of HDAC3 is not associated with some cancer progression. Liu et. al. (2013) reveals that the elevation of HDAC3 is linked to poor outcomes in liver cancer [42]. Harada et. al. (2017) demonstrated that the elevation of HDAC3 is not associated with the progression of multiple myeloma [43]. In addition, HDAC3 is an epigenetic regulator of a range of cell signaling pathways and also knockdown of HDAC3 results of the G0/G1 cell cycle arrest which in turn causes colorectal, prostate, melanoma, and acute myeloid leukemia. However, the HDAC3 enzyme forms a stable complex with the nuclear receptor corepressor (N-CoR) and the silencing mediator of retinoic and thyroid receptors (SMRT). This complex is crucial to trigger the hypoacetylation of histone tail for transcriptional repression in different cancer including leukemia and lymphoma [44-45].

While therapeutic effects of HDAC inhibitors ($HDAC_i$) have been studied on different types of tumors and cancer cell lines. Several inhibitors are undergoing clinical trials. Thus far, six $HDAC_i$ have been approved by US Food and Drug Administration (US-FDA) and China FDA (CFDA) such as romidepsin (FK228), vorinostat (SAHA), panobinostat (LBH589), belinostat (PXD101), chidamide (CS055) and entinostat (MS-275). Among 18 family members of HDACs, histone deacetylase 3 (HDAC3) is a fateful member of the class I HDACs and significantly contributes to several diseases/disorders, including cancer. Evidence revealed that HDAC3 was involved in and correlated with various cancer related

processes, including migration, proliferation, malignancy, differentiation, and apoptosis that include ovarian cancer, colorectal cancer, ovarian cancer, gastric cancer, etc. (**Figure 1.3**) [46]. Apart from cancer, it has a role in other diseases including rheumatoid arthritis (RA) [47], diabetes [48], cardiovascular diseases [49], neurodegenerative diseases [50], HIV [51], Kidney disorder [52].

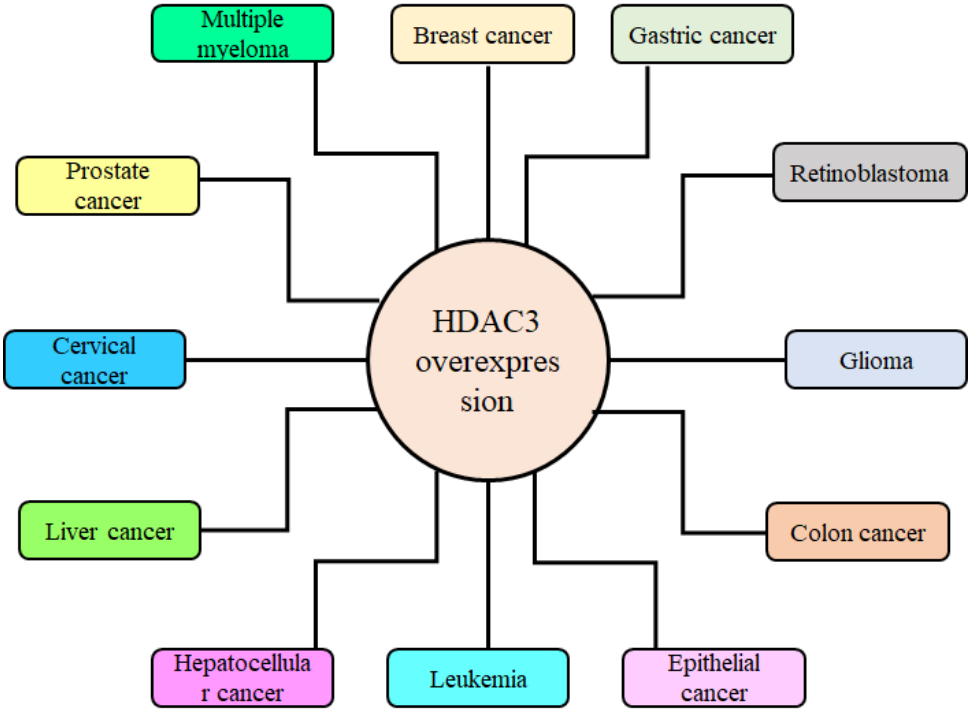

Figure 1.3: The overexpression of HDAC3 causes a number of physiological conditions, as shown in the schematic diagram.

1.5. Structure of HDAC3

HDAC3 belongs to class I HDAC family and it was discovered in 1977 after HDAC1 and HDAC2. The homology sequence of HDAC3 is resembled with *Rpd3* protein of yeast, while HDAC1 and HDAC2 are not encoded in a similar manner. HDAC3 has an extra phenylalanine at position 199, although HDAC1 and HDAC2 have tyrosine residue at this position. Position 92 of HDAC3 is an aspartate residue, but HDAC1 has glutamate residue at this position. All class 1 HDACs require the recruitment of multi-subunit corepressors for their enzymatic activity. HDAC3 is consist of four distinct splicing variants have been found as HD3α, -β, -γ, and -δ [53]. Also, HDAC3 is found in the nucleus, cytoplasm, and plasma membrane along with transcriptional repressor NCoR, SMRT [54], or Ski [55], which differentiate it from other HDACs (**Figure 1.4A**). However, it suggests that HDAC3 has a unique property that is not completely understood yet [54]. Watson and co-workers [56]

revealed that the HDAC3 complex with SMART-DAD activates the HDAC3 functional activity.

In class 1 HDACs, HDAC1 and HDAC2 are found with three corepressors such as CoREST/Kiaa0071 [57], NuRD [58], and Sin3A [58,59], whereas HDAC3 recruited specially to the homologous NCoR complex or SMRT complex for its enzymatic activity. HDAC3-SMRT complex is found to exhibit HDAC3 activity. Activation of HDAC3 is mediated by deacetylase activating domain (DAD) that include two SANT motif, present in SMRT. Therefore, DAD mutation that denies HDAC3 interaction also removes HDAC activity restoration [60]. It has been hypothesized that the chaperone complex including the TCP-1 ring complex (TRiC) is necessary for the assembly of the HDAC3 and SMRT-DAD. However, HDAC3 does not form any complex with SMRT-DAD complex when expressed in bacterial cells. Somoza et al. demonstrated that HDAC3 is 41% similar to HDAC8 and HDAC2 [61]. Watson et al. [56] showed that the N-terminal helix of the DAD undergoes a significant structural change when it forms a complex with HDAC3, such that it no longer forms a part of the structure but lies along with the surface of the HDAC3 and engages numerous intermolecular interactions. This interaction forms helix H1, loop L2, helix H2, and strand S2. This region is slightly different from HDAC8. In HDAC3 helix H1 is distorted and is called pseudo helix. Due to this difference, HDAC8 is active without interaction with the co-repressor, a small molecule referred to as inositol-1,4,5,6-tetrakinase phosphate (Ins (1,4,5,6) P4) plays an important role to make the interaction between HDAC3 and SMRT-DAD complex (**Figure 1.4B**). This small molecule acts as an "intermolecular glue", present between HDAC3 and SMRT-DAD complex, which contributes five hydrogen bonds and salt bridges to the Ins (1,4,5,6) P4. A careful examination of structure suggests that SMRT, Ins (1,4,5,6) P4. HDAC3 are mutually interdependent such that SMRT-DAD and Ins (1,4,5,6) P4 are required for activation of the HDAC3 activity [62]. An acetate ion forms a hydrogen bond with catalytic Zn and His134, His135, and Tyr298 (**Figure 1.4C**). The active site of the HDAC3 is given in **Figure 1.4D**.

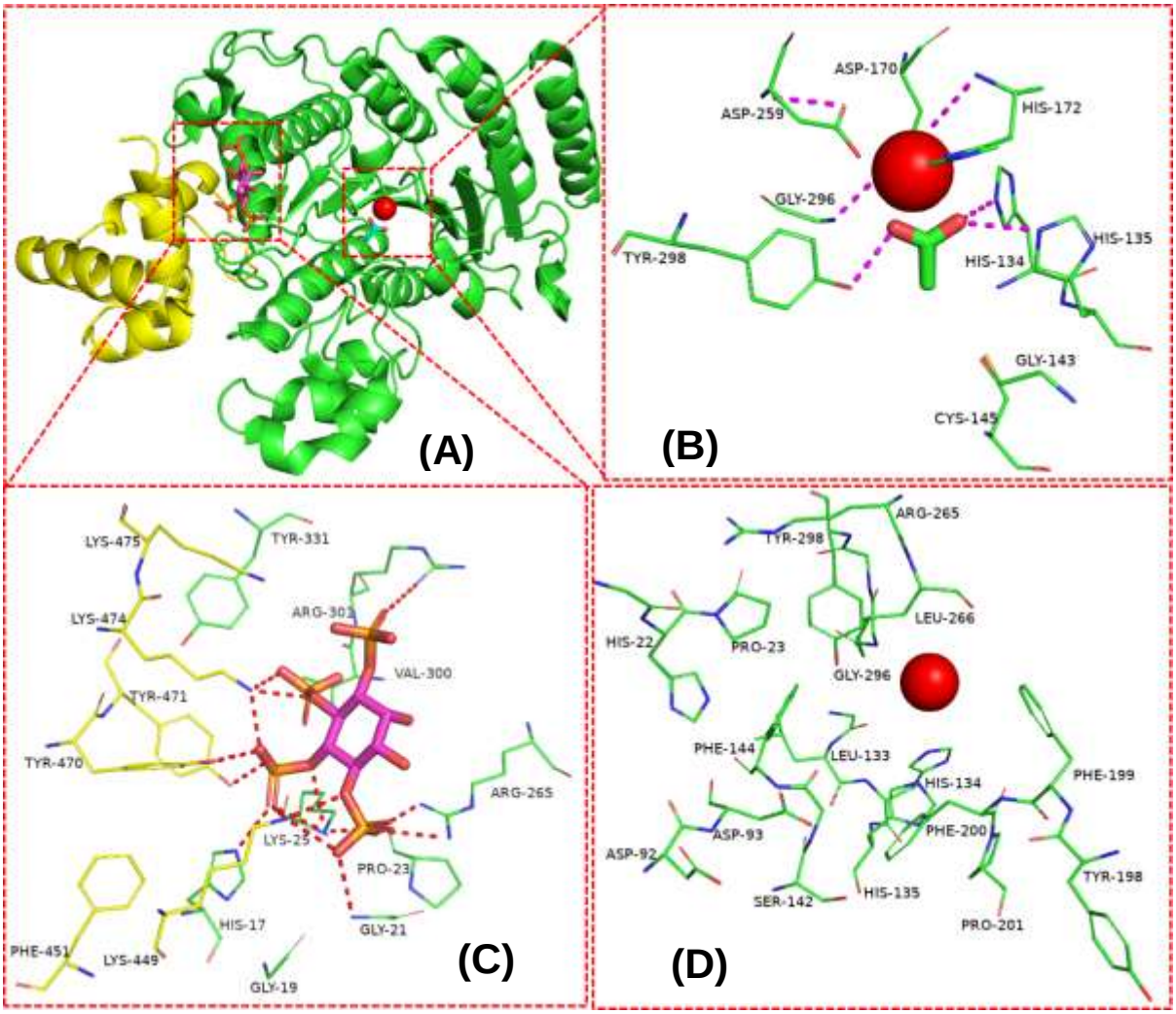

Figure 1.4: (A) HDAC3-SMRT-DAD (yellowish color) complex. **(B)** Intermolecular interactions of acetate ion with zinc ion (red color) in the active site of HDAC3. **(C)** Inter molecular interaction of Ins (1,4,5,6) P4 with the HDAC3 residue which attached HDAC3 and N-CoR. **(D)** Active site residue of HDAC3

1.6.Pathophysiological role of HDAC3

HDAC3 regulates a number of pathophysiological processes including cancer, aging, kidney disease, cardiovascular disease, neurodegenerative disease, diabetes, bone disorder and embryonic development, and inflammation. Here, we discussed some major diseases associated with HDAC3 with possible mechanisms.

1.6.1. Kidney disease

Kidney disease is associated with epigenetic modification such as DNA methylation, and protein/histone modification [63]. HDAC alteration is detected in many experimental animal models of kidney disease [64]. During kidney development a transcription repressor protein

namely cut like homeobox 1 (Cux1) is overexpressed and forms a transcriptional repressor complex with Groucho 4 (Grg4), HDAC1, and HDAC3. Results in inhibition of transcription of p27kip1. The p27kip1 is a cell-cycling kinase inhibitor that binds to the cyclinE/cdk2 and inhibited the G1/S phase transcription phase. This G1/S phase is required for cell cycle progression. So, during kidney development inhibition of p27kip1, leads to activation of the G1/S transcription step and kidney development [65] (**Figure 1.5**). But overexpression of HDACs leads to or potentiates several kidney diseases like adenine-induced chronic kidney disease. Adenine in the diet is readily converted into 2,8, dihydroxy adenine which is an insoluble crystal and blocks renal normal function, leading to damage of renal tubules and also hyperactivity of transforming growth factor β (TGFβ) that increases HDAC3 in renal cells. The HDAC3 involved kidney disease due to irregulate of the PPARγ / Klotho pathway. The peroxisome proliferation-activated receptor gamma (PPARγ) mainly protects renal cells and kidneys by regulating the transcription of genes involved in lipid/protein metabolism, oxidative stress, and insulin action [66]. In kidney disease, PPARγ is found to be suppressed. It means PPARγ is inversely proportional to kidney disease. Studies have shown that activation of PPARγ can protect against kidney disease by improving glucose and lipid metabolism, reducing inflammation, and promoting cell survival. Klotho has also been found to have a protective effect against kidney disease by reducing inflammation, oxidative stress, etc. The lysine residue of PPARγ such as K240, and K265 are HDAC3 sensitive. Thus, administration of HDAC3 inhibitors increases PPARy acetylation. The acetylation of PPARγ translocate to the nucleus and binds to specific regulatory regions in the DNA that are PPAR responses elements, within the Klotho promoter gene and increases the level of Klotho by transcriptional activation of Klotho gene in kidney disease (**Figure 1.6**). Thus, targeting the HDAC3 selectively might be beneficial for kidney disease. In 2020, Chen and co-workers [67] reported several pathophysiological pathways/ mechanisms of renal fibrosis. In renal fibrosis, TGFβ extremely releases and activate Smad 3 which increases the formation of myofibroblast and HDAC3 transcription causes renal fibrosis. Then HDAC3 complexes with NCoR and NF- κB transcriptionally inhibit major antifibrosis factor Klotho via deacetylating the Klotho promoter and lead to renal fibrosis. Selective HDAC3 inhibitor (RGFP966/compound **04**) (**Figure 2.1**) was found to reduce renal fibrosis via de-repressing of Klotho (anti-aging protein).

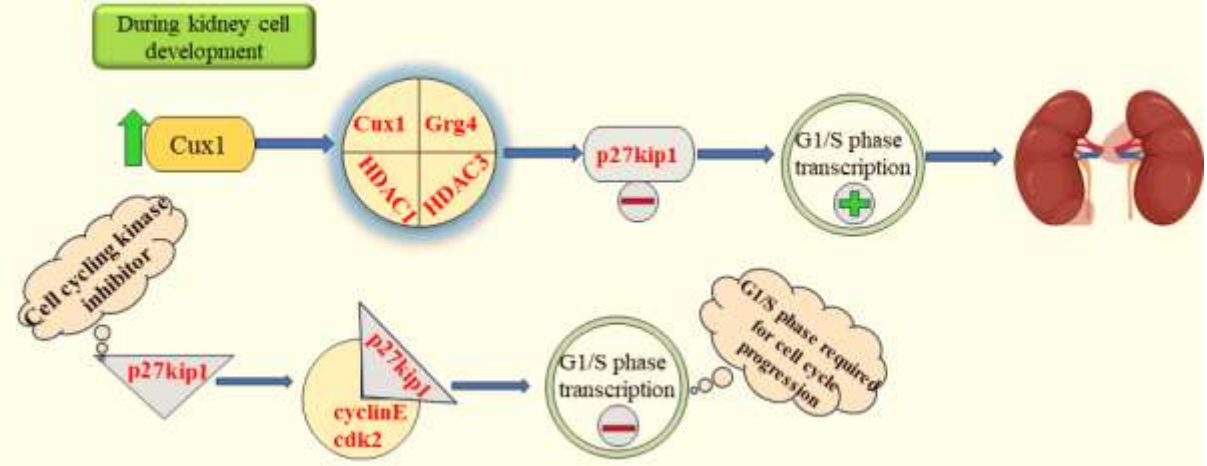

Figure 1.5: Kidney development process

L. Brilli et al. [68] revealed how HDAC*i* is used to treat several kidney diseases. It has been seen that HDAC*i* have anti-fibrotic effects on acute and chronic disease. Mishra et al. [69] demonstrated that TSA (compound **2**) decreased proteinuria with systemic lupus erythematosus (SLE)-induced in mice. HDAC*i* such as panobinostat (LBH589/compound **5**) (**Figure 2.1**) and novel γ-lactam-based HDAC*i* KBH-A145 (compound **13, Figure 2.1**) arrest the G2-M phase in renal cell carcinoma (RCC). Also, compound **5** reduces both protein levels of aurora A and aurora B kinase (present in higher amounts in RCC) via inhibition of HDAC3 and HDAC6 [70,71].

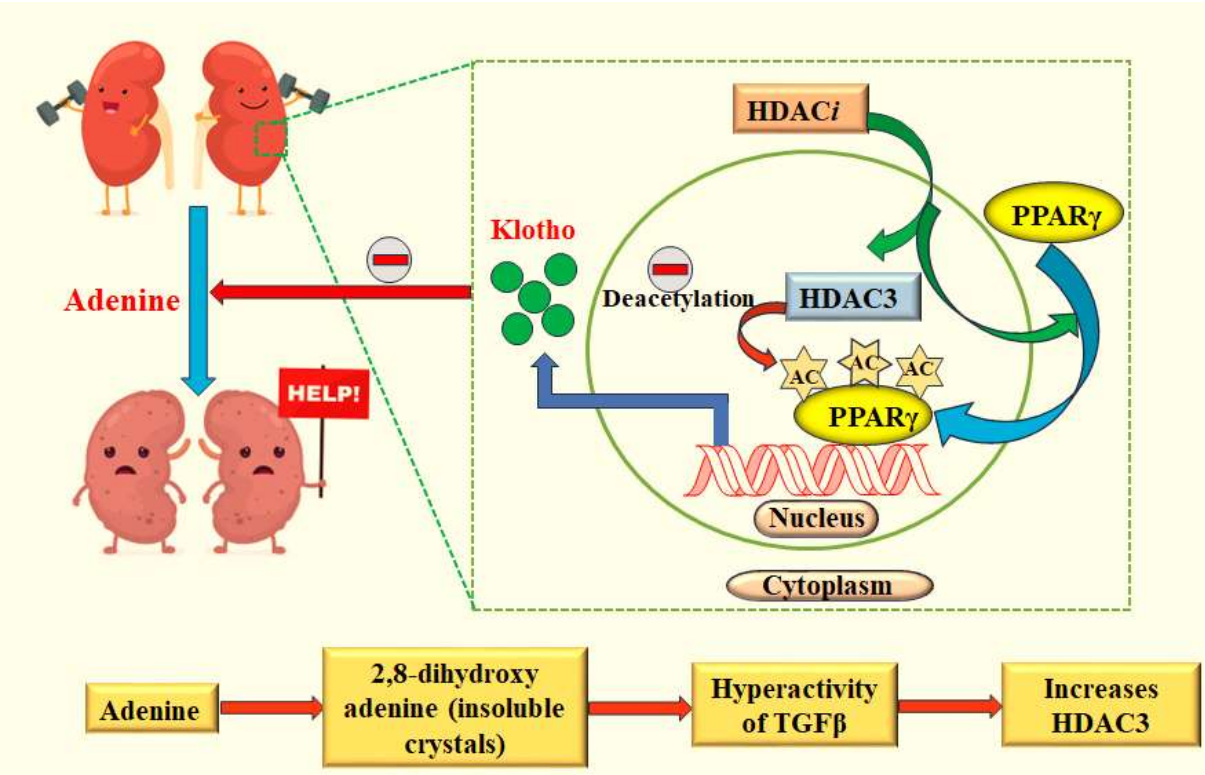

Figure 1.6: Role of HDAC3 inhibitors in kidney disease.

1.6.2. Cardiovascular disease

The most common cardiovascular disease that has contributed significantly to global morbidity and death rates is atherosclerosis. HDAC3 has been implicated in the development and progression of cardiovascular disease through several mechanisms such as (a) lipid metabolism, (b) oxidative stress, and (c) inflammation (**Figure 1.7**) [72]. HDAC3 plays a role in regulating lipid metabolism by deacetylating and activating transcription factors that control lipid metabolism genes. In particular, HDAC3 has been specifically demonstrated to control the expression of *ABCA1* and *ABCG1* genes, which are involved in fatty acid oxidation [73], lipid uptake, and lipogenesis. The *ABCA1* is mainly an ATP-binding cassette transporter gene that is involved in the efflux of cholesterol across the cell membrane to the outside of the cell [74]. Then, these substances are taken up by a protein called apolipoprotein A-I (apoA-I), which is combined with cholesterol and phospholipids to form high-density lipoprotein (HDL), often called "good lipid" because it reduces cardiovascular diseases [75]. Similarly, ABG1 is the human protein code for ATP-binding cassette sub-family G member 1. It is involved in the transport of cholesterol and phospholipids by macrophages and may also control the homeostasis of lipids in other cell types [76,77]. Dysregulation of these pathways can lead to the accumulation of lipids and the development of atherosclerosis [72]. Huang et al., [78] reported overexpression of HDAC3 leads to the downregulation of cholesterol transporter genes such as *ABCA1*, and *ABCG1*, dependent on the expression of liver X receptor alpha (LXRα). This study revealed that overexpression of HDAC3 could inhibit the expression of LXRα [79]. In conclusion, inhibition of LXRα by HDAC3 decreases the downregulation of *ABCA1* and *ABCG1* and increases lipid/cholesterol accumulation, and accelerates the development of atherosclerosis leading to cardiovascular diseases [80]. Again, HDAC3 can regulate the expression of genes involved in oxidative stress response and antioxidant defense. For example, HDAC3 can repress the transcription of the antioxidant enzyme, heme oxygenase-1 (HO-1), which plays an important role in preventing oxidative stress in cells [81]. When HDAC3 activity is increased, it can lead to decreased expression of HO-1 and other antioxidant enzymes, which results in decreased cellular antioxidant capacity and increased susceptibility to oxidative stress [81]. Oxidative stress occurs when there is an imbalance between the production of reactive oxygen species (ROS) and the antioxidant defense system, leading to cellular damage and dysfunction [82]. HDAC3 can also contribute to oxidative stress by regulating the activity of enzymes involved in ROS production. For

example, HDAC3 can promote the expression of NADPH oxidase (NOX), an enzyme that generates ROS in various cells, including vascular smooth muscle cells and endothelial cells [73]. Increased ROS production by NOX and other enzymes can lead to oxidative damage to lipids, proteins, and DNA, which can contribute to the development of cardiovascular diseases such as atherosclerosis and hypertension [83]. HDAC3 also produces inflammation by regulating the expression of genes involved in the inflammatory response. When HDAC3 activity is increased, it can lead to decreased expression of anti-inflammatory genes (such as IL-10) and increased expression of proinflammatory genes (such as TNF-α, IL-1β). HDAC3 removes acetyl groups from histone proteins, leading to a more compact structure and decreased accessibility of DNA to transcription factors [84]. The IL-10 is an anti-inflammatory cytokine that plays a crucial role in the immune response by inhibiting the production of proinflammatory cytokines such as TNF-α, and IL-1β. The IL-10 gene is regulated by various transcription factors, including NF-κB and STAT3, which bind to specific regions of the IL-10 promoter and enhance the action of anti-inflammatory action [85]. When HDAC3 activity is increased, it can lead to deacetylation of histones at the IL-10 promoter and enhancer regions, which decreases the accessibility of these regions to transcription factors [84]. This decrease in the accessibility can lead to a decreased binding of NF-κB and STAT3 to the IL-10 promoter and enhancer regions, which results in decreased transcription of the IL-10 gene [84,85].

Moreover, overall increased HDAC3 activity can lead to a decreased expression of anti-inflammatory genes like IL-10 through epigenetic modification and transcriptional regulation. Chen et al., has pointed out that endothelial-to-mesenchymal transition (EndMT) is a crucial mechanism in vascular inflammation in atherosclerosis by forming inflammatory cytokines that induce mesenchymal cell from the endothelial cell [86].

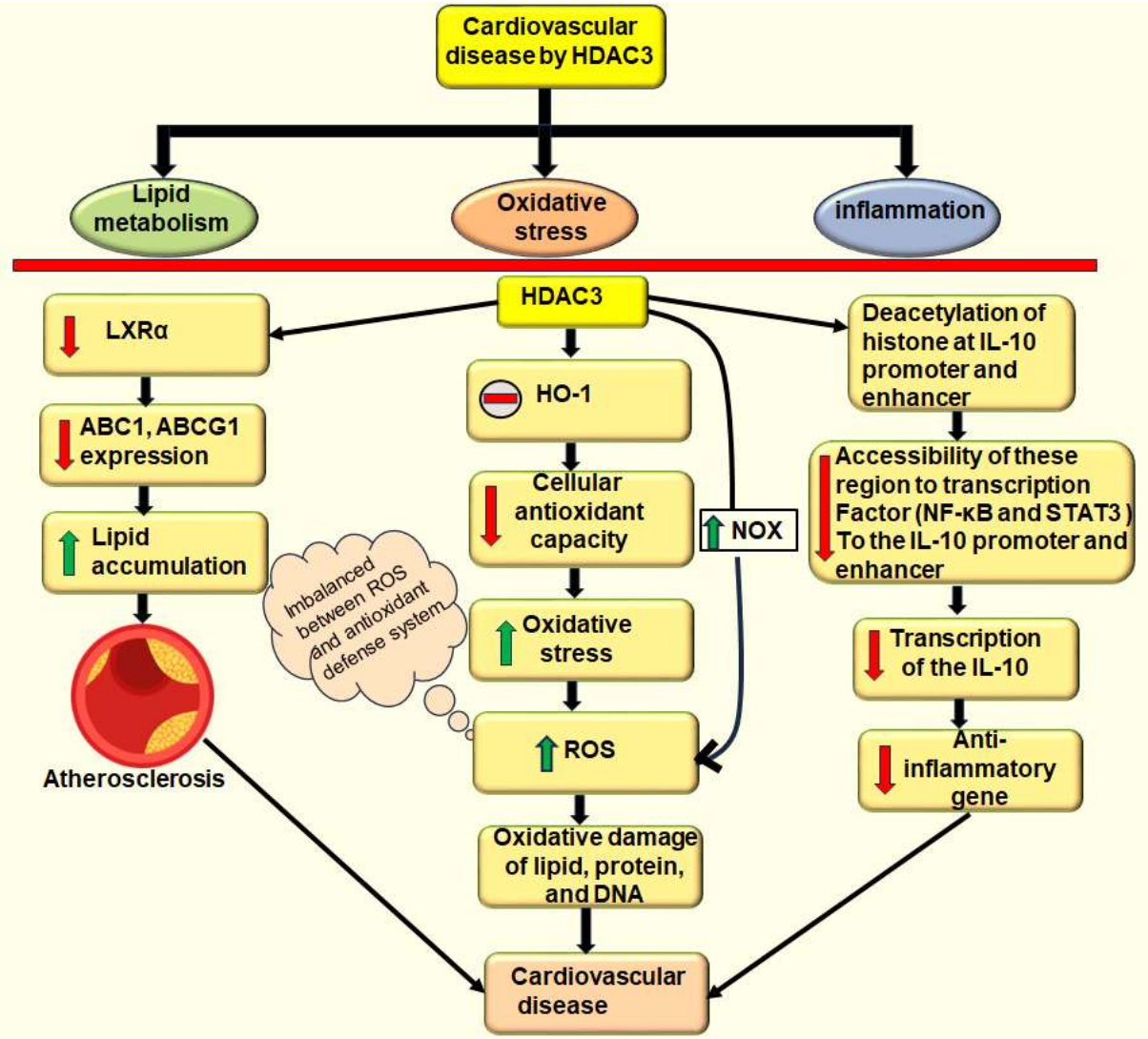

Figure 1.7: Development of cardiovascular disease by overexpression of HDAC3

1.6.3. Diabetes

Diabetes is a metabolic disorder that occurs when your blood glucose level is too high. Diabetes is mainly categorized into two classes, *i.e.*, diabetes mellitus and diabetes insipidus caused due to lack of insulin and vasopressin or anti-diuretic hormone (ADH). Particularly Type 1 and Type 2 diabetes, have received more attention recently as possible signals that HDAC inhibition may be beneficial. In type 1 diabetes (insulin-dependent diabetes mellitus), pancreatic β cells are destroyed due to an autoimmune inflammatory mechanism. In addition, type 2 diabetes is caused by several environmental variables like obesity, stress, lack of exercise, and also some genetic factors related to decreased insulin production as well as insulin resistance [87]. Meier et al. [88] revealed that HDAC3 inhibitors protect β cells from cytokinin-induced apoptosis which is responsible for insulin production. This study showed pancreatic β cell destruction is caused by proinflammatory cytokines (namely *IL-1β*), which

activate the inflammatory transcription factors NF-κB and triggers apoptotic signaling. Therefore, selective HDAC3 reduced cytokinin-mediated destruction of β cells. Peroxisome proliferator-activated receptor gamma (PPARγ), a transcription factor, was shown to be crucial in the control of glucose metabolism. Activation of PPARγ by phosphorylation, and acetylation increases insulin sensitivity in type 2 diabetes [89]. HDAC3 is an enzyme, present in cytoplasm with inhibitor IκBα. After degradation of IκBα, it enters into the nucleus and binds to the transcription factor resulting in the production of inflammatory cytokines such as tumor necrosis alpha (TNFα) that prevent the PPARγ from being activated. Moreover, HDAC3 inhibitors acetylate the histone protein of PPARγ and activate PPARγ target genes such as aP2 and adiponectin which increases glucose metabolism. Therefore, inhibition of HDAC3 is an important target for the activation of PPARγ. Since there are no effective treatments for type 1 diabetes, maintaining the function of beta cells by using any drug or medicine is a critical strategy to maintain beta cell function. On the other hand, type 1 diabetes (insulin dependent mellitus) is caused by the destruction of β cells, mediated by pro-inflammatory cytokines (*IL-1β*) induced by β cell apoptosis. This cytokine activates transcription factor NF- κB and triggers apoptosis. Also, *TNFα* and interferon gamma (*IFNγ*) play important roles in the destruction of β cells. However, class 1 HDAC inhibitors was found to reduced cytokines-mediated cell damage. It was observed that RNA*i*-mediated HDAC inhibition may lead to a reduction in *IL-1β* and IFNγ-induced expression of inducible nitric oxide synthase (iNOS) means a decrease in nitric oxide, an NF-κB-regulated pro-inflammatory mediator [90]. After a detailed study, it was seen that selective HDAC3 have a better effect at reducing β cell apoptosis and decreasing nitrite conc. and restoring glucose-stimulated insulin secretion (GSIS) than broad-spectrum HDAC inhibitors. Selective HDAC3 inhibitors have better cytokine-induced apoptosis, and could better restore GSIS than respective HDAC1 and HDAC2 inhibitors. Thus, selective HDAC3 inhibition may be a good choice for reducing cytokinin-induced beta cell apoptosis [91]. Yao et al. reported [92] that Geniposide, a naturally occurring substance isolated from gardenia fruits is important for β cell regeneration by increasing T-cell factor 7-like 2 (TCF7L2) through activating Wnt/beta-catenin signaling expression. In 2015, Wagner et al. [93] another study published findings of selective HDAC3 inhibitors used as a potential therapy to protect β cell apoptosis from inflammatory cytokines via targeted small interfering RNA (siRNA). It was found that BRD3308 (compound **8**) (**Figure 2.1**), selective HDAC3 inhibitors (IC_{50} = 64 nM) protect the β-cell by suppressing cytokine-induced caspase-3 activity in rat INS-1E insulinoma cells

and had no effects on human megakaryocyte differentiation (a bone, marrow toxicity) whereas, HDAC1, HDAC2 selective inhibition showed toxicity.

Tian et al. [94] showed that lesogaberan (AZD3355) could be repurposed for the treatment of diabetes. Lesogaberan is a GABA receptor agonist which was used in gastroesophageal reflux disease (GERD). But authors tested human islets that lesogaberan increases islet cell proliferation as well as beta cell replication in vitro.

1.6.4. Neurodegenerative disease

The histone deacetylase enzyme family, which includes HDAC3, is essential for the control of gene expression by removing acetyl groups from histones and non-histone proteins. The majority studies revealed that HDAC3 is substantially expressed in the brain compared to other HDACs [95-97]. HDAC3 has been implicated in the development of several neurodegenerative diseases, including Alzheimer's disease (AD) [98], Parkinson's disease (PD) [99], and Huntington's disease (HD) [100]. HDAC3 has been demonstrated to contribute to the development of amyloid beta (Aβ) plaques and the buildup of hyperphosphorylated and acetylated tau, two hallmarks of the illness in AD. A selective HDAC3 inhibitor (RGFP-966/ compound **4**) (**Figure 2.1**) was to found to increase brain-derived neurotrophic factors (BDNF) expression, as well as decrease Aβ accumulation to improve learning and memory [98]. In addition, McQuown and his co-workers [97] have revealed that focal deletion of HDAC3-FLOX genetically modified mice of HDAC3, as well as HDAC3 inhibition via RGFP136 (compound **6**) (**Figure 2.1**), increases long-term memory. The Kwapis and co-workers [101] have shown that expression of Nr4a-CREB genes increases long-term memory. HDAC3 negatively regulates the expression of these genes which are involved in long-term memory. Thus, inhibition of HDAC3 promotes the expression of Nr4a genes which might be an effective strategy to improve long-term memory functions. In Parkinson's disease (PD), HDAC3 is an enzyme that plays a crucial role in regulating gene expression by removing acetyl groups from histone proteins, leading to chromatin condensation and transcriptional repression. Recent studies suggested that HDAC3 plays a key role in the development of PD through its interaction with leucine-rich repeat kinase 2 (LRRK2) [102].

HDAC3 plays a critical role in the development of or promotion of neurodegenerative diseases. Bates and coworkers [103] demonstrated that Huntington's disease is caused by the expansion of the polyglutamine tract. Expansion of polyglutamine alters transcription by

sequestering glutamine transcriptional regulation thereby dysregulating their function protein loss of cAMP-response element binding protein (CREB) and CBP Enhanced polyglutamine toxicity in neurons. Knockdown of HDAC3 suppressed neuronal toxicity and neuronal expression of HDAC3 restore expanded polyglutamine tract (Htn-Q150).

In 2021, Hecklau and co-workers [104] reported the importance of HDAC3 in Huntington's disease (HD) in mice. Huntington's disease is a neurodegenerative disease caused by modification/alteration of epigenetics, most prominent in the striatum and spread in the brain region in chronic conditions. Several genes are repressed, associated with HD namely brain-derived neurotrophic factor (Bdnf), dopamine receptor 2 (Drd2), and preproenkaphalin (Penk). On the other hand, epigenetic alterations such as histone acetylation, ubiquitination, and DNA methylation contribution to gene expression of HD. HAT and HDAC are associated with hyperacetylation and deacetylation of histone resulting in gene expression and gene repression. Mutant Huntingtin (HTT) gene directly binds to the HATs and reducing their activity results in hypoacetylation and gene repression. Histone hypoacetylation at promoters of the downregulated gene was shown in several HD models. Thus, inhibition of HDAC neuroprotective effects can be achieved. RGFP109 (compound **7**) is a class 1 selective inhibitor for HDAC1 and HDAC3 that very slightly improves transcriptional dysregulation and short term motor skill learning deficits in HD mice [104].

Several authors reported detailed mechanisms of HDAC3 [105,106] in memory and learning. The authors demonstrated that CREB is a transcriptional factor. It is activated by several pathways mainly the cAMP-PKA pathway which phosphorylates CREB and activates it. Once activated, it binds to cAMP response elements (CREs) in the target gene and leads to the expression of a wide range of proteins related to memory formation. CREB-binding protein (CBP) is a co-activator protein that enhances CREB's transcription activity. The CBP has histone acetyltransferase activity, which means that it adds an acetyl group to histone proteins associated with DNA. This leads to an open chromatin structure that allows other transcription factors and machinery to access the DNA, promoting gene transcription. HDAC enzyme that deacetylates the lysine residue and represses the gene transcription. Therefore, HDAC inhibitors block the activity of HDACs. When HDACs are inhibited histone acetylation increases, leading to an increase in accessibility of chromatin structure. This modification led to increased transcription of CREB and coactivators like CBP that facilitate gene expression related to memory and the learning processes (**Figure 1.8**).

Li et al. [107] demonstrated that neuroinflammation is an abnormal activation of inflammatory cells after intraventricular hemorrhage (IVH). Microglial activation induces the production of pro-inflammatory genes such as TNF-α, IL-1B, IL-6, etc. resulting in inflammation in cells and increases cell death. HDAC3 inhibitors like BRD3308 (compound **8**) (**Figure 2.1**) was found to suppress HDAC3 and showed anti-inflammatory activity. Also, HDAC3 inhibition, increases the expression/activation of PPARγ target genes. The PPARγ activation can decrease inflammation by blocking the family of nucleotide-binding domain, and leucine-rich-containing family, pyrin domain-containing-3 (NLRP3) signaling pathway and neuronal function in mice models because HDAC3 is widely expressed in the brain [107,108].

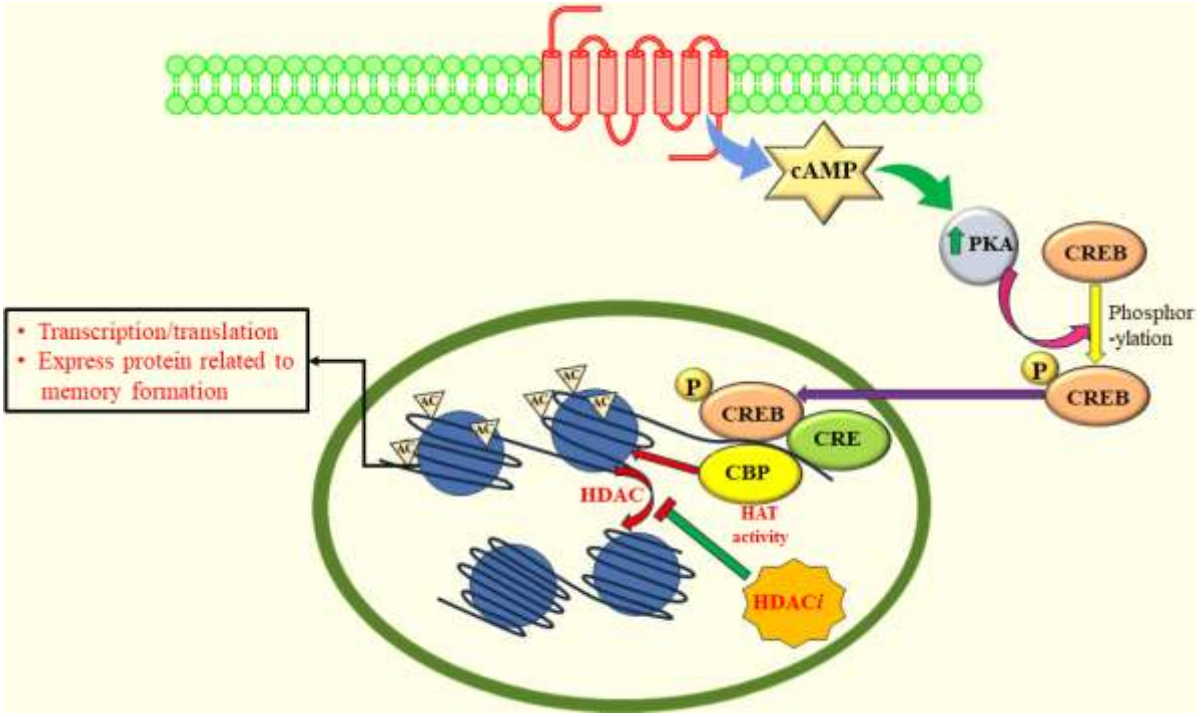

Figure 1.8: Expression of protein related to memory formation through activation of CREB.

1.6.5. Bone disorder

Bone disorders can be caused by several factors such as genetics, hormones, aging injuries, and infections. Bone is a dynamic tissue with variety of forms and purposes. It has been shown that most bone fractures heal completely within a few weeks or months due to the recovery of genomic material of bones. Plasticity in the genome or epigenome provides cells that are the ability to protect fractured bones. Osteoporosis and osteoarthritis are two common diseases that affect the integrity and functioning of the bones [109,110]. Many illnesses may be significantly influenced by epigenetic alteration according to the newly published paper

discussed earlier. The HDAC family member such as HDAC1 and HDAC3 both are abundant in human bone and articular cartilage [111]. HDAC3 is a member of the class1 family and four distinct splicing variants have been found as HD3α, -β, -γ, and -δ [112] and functionally distinct from HDAC1 and 2 because of distinct interaction with NCoR-SMART corepressor [54] or Ski [55,113,114]. Still, HDAC*i* action is not properly clear. Valproic acid (compound **9, Figure 2.1**) is one of the oldest drugs in HDAC. Two consecutive studies have seen that on long-term administration of compound **9** (**Figure 2.1**) bone mineral density decreased or increased or unchanged and bone resorption decreased or increased or unchanged [115,116]. Senn et al., [117] and Mc-Gee-Lawrence et al. [118] reveal that in vivo treatment of rat models with valproate compound **9** (**Figure 2.1**) and vorinostat (SAHA)/ compound **1** (**Figure 2.1**) caused bone loss. Distinguee, Cantley et al. [119] reveals that HDAC inhibitors inhibit osteoclasts and joint destruction in animal models of chronic inflammatory disease such as rheumatoid arthritis and periodontal disease. In summary that in vivo activation of HDACs is generally unfavorable for bone development because the loss of HDAC function is especially susceptible to mesenchymal progenitors (bone-forming properties).

Culley et al. [120] revealed that the administration of TSA (compound **2, Figure 2.1**) reduced the damage of cartilage caused by cytokinin-induced MMP expression. Similar results were obtained by Chen et. al. [121,122] Huh et al. [123] Wang et al. [124] where, TSA (compound **2**) protected cartilage and reduced MMP and cathepsin expression.

Xu et al. [125] reveal that osteogenic differentiation is the process by which mesenchymal stem cells (MSCs) differentiate into osteoblasts, the cells that form the new bones. HDAC3 inhibitors can enhance osteogenic differentiation by increasing the expression of osteoblast-specific genes and proteins.

Another article says that the bone marrow microenvironment is the niche where hematopoietic stem cells (HSCs) and multiple stem cells (MSCs) reside and interact with each other or other cells. The bone marrow disorders, such as multiple myeloma (MM), are a type of blood cancer that originates from plasma cells. MM cells induce osteoclast activation and osteoblast inhibition, leading to bone destruction and impaired bone formation. HDAC3 inhibitors can target the bone marrow microenvironment by decreasing MM cell proliferation and survival, boosting MSCs-mediated cytotoxicity against MM cells, and regaining osteoblast function [126].

1.6.6. Inflammation

Inflammation is a protective response characterized by a series of chemical reactions resulting in vasodilation, swelling, and migration of immune cells and plasma proteins to the infection site. Among the latter, nuclear factor-κB (*NF-κB*) has been found in most of the cells. It plays a central mediator of pro-inflammatory gene and cytokines expression such as *IL-1* and *TNFα* [127]. In many inflammatory diseases such as rheumatoid arthritis, atherosclerosis, asthma, and multiple, it was noticed that *NF-κB* is active and expressed many pro-inflammatory genes. For that reason, *NF-κB* is a crucial target for the therapy of several inflammatory diseases [128]. Histone proteins that have undergone post-translational modification control the expression of the inflammatory genes. Histone deacetylase removes the acetyl group from histone protein and thereby repression of gene expression whereas, histone acetyltransferase increased the level of transcriptional activity and leads to the expression of pro-inflammatory genes. Apart from histone protein they (HAT and HDAC) also acetylate or deacetylate non-histone proteins such as *NF-κB*. It (*NF-κB*) is present in homo or hetero dimers namely p50 and p65 (ReLA) [129]. Acylation of a particular position in NF-κB-p65 has been shown to regulate several transcriptional activities, DNA binding capacity, and binding to IF-κB. Seven NF-κB-p65 lysine residues, including 122, 123, 218, 221, 310, 314, and 315, have been identified as being acetylated. Moreover, it has been seen that acetylation of specific residues such as 122, 123, 314, and 315 negatively regulates the *NF-κB* regulation means acetylation of specific residues does not produce any pro-inflammatory gene. Also, it has been shown that HDAC3 is involved in the removal of the acetylation of the specific lysine residue of the inhibitory *NF-κB*-p65 subunit and leads to the expression of the pro-inflammatory gene. Moreover, HDAC3 is important for the removal of the acetylation of *NF-κB*-p65 from these specific lysine residues. Therefore, HDAC3 is a crucial positive regulator of inflammatory signaling caused by IL-1 [130,131]. But the proper mechanism of HDAC3 *NF-κB*-p65 inflammation is not clear, research is going on till now.

Kim et al. [132] reported HDAC3 expression results in allergic skin inflammation in the mouse model. The result showed that HDAC3 induction leads to the expression of monocyte chemoattractant protein 1 (MCP1). This MCP1 enhanced the expression of β-hexosaminidase which led to the release of histamine and exerted skin inflammation.

Chen et al. [133] reported spinal cord injury mediated *NF-κB*. The *NF-κB* present in the cytoplasm with inhibitory protein IκB in an inactive state. The activation of *NF-κB* initiated by IκB kinase (IKK), which degrades *NF-κB* protein and trans-locates *NF-κB* protein in the

nucleus. Also, STAT enters into the nucleus from the cytoplasm and activates its target gene at chromosome 19q13. The *NF-κB* binds to this target gene that encodes chemokines and cytokines. Acetylated histone protein reduced inflammation. A recent study by Chen et al. [134] showed how VPA, a HDAC inhibitors reduce inflammation and neuronal cell death.

1.6.7. Role of HDAC3 in cancer

The HDAC family of enzymes, which includes HDAC3, regulates gene expression by removing acetyl groups from histones and other proteins. Several forms of cancer have been linked to the onset and development of HDAC3 activity disruption. One of the mechanisms by which HDAC3 contributes to cancer is through the repression of the tumor suppressor gene. HDAC3 can deacetylate histones and other proteins that interact with DNA, which causes compaction of chromatin and the silencing of tumor suppressor genes.

HDAC3 regulate gene expression by removing acetyl groups from histones and other proteins. Abnormal HDAC3 activity has been implicated in the development and progression of several types of cancer.

One of the mechanisms by which HDAC3 contributes to cancer is through the repression of tumor suppressor genes. HDAC3 can deacetylate histones and other proteins that interact with DNA, leading to the compaction of chromatin and the silencing of tumor suppressor genes [135]. For example, HDAC3 has been shown to repress the expression of the p21 gene in colon cancer cells, leading to increased cell proliferation and survival [136]. In breast cancer it has been shown that HDAC3 increases the expression of β-catenin which is responsible for breast cancer, the knockdown of HDAC3 reduces the expression of β-catenin and is effective in inhibiting breast cancer [137]. HDAC3 can also regulate the expression of various oncogenes and tumor suppressor genes responsible for cell proliferation, lack of differentiation, migration, and cell invasion. Cui et. al [138] revealed that overexpression of HDAC3 correlated with human epidermal growth factor 2 (HER2) overexpression led to the development of cancer. So selective HDAC3 inhibitors may be beneficial in overexpression of HER2 in malignant breast cancer. Several studies have shown that HDAC3 inhibitors can inhibit cancer cell growth and induce apoptosis in cancer cells. For example, the HDAC3 inhibitor RGFP966 (compound **4, Figure 2.1**) has been shown to repress the expression of programmed death ligand 1 (PD-L1) is expressed on the surface of the tumor cells. HDAC3 inhibition has also been shown to sensitize cancer cells to chemotherapy and radiation therapy [139].

In summary, HDAC3 plays a critical role in regulating gene expression in cancer cells and contributes to the development and progression of cancer. HDAC3 inhibitors represent a promising therapeutic approach for the treatment of cancer.

Chapter 2: Literature Review

HDAC inhibitors have been found or created in a broad variety of forms, including vorinostat (SAHA), panobinostat, romidepsin, and belinostat, among others. Unfortunately, the majority of inhibitors do not particularly target HDAC1, HDAC2, or HDAC3 activity. Given that HDAC3 plays a significant role in a number of pathophysiological diseases, targeted HDAC3 inhibition is a possible treatment approach. Hydroxamate, benzamide, hydrazide, and thiols are some of the many materials that are used to make different types of HDAC inhibitors, which come in a range of shapes and functions [140]. For its catalytic activity, HDAC3 possesses a zinc-binding group that is comparable to that of other HDACs. Numerous HDAC3 inhibitors derived from natural materials have also been discovered [141]. Nevertheless, isoenzyme selective HDAC inhibitors are infrequent. Selectivity is crucial because HDAC3 is involved in many illnesses. In this section we have described effective and selective HDAC3 inhibitors to understand the significance of various diseases. Some important inhibitors were given in **Figure 2.1.**

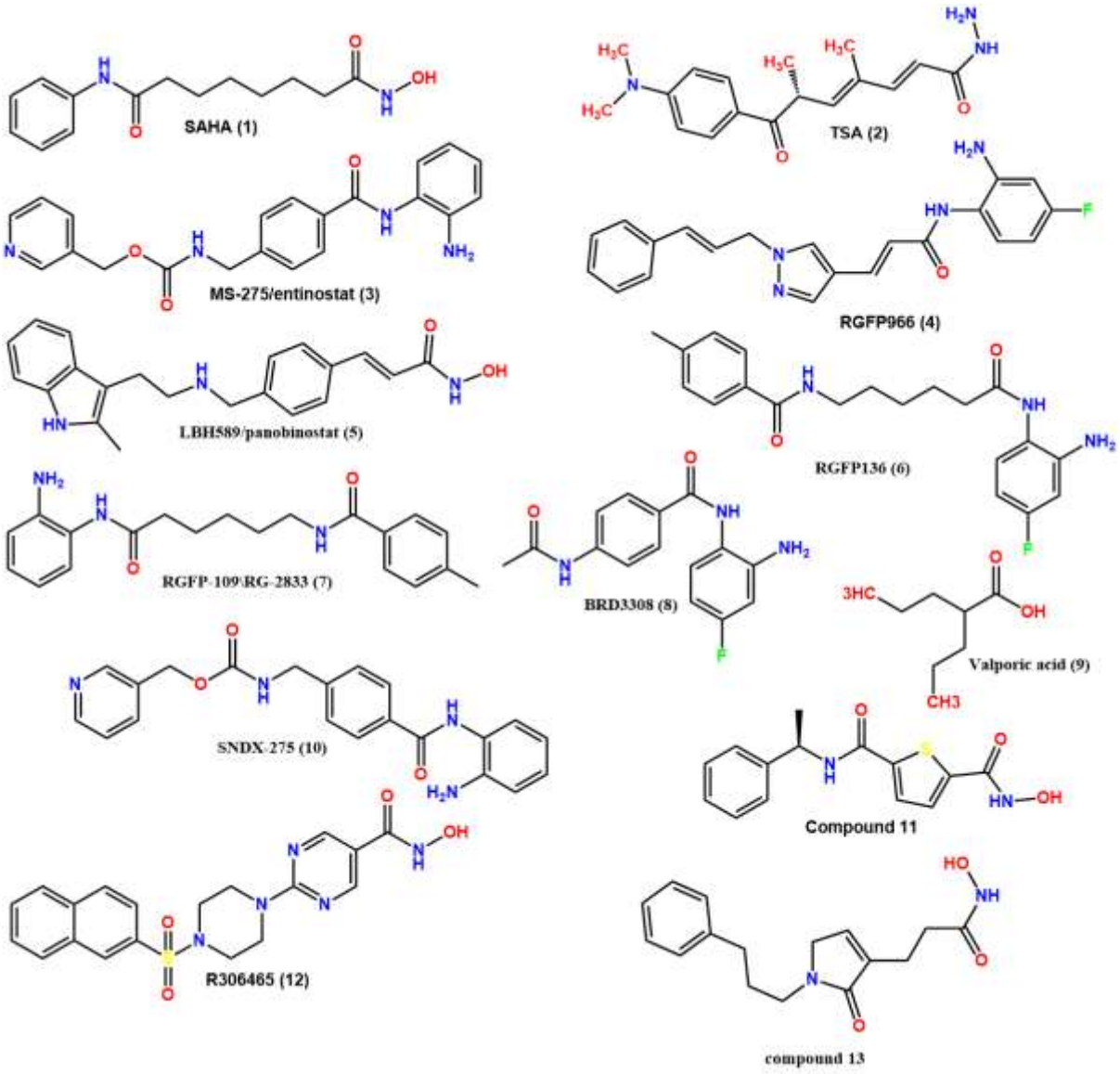

Figure 2.1: Some important HDAC3 inhibitors (**1-13)**

2.1. An overview of HDAC3 inhibitors

2.1.1. Hydroxamate based HDAC3 inhibitors

In 2017, wang et al., [142] reported thienopyrimidine hydroxamic acid-based HDAC inhibitors. It has been observed that thienopyrimidine plays a vital role in several diseases such as antidiabetic, anti-inflammatory, and antitumor. So, workers attempted to modify the cap group for such a compound using substituted 4-anilinothienol [3,2-d] pyrimidine moiety without changing the carbon linker and zinc-binding group. It was interesting to note that compounds **14** and **15** (**Figure 2.2**) show almost similar potent and selective HDAC3 inhibitory activity (IC_{50} = 19.80 nM, and IC_{50} = 21.37 nM). Compounds **14** and **15** showed good anti-proliferative activity in different cell lines such as RPMI 8226 (IC_{50} = 1580 nM,

IC_{50} = 1260 nM), HCT (IC_{50} = 2090 nM, IC_{50} =1330 nM). It was observed that compound **15** is slightly better than compound **14** based on antiproliferative activity.

Zhang et al. [143] synthesized and evaluated some bisthiazole histone deacetylase inhibitors. Compound **16** (**Figure 2.2**) was a potent HDAC3 inhibitor (IC_{50} = 3.02 nM) over other HDACs. It was noticed that the alpha substituent benzyl linker group increased the metabolic stability. Compound **17** (**Figure 2.2**) with (S)-methyl-substituted is six-fold more potent than its enantiomer compound **18** (IC_{50} value of 42.51 nM and 260 nM) (**Figure 2.2**). Compound **16** showed the most potent antiproliferative activity against T47D and NCI-N87 cells with IC_{50} values of 40.81 nM and 28.33 nM.

In 2017, Lai et al. [144] reported cyclic tetrapeptide HDAC inhibitors as a potential therapeutic target for spinal muscular atrophy (SMA) is an autosomal neuromuscular disorder. This is caused by a decreased spinal motor neuron (SMN) protein expression. In this regard, the worker screened the cyclic tetrapeptide HDAC*i* library to get a potent compound that elevates the expression of SMN protein. Compound **19** (IC_{50} = 8 nM) (**Fig. 2.2**) showed highly effective HDAC3 inhibitory activity also SMN mRNA increased 1.4-2.2 and 2-3-fold at 100 nM and 1000 nM concentration.

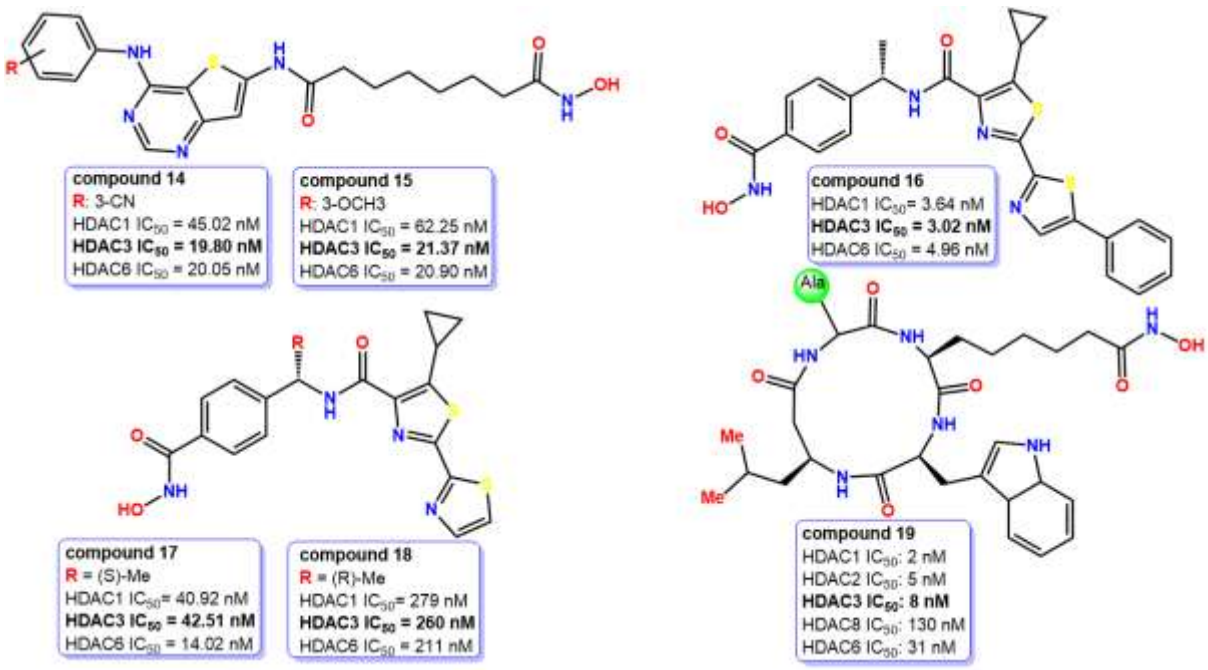

Fig. 2.2: Structure of potent hydroxamate HDAC3 inhibitors (compound **14-19**) and their HDAC isoform inhibitory activity

In 2018 Zhu et al. [145] reported a series of camptothecin prodrugs as potential HDAC inhibitors as well as cytotoxicity in several cancer cell lines. Most of these compounds showed potency and selectivity towards HDAC3 over other HDACs. Compounds **20** and **21 (Figure 2.3)** showed similar HDAC3 inhibitory activity (IC_{50} = 100 nM, IC_{50} = 100 nM). Therefore, these compounds also showed antiproliferative activity in a variety of A549 and HCT116 cell lines. It is interesting to note that compound **20** showed excellent cytotoxicity namely A549 (IC_{50} = 245 nM), HCT116 (IC_{50} = 46.22 nM) almost 2-times more cytotoxicity/antiproliferative activity than compound **21**, A549 (IC_{50} = 612.46 nM), HCT116 (IC_{50} = 88.00 nM). It is due to increasing carbon length, and increased hindrance at the C-20 position, resulting in decreased cytotoxicity.

Zhang et al. [146] reported some colchicine-based SAHA-linked hydroxamate as effective and selective HDAC inhibitors. Among these compounds, **22 (Figure 2.3)** showed the most potent HDAC activity such as HDAC3 (IC_{50} = 830 nM), HDAC1 (IC_{50} = 720 nM), and HDAC6 (IC_{50} = 440 nM). However, compound **23 (Figure 2.3)** showed G2/M peak after treatment with BEL-7402 cells with a low concentration of compound **23**. It also showed potent cytotoxicity efficacy against five cancer cell lines namely A431 (IC_{50} = 242 nM), A549 (IC_{50} = 4672 nM), HCT-116 (IC_{50} = 903 nM), MCF-7 (IC_{50} = 825 nM), PC-3 (IC_{50} = 813 nM). This suggested that colchicine moiety is suitable as a capping group for HDAC inhibitors. Also requires an appropriate linker group to the chelation with zinc ion at the bottom of the active site.

In 2013, Zhang et al. [147] also reported novel podophyllotoxin derivatives as a dual inhibitor of topo II and HDAC. It has been noticed that the aromatic capping group plays a vital role to contribute the activity. Also, meta-substitution compounds (compound **24, Fig. 2.3**) showed better activities compared to para and ortho substitution analogs. Compound **24** showed the most potent HDAC3 inhibitory activity (IC_{50} = 9.6 nM), almost 13-fold more potent than reference compound SAHA (IC_{50} = 131 nM) (compound **1**, **Figure 2.1**). Compound **24** exhibited strong anti-proliferative activity towards HCT116 colon carcinoma cells at micromolar level (IC_{50} = 3330 nM).

Luo et al. [148] synthesized some piperamides and evaluated them for inhibitory activity against histone deacetylase as well as HCT-116 human cancer cell line. Compounds **25** and **26** (**Figure 2.3**) with zinc binding group namely hydroxamic acid exhibited potent and selective HDAC3 inhibitory activity. But compound **25** (IC_{50} = 760 nM) is approx. 2-fold

more potent than compound **26** (IC_{50} = 1520 nM). It has been stated that the inhibitory activity of compound **25** is more potent than compound **26** due to the presence of a sterically restricted double bond located adjacent to the phenyl group that influences the shape of the molecule and contributes to better activity towards HDAC3 selectivity. Both of them showed moderate to good antiproliferative activity against HCT-116 (compound **25**: IC_{50} = 4400 nM; compound **26**: IC_{50} = 3500 nM).

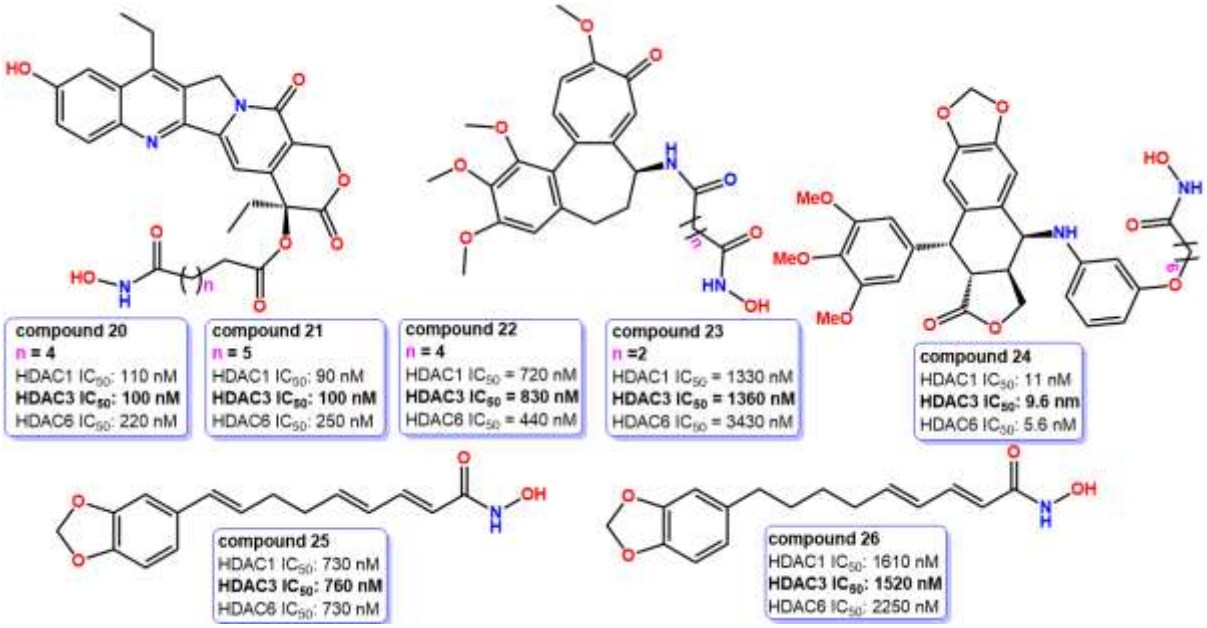

Figure 2.3: Structure of potent hydroxamate HDAC3 inhibitors (compound **20-26**) and their HDAC isoform inhibitory activity.

In 2009, Tapadar and coworkers [149] reported a series of isoxazole moieties containing hydroxamate acid exhibited potency against HDAC and inhibitory activity against five pancreatic cancer cells. Compounds **27** and **28** (**Figure 2.4**) with phenyl thiazole and amino-substituted phenyl thiazole as a capping group are required for more HDAC3 inhibitory activity. It was noticed that compounds **27** (IC_{50} = 30 nM) and **28** (IC_{50} = 25 nM) minimum 2-fold more potent HADC3 inhibitory activity than other HDAC. Both of them showed good to moderate cytotoxicity but compound **27** showed higher cytotoxicity as compared to compound **28** against variety of cell line such as BxPC-3 (IC_{50} = 3000 nM, 10500 nM), HupT3 (IC_{50} = 1000 nM, 2840 nM), Mia Paca-2 (IC_{50} = 4000 nM, 9000 nM), Panc 04.03 (IC_{50} = 4000 nM, 14400 nM) and Su.86.86 (IC_{50} = 1000 nM, 15000 nM).

Ghosh and coworkers [150] synthesized of biphenyl cap containing a hydroxamate motif with a 6-methylene linker as potent neuroepigenetic regulation. Compound **29** (IC_{50} = 2 nM) (**Fig.**

2.4) exhibited 10-fold more potent than reference compound SAHA (IC_{50} = 21 nM) (compound **1**, **Figure 2.1**) towards HDAC3 inhibition. It was found that at both 1000 nM and 10000 nM acetylation of histone H3K9 and H4K12 in mouse forebrain was greater than SAHA, resulting in cognition enhancement in normal and aged mice.

Several β carboline-based hydroxamic acids were synthesized and evaluated by Ling et al., [151]. All the compounds not only showed excellent HDAC 1/2 and 3 activities but also displayed good inhibitory proliferation of the human cancer cell line. Compound **30** (IC_{50} = 0.75 nM) (**Figure 2.4**) showed potent and selective HDAC3 inhibition as compared to other HDACs, also more potent than the reference compound SAHA (IC_{50} = 153 nM). It was also affecting cytotoxicity in several cancer cell lines namely, HCT116 (IC_{50} = 780 nM), SUMM-7721 (IC_{50} = 870 nM), HepG2 (IC_{50} = 530 nM), Mcf-7 (IC_{50} = 1560 nM), Huh (IC_{50} = 960 nM), which was approx. three to ten-fold more potent than the reference compound SAHA (IC_{50} = 4480-6250 nM). It was interesting to note that the activity of compound **30** is more potent due to the presence of the 4-methyl phenyl group at the position of C1.

Further, Ling et al. [152] reported β-carboline moiety containing a hydroxamate group connected via hydro cinnamic acid as a potential HDAC inhibitor and potent cytotoxicity activity against cancer cell lines at the micromolar level. This study reveals that β-carboline is a new lead compound used for the treatment of cancer. Compound **31** (IC_{50} = 148 nM) (**Figure 2.4**) showed good inhibitory activity towards HDAC3. Moreover, Compound **31** (IC_{50} = 1000 -2900 nM) was found to have a minimum of 3-fold more antiproliferative activity of human HCC cells as compared to SAHA (IC_{50} = 4700-5900 nM). Compound **31** showed effective cytotoxicity against different cancer cell lines namely, SMMC-7721 (IC_{50} = 2900 nM), HepG2 (IC_{50} = 1400 nM), Bel7402 (IC_{50} = 1000 nM), Huh7 (IC_{50} = 1100 nM).

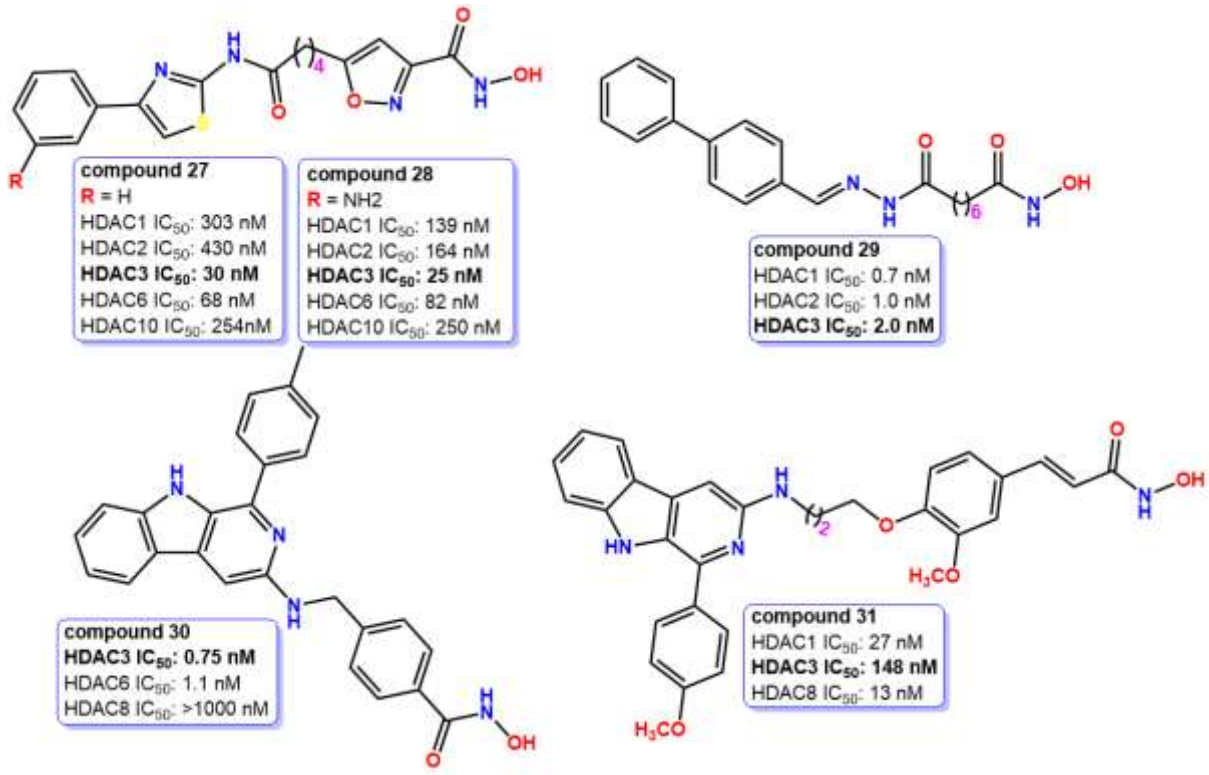

Figure 2.4: Structure of potent hydroxamate based HDAC3 inhibitors (compound **27-31**) and their HDAC isoform inhibitory activity.

Tashima and coworkers [153] designed and synthesized carbostyril-containing pan-histone deacetylase inhibitors. Compound **32 (Figure 2.5)** with hydroxamate as a zinc-binding group showed >7-fold more potent HDAC3 (IC_{50} = 15 nM) inhibitory activity than SAHA (IC_{50} = 110 nM). It is interesting to note that compound **32** with a linker cyclohexene ring with trans form makes compounds more solubility in nature and increases their activity. This cyclohexyl linker group showed the best interaction with HDAC proteins.

Tng et al. [154] reported a series of achiral AR-42 (compound **33**/AR42: IC_{50} = 12 nM) (**Figure 2.5**) analogs. It has been stated that chiral 2-aryl butyrate is not necessary for potency. Compounds **34** (IC_{50} = 2 nM) (**Figure 2.5**) and **35** (IC_{50} = 2 nM) (**Figure 2.5**) showed similar activity against HDAC3 inhibition and were six-fold more potent than compound **33**. Replacement of the chiral isopropyl group and tertiary benzylic position of compound **33** by achiral five and six-membered rings in compounds **34** and **35** results in entangle of racemization and makes it more favorable properties than chiral AR-42 and more selectivity and cytotoxicity against human cancer cell line. Compounds **34** and **35** both showed excellent cytotoxicity against different cancer cell lines such as HeLa (IC_{50} = 500 nM, 30 nM), MM96L (IC_{50} = 50 nM, 20 nM), HT-29 (IC_{50} = 100 nM, 40 nM), MDA-MB-

231 (IC_{50} = 200 nM, 100 nM), and A549 (IC_{50} = 1200 nM, 100 nM) than compound **33**/AR-42, Cytotoxicity of compound **33** showed in different cancer cell line namely HeLa (IC_{50} = 700 nM), MM96L (IC_{50} = 300 nM), HT-29 (IC_{50} = 600 nM), MDA-MB-231 (IC_{50} = 1500 nM), and A549 (IC_{50} = 1500 nM). Compound **34** were 2-7-folding more cytotoxicity than compound **33** whereas, compound **35** showed 15-23-fold cytotoxicity than compound **33**. Both compounds **34** and **35** demonstrated up to 8 times and 20 times more cyto-selectivity over neonatal foreskin fibroblasts (NFFs).

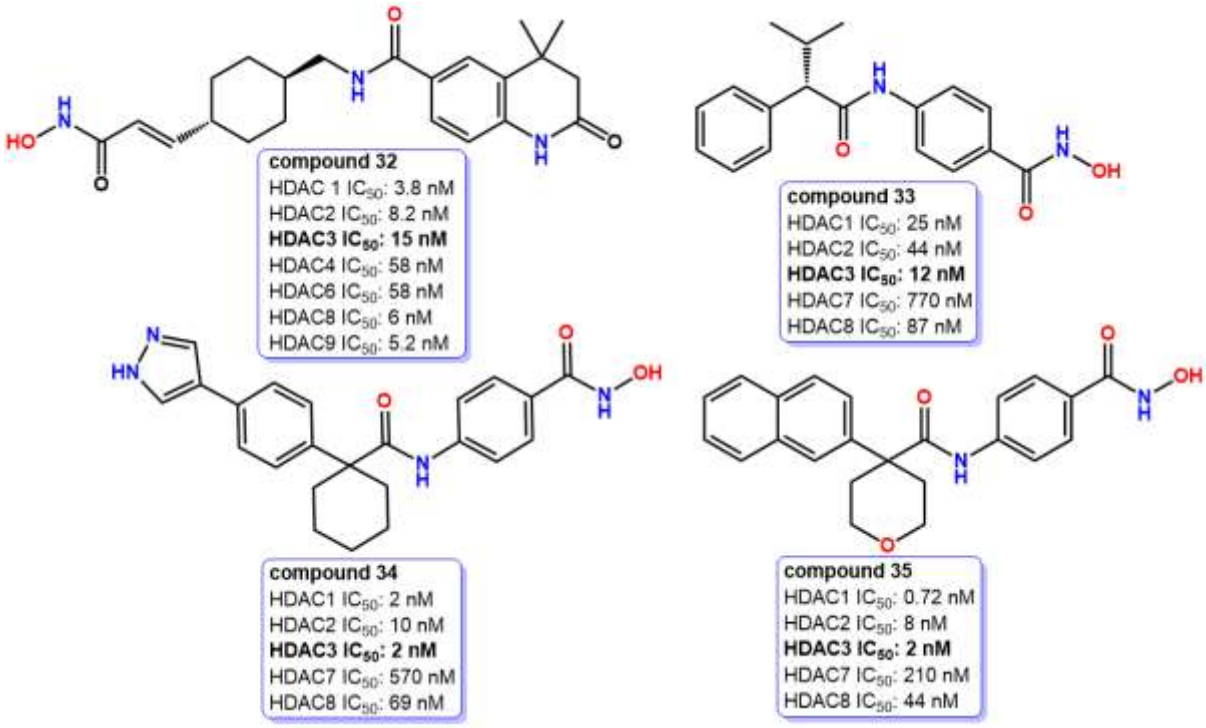

Figure 2.5: Structure of potent hydroxamate-basedHDAC3 inhibitors (compound **32** -**35**) and their HDAC isoform selectivity

Jin et al. [155] designed and synthesized indoline-2-3-dione derivative as a potent anti-proliferative activity. Compound **36** (IC_{50} = 10.13 nM) (**Figure 2.6**) showed the best efficacy to the HeLa cell nuclear extract inhibitory activities. Also, it showed good HDAC3 inhibitory (IC_{50} = 25.01 nM) activity which is 5-8-fold more potent HDAC3 inhibitory activity than other HDACs and 2-fold more potent than SAHA (IC_{50} = 52.99 nM), used as a positive control. It has been demonstrated that adding a side chain at the R1 position decreases the potency of that compound. To explore compound **36** with bromide group instead of fluorine at the R2 position of the benzamide group increases HDACs inhibitory activity. Bromine is a little bit weaker negative inductive effect than fluorine so its little bit attracts π-electrons from the benzene ring than fluorine and increases π-electron density in benzene, resulting in π-π

interaction between the active site of HDACs and ligand being a little bit stronger. Also, the six-membered heterocyclic ring and a 2-carbon side chain of the R3 position increase the potency of the HDAC inhibition because the six-membered is more stable than others and makes a stable hydrophobic interaction whereas the 2-carbon side chain better occupy to the active site of the HDAC. Compound **36** also showed good antiproliferative effects on twelve cancer cell lines (IC_{50} = 140 nM -100840 nM).

In 2014, Li and coworkers [156] developed 3-hydroxycinnamide-baseed HDAC inhibitors as an anti-tumor activity. Compound **37** (IC_{50} = 28.7 nM) (**Figure 2.6**) showed 2-fold more potent HDAC3 inhibitory activity than SAHA (IC_{50} = 56.8 nM). But compound **38** (IC_{50} = 410 nM) (**Figure 2.6**) showed the most potent antiproliferative activity using the myeloma cell U266 cell line. Further its cytotoxicity assays against more than ten cancer cell lines and showed slightly better activity than SAHA.

Shouksmith and coworkers [157] developed an HDAC inhibitor (compound **39, Figure 2.6**) for the treatment of pancreatic ductal adenocarcinoma (PDAC) because there is no proper treatment for PDAC. It has been seen that HDAC inhibitors effectively kill the pancreatic cancer cell. So, workers developed compound **39** which exhibits good inhibitory activity against HDAC3 (IC_{50} = 654 nM). Docking analysis of compound **39** with HDAC3 (PDB ID: 4A69) reveals that the perfluorinated ring of compound **39** interacts with the active site residue of the HDAC3 with minimal steric hindrance. Also, compound **39** showed good cytotoxicity against several prostate cancer cell lines. Compound **39** at 10 µM concentration showed the highest HDAC3 inhibitory activity (98%). Further, workers [158] continued their study, compound **39** was identified as the preclinical study of acute myeloid leukemia and screened low molecular weight molecules. Compound **40** (**Figure 2.6**) showed good HDAC3 (IC_{50} = 187 nM) inhibitory activity and higher cytotoxicity against MV4-11 (IC_{50} = 576 nM) cells. The lower molecular weight of compound **40** suggested exhibiting membrane permeability and improved oral bioavailability.

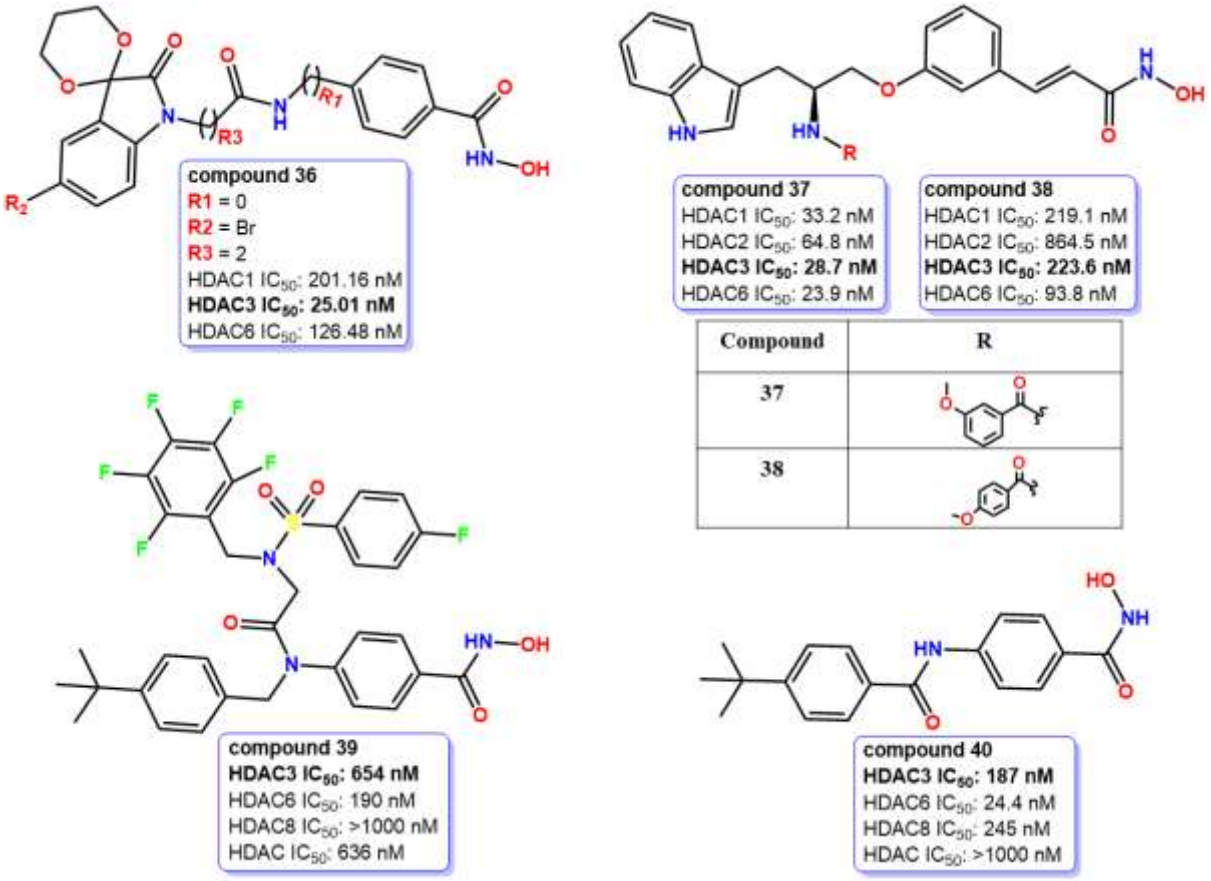

Figure 2.6: Structure of hydroxamate-based HDAC3 inhibitors (compound **36-40**) and their HDAC isoform selectivity.

Zhang and coworkers [159] designed and developed of series of novel hydroxycinamide-based HDAC inhibitors. Among them, compound **41** (IC_{50} = 280 nM) (**Figure 2.7**) showed better HDAC3 inhibitory activity over other HDACs. Compound **41** was shown cytotoxic against a variety of cancer cell lines namely U937 (IC_{50} = 1800 nM), PC-3 (IC_{50} = 3700 nM), A549 (IC_{50} = 4400 nM), ES-2 (IC_{50} = 5400 nM), MDA-MB-231 (IC_{50} = 3100 nM), HCT116 (IC_{50} = 5500 nM). Further, Li and co-workers [160] studied to design more potent N-hydroxycinnamide-based HDAC inhibitors. Although all of these compounds showed moderate to potent HDAC1 and HDAC3 selectivity over HDAC2 and HDAC6 in the nanomolar range. The most potent HDAC3 inhibitor from this HDAC inhibitor is compound **42** (IC_{50} = 3.2 nM) (**Figure 2.7**). Although compound **43** (**Figure 2.7**) showed better cytotoxicity against different cancer cell lines. HDAC inhibitors are very much sensitive to the U937 monocyte lymphoma cancer cell line and compound **43** (IC_{50} = 160 nM) was 9-fold more potent than SAHA (IC_{50} = 1450 nM).

Yang et al. [161] designed and synthesized a series of 4-anilinothienol [2,3-d] pyrimidine-based hydroxamic acid derivatives. It was found that most of the compounds showed good to excellent HDAC1, 3, and 6 inhibitory activities. Among these, compounds **44** (IC_{50} = 2.92 nM) (**Figure 2.7**) showed the most potent HDAC3 inhibitory activity but compounds **45** (IC_{50} = 2390 nM, 1610 nM) (**Figure 2.7**) and **46** (IC_{50} = 1410 nM, 2550 nM) (**Figure 2.7**) showed better cytotoxicity activities against RPMI 8226 and HCT-116 cell lines, similar to SAHA (IC_{50} = 2390 nM, 3450 nM). Also, compounds **45** (IC_{50} = 3.56 nM) and **46** (IC_{50} = 3.52 nM) showed good HDAC3 inhibitory activity. DACs surface. The best chain length of six (n = 4) was taken as the best inhibition with minimum IC_{50} values.

Abdelkarim et al. [162] designed and synthesized amine-based HDAC inhibitors. This study revealed the presence of secondary amines in a compound exhibiting higher potency against HDAC. The 1H-indol-2-ylmethyl (compound **47, Figure 2.7**) exhibited higher potency against HDAC3 inhibitors (IC_{50} = 25 nM). Then cytotoxicity of the compound **47** was determined against various cancer cells (HT-29, SH-SY5Y, and MCF-7). In the case of HT-29, and SH-SY5Y cells inhibition at 48 hr for 10 μM of compound **47** was 2100 nM and 1300 nM. In the case of the MCF-7 cell percentage of inhibition of compound **47** at 48 hr for 10 uM was 71% which was slightly better than SAHA. Compound **47** is also metabolically stable and plasma brain concentration displays well. Overall compound **47** exhibits excellent drug-like properties and therapeutic efficacy.

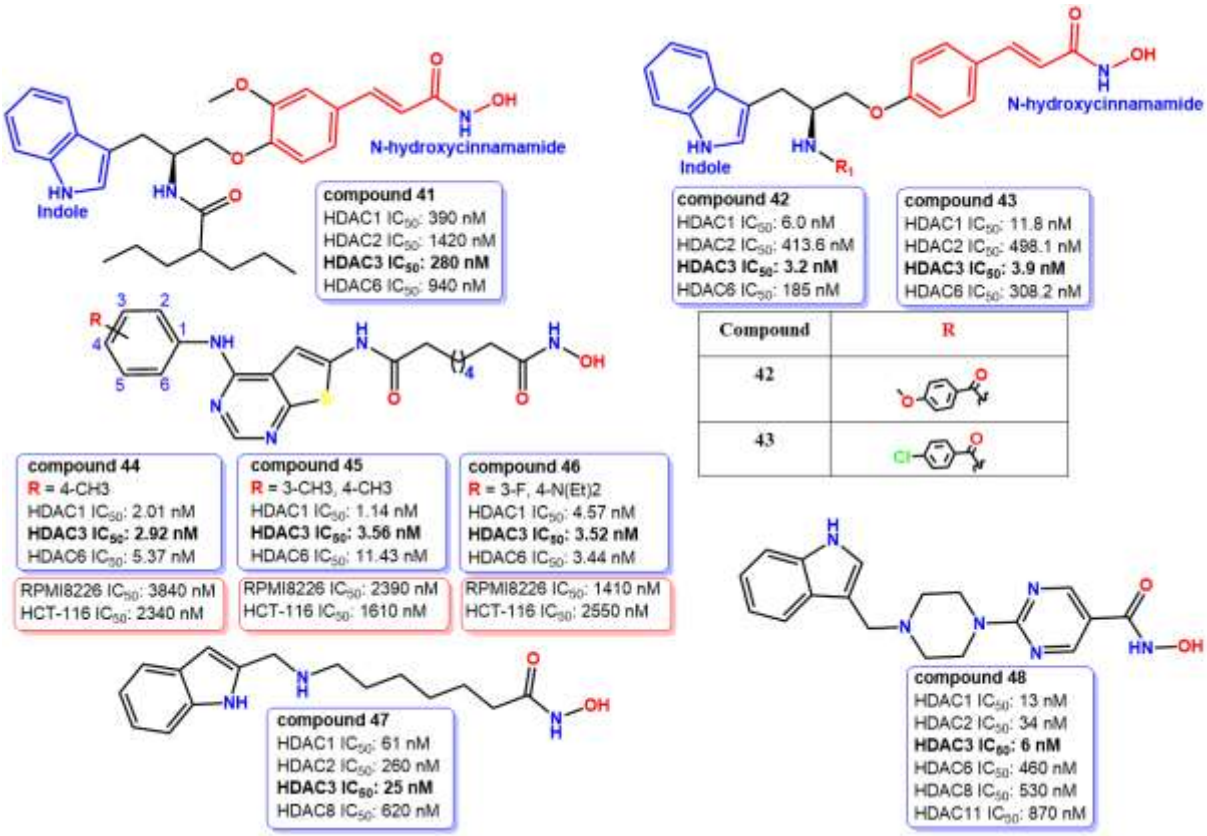

Figure 2.7: Structure of hydroxamate-based HDAC3 inhibitors (compound **41-48**) and their HDAC isoform selectivity.

Fischer et al. [163] reported some hydroxamic acid derivatives of KH series HDAC inhibitors. Among these KH groups, KH-16 (yanostat) showed high potency towards HDAC3 (IC_{50} = 6 nM) inhibition and it is superior to the SAHA. Here, KH-16 denoted as compound **48 (Figure 2.7)**, is used to assess the apoptosis in HEL erythroleukemia cells. It was observed that apoptosis triggered at 30 nM and with an IC_{50} value of 110 nM which was approx. 11-fold more potent than the reference compound SAHA (IC_{50} = 1214 nM). Then rationalize the high potency compound **48** was used to dock in HDAC3 crystal structure. The capping group (Indole) of compound **48** makes a hydrogen bond between the indole NH group with Asp92 to stabilize the orientation of the capping group. Also, carbonyl and the hydroxyl group of compounds **48** make hydrogen bonds with the residue of Tyr298, His172, and His135 (**Figure 2.8**). These unique interactions with HDAC3 make the compound **48** higher potency.

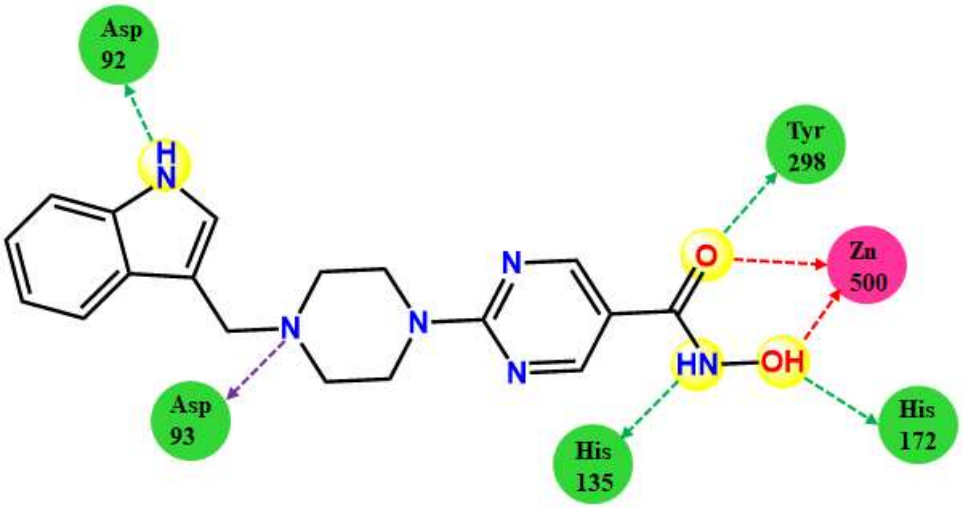

Figure 2.8: Schematic representation of interactions with compound **48** in HDAC3 active site residue.

2.1.2. Benzamide based HDAC3 inhibitors

An attempt was made by Mahboobi and co-workers [164] to design and develop a potent anti-cancer drug by a combination of EGFR/HER2 kinase and HDAC inhibitory activity. It was noticed that compound **49** (**Figure 2.9**) showed both good inhibition and cytotoxicity activity. It was observed that a change in the substitution (in para position) pattern drastically decreases the HDAC inhibitory activity (IC_{50} = >32000 nM) (**Figure 2.9**). Compound **49** showed good cytotoxicity but it is more selective and has good HDAC (IC_{50} = 47 nM) and rHDAC3 (IC_{50} = 66 nM) inhibitory activity due to substitution in the meta position. Lastly, cytotoxic activity was determined in EGFR (compound **49**: IC_{50} = 18 nM) or HER2 (compound **49**: IC_{50} = 11 nM) overexpressing cancer cell line.

Wong et al. [165] used non-hydroxamate-based 2-aminoanilides compounds for selective HDAC inhibitory activity. Then selectivity was assessed by the p21 and klf2 gene assay in Hela and A204 cells. It has been noticed that 2-aminoanilides play an essential role in interacting with the HDAC3 active site. Compound **50** (IC_{50} = 360 nM) (**Figure 2.9**) has almost 3-fold greater potency towards HDAC3 than reference compounds such as SNDX-275 (IC_{50} = 1000 nM) (compound **10**, **Figure 2.1**) and p21/klf2 selectivity. So, it has been suggested that 2-aminoanilides may be part of the selectivity towards the HDAC3 selectivity that acts as a potent anticancer activity.

Hu and coworkers [166] attempted to design some novel benzamide-peptide histone deacetylase inhibitors by solid phase peptide synthesis (SPSS). It has been noticed that all the

compounds have moderate to good HDAC3 inhibitory activity. An interesting trend was found that the activity of these series of compounds drastically changes by some modifications.

N1, N7-bis (2-aminophenyl) heptane diamide > cyclo tetrapeptide > linear tetrapeptide

The most potent HDAC3 inhibitor of this series is compound **51** (IC_{50} = 1300 nM) (**Figure 2.9**) due to the presence of N1, N7-bis (2-aminophenyl) heptane diamide. Surprisingly, compound **52** (**Figure 2.11**) showed the best HDAC3 selectivity over other HDACs.

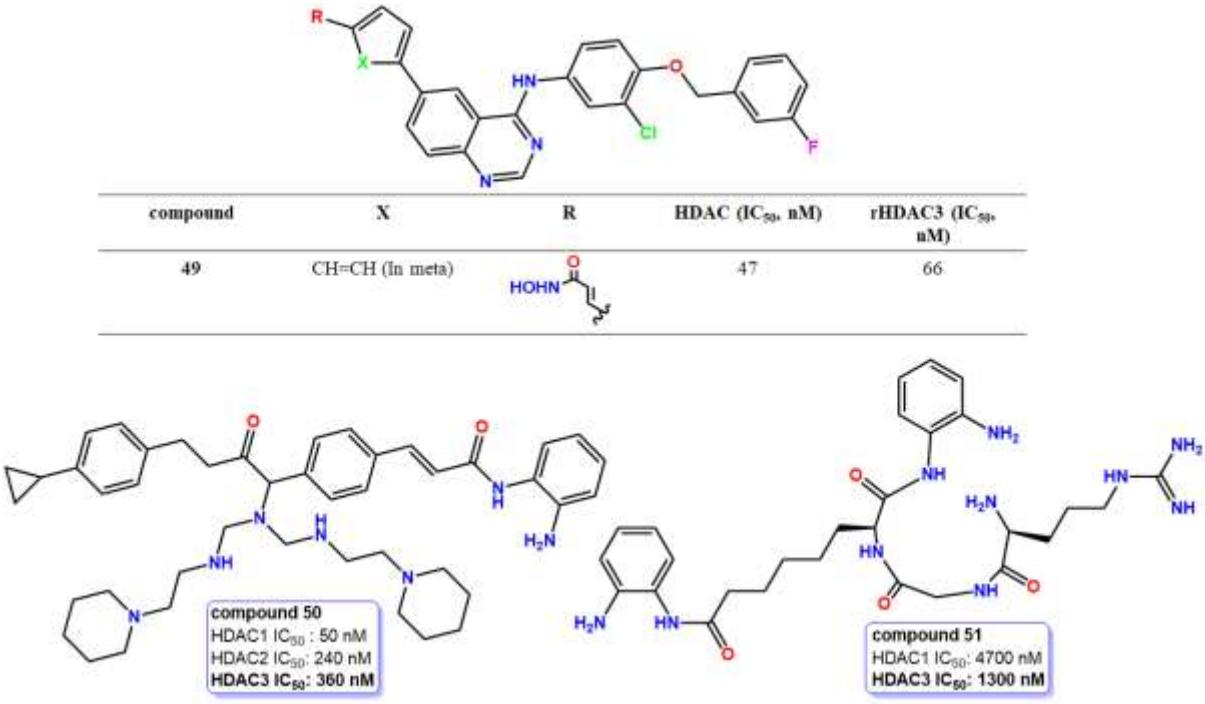

compound	X	R	HDAC (IC_{50}, nM)	rHDAC3 (IC_{50}, nM)
49	CH=CH (In meta)	HOHN	47	66

Figure 2.9: Structure of benzamide-based HDAC3 inhibitory activity (compound **49-51**) and their HDAC isoform selectivity.

Zhang et al. [167] developed some pazopanib-based HDAC inhibitors. All the compounds showed moderate to potent HDAC3 inhibitory activity. But compound **53 (Figure 2.11)** showed greater HDAC3 inhibitory (IC_{50} = 430 nM) activity as well as potent antiproliferative activities. It had been noticed that ortho-amino anilide analog with para-substituted pazopanib (compound **53**) is important for its greater activity. It was worth noting that compound **53** (IC_{50} = 1070 nM) exhibited more antiproliferative activity than SAHA (IC_{50} = 1510 nM) against HT-29.

In 2021, Routholla and co-workers [168] designed and synthesized some benzamide-based selective HDAC3 inhibitors. Compound **54** (IC_{50} = 1586 nM) (**Figure 2.11**) showed 16-30-

fold more potent HDAC3 inhibitors as compared to other HDACs. Interestingly, it was observed that the quinoline group at the cap position was beneficial for selective HDAC3 inhibitors. But, compound **54** did not show the highest cytotoxicity against different cancer cell lines such as 4T1 (IC_{50} = 10290 nM), B16F10 (IC_{50} = 18550 nM), MDA-MB-231 (IC_{50} = 13870 nM), HEK-293 (IC_{50} = 449700 nM). Then, molecular docking was performed on the selected compound. It was observed that both hydroxyl function and carbonyl oxygen adjacent amide are involved in coordination with zinc ions. Also, this carbonyl group makes a hydrogen bond interaction with Tyr298. The amide group of compounds **54** formed a hydrogen bond with the Gly143 residue of the active site HDAC3 enzyme. Additionally, the benzene ring of the compound is involved in π-π stacking interaction with His135 residue (**Figure 2.10**). Molecular docking revealed a good fit with a docking score that correlated with in-vitro HDAC3 inhibitory assay. Altogether results obtained from different assays pointed out that compound **54** might be useful for promising anticancer therapeutics.

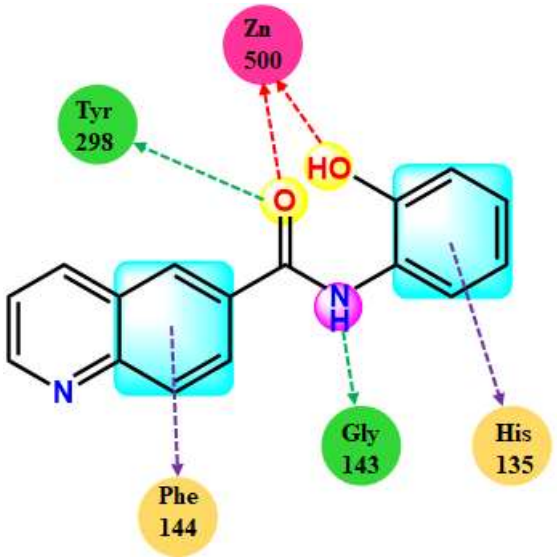

Figure 2.10: Schematic representation of compound **54** interactions with HDAC3 active site residue.

Wang et al. [169] designed and synthesized three series of novel polysubstituted N-alkyl acridone derivative HDAC inhibitors. Among them, compound **55** (**Figure 2.11**) showed good HDAC3 (IC_{50} = 225 nM) inhibitors. Also, it showed potent anti-proliferative activity against leukemia cells such as HCT-116 (IC_{50} = 4210 nM), and HL-60 (IC_{50} = 1240 nM) cells.

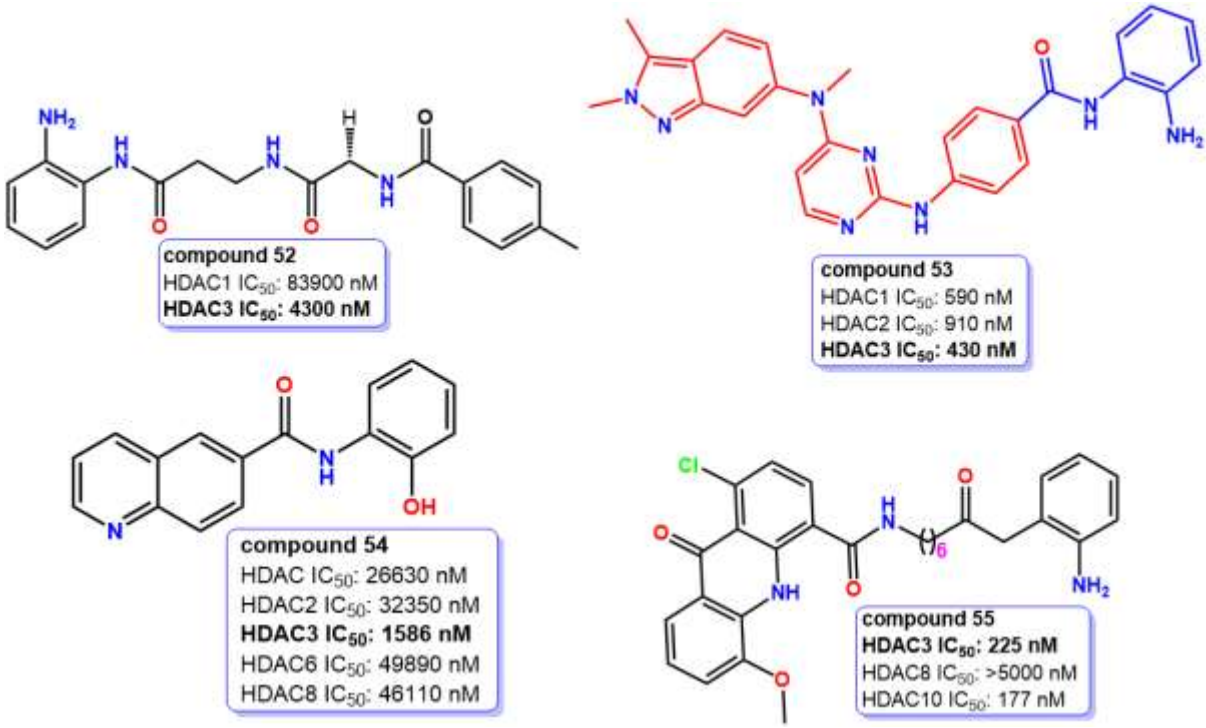

Figure 2.11: Structure of benzamide-based HDAC3 inhibitory activity (compound **52-55**) and their isoform selectivity.

Trivedi et al. [170] designed and synthesized a new compound (compound **56, Figure 2.12**) possessing 2-amino benzamide moiety as a zinc-binding group by a combination of BG45 and CI-994 (both are prototype isoform selectivity) that may lead to selective HDAC3 selectivity. Compound **56** showed good HDAC3 inhibition (% of inhibition in HDAC3 assay at 1 μM: 43.54) due to the presence of pyrazine ring in the system involving in π-π interaction or charge transfer mechanism that was seen by analyzing HOMO and LUMO orbital maps. Further, changes in the pyrazine ring and para position of benzamide moiety by substituting other groups. Compound **57** (**Figure 2.12**) demonstrated excellent HDAC3 (IC_{50} = 245 nM) inhibition and 11.68-fold selectivity in HDAC3 inhibition over pan HDAC compared to CI-994 (5.85-fold), BG45 (9.9-fold). Compound **57** was found to be a more potent antiproliferative activity against different cancer cell lines such as B16F10 (IC_{50} = 5330 nM), and HeLa cells (IC_{50} = 3980 nM).

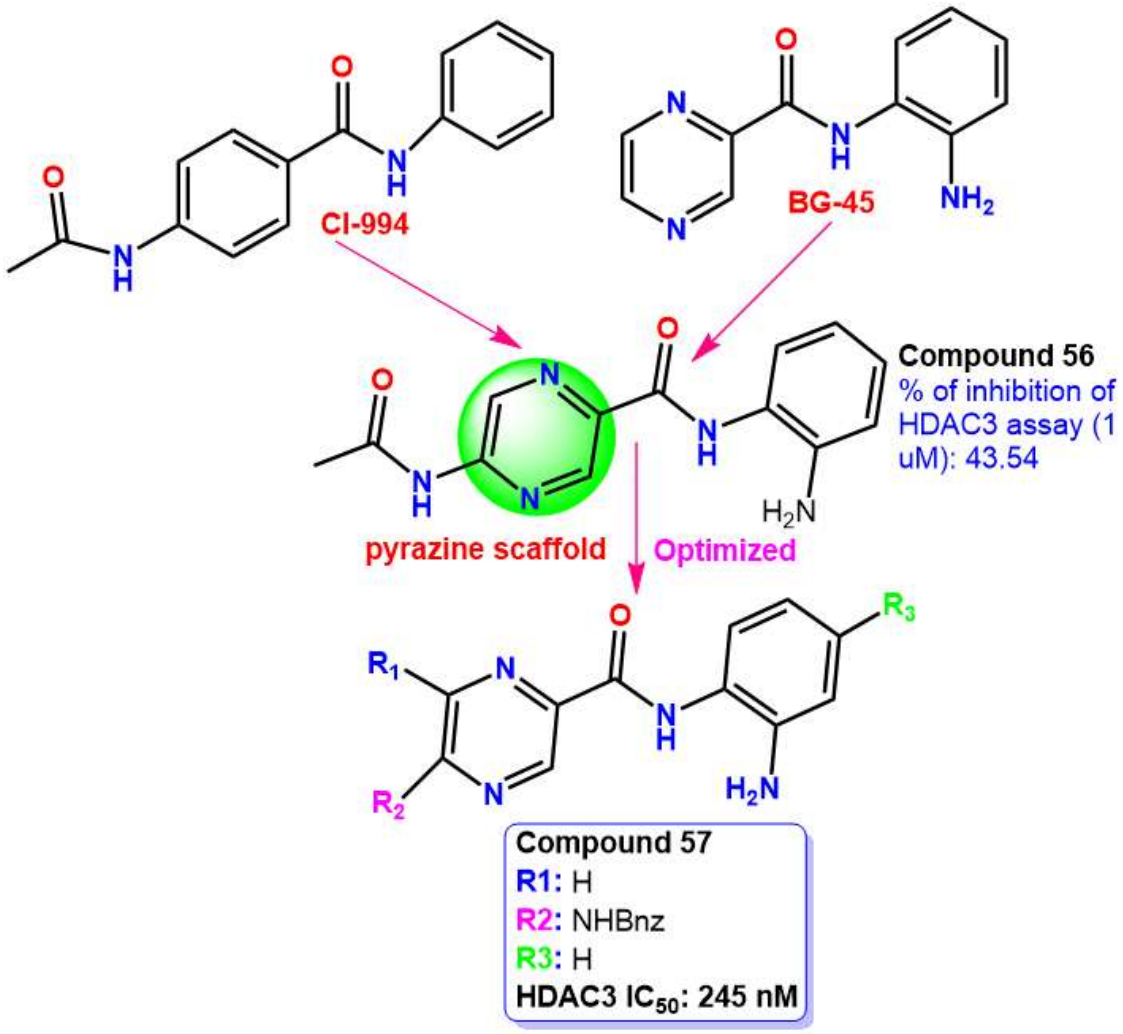

Figure 2.12: Design of compound **56** using CI-994 and BG-45 and optimize it to convert **57.**

Suzuki et al. [171] screened 504 molecule members of triazole library against HDAC3. It was observed that o-aminoanilides containing molecules such as T247 (compound **58, Figure 2.14**) and T326 (compound **59, Figure 14**) showed the most potent HDAC3 over other HDAC. Compound **58** (IC_{50} = 240 nM) and compound **59** (IC_{50} = 260 nM) displayed greater activity than vorinostat (IC_{50} = 270 nM). The vorinostat total inhibited HDACs, HDAC1, HDAC3, HDAC6, and HDAC8 whereas compound **58** and compound **59** only inhibited HDAC3. So, these both compounds can be used as potent and selective HDAC3 inhibitors. Further, cytotoxicity was checked in different cancer cell lines for both compounds **58** and **59** in HCT116 (IC_{50} = 1900 nM, 1400 nM) and prostate cancer 3 (IC_{50} = 940 nM, 1000 nM) cell line. Then, molecular docking was performed for the best active compound **58** on the crystal structure of HDAC3 (PDB ID: **4A69, Figure 2.13**). Molecular docking of compound **58** revealed that the o-aminoanilides group bidentate coordinated with zinc ions through amino and carbonyl groups. Also, the NH_2 group of the o-aminoanilide group formed a hydrogen

bond with His134 and Gly143, and the phenyl triazole part of this compound best fitted in the active site of the HDAC3 via hydrophobic interaction with several residues such as Phe144, Phe200, Leu266. The thiophene ring of the compound makes hydrophobic interaction with Pro23 and Phe144 residue. This interaction suggests the significance of the whole group for its higher potency.

Peng et al. [172] designed and synthesized by combining pharmacophore SMART (tubulin inhibitors) and MS-275 (HDAC inhibitor). Among them, compound **60 (Figure 2.14)** showed good HDAC3 inhibitors. Compound **60** showed 301-1423-fold more potent HDAC3 (IC_{50} = 30 nM) inhibitory activity than other HDACs and also selectivity (HDAC3 = >1000) over other HDACs. This compound also showed very good cytotoxicity activity than others in different cancer cell lines such as HCT-116 (IC_{50} = 50 nM), B16-F10 (IC_{50} = 70 nM), Jurkat (IC_{50} = 30 nM), A549 (IC_{50} = 140 nM). Not only potent cytotoxicity against different cancer cell lines but also potent against different HDAC-resistant cells such as YCC11 (IC_{50} = 300 nM), and YCC3/7 (IC50 = 560 nM). Then molecular docking study was performed in compound **60** to investigate binding interaction with HDAC3 (PDB ID: **4A69, Figure 2.13**). It was seen that compound **60** bidentate chelate with Zn^{+2} ion forms a hydrogen bond with Leu29. The CAP group, 3,4,5-trimethoxyphenyl group forms hydrogen bonds with the Phe199 residue, and aliphatic chains occupy the hydrophobic group. Also, it has been observed that the benzamide group forms a π-π stacking interaction with Tyr107 of the active site of HDAC3. This mode of interaction explains the higher potency of compound **60**.

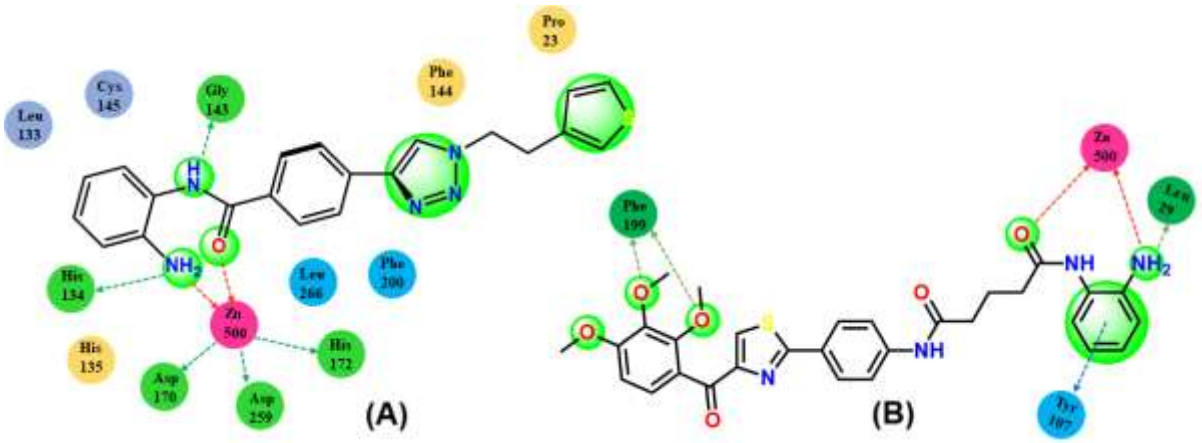

Figure 2.13: Schematic diagram of docking performance of compounds **58 (A)** and **60 (B)** in HDAC3 enzyme.

Ding et al. [173] synthesized a series of N-acyl-o-phenylenediamine with phenyl sulfonyl furoxan-based HDAC inhibitors that are responsible for nitric oxide release. Phenylsulfonyl

furoxan was mainly responsible for releasing nitric oxide. There are large of evidence suggests that high concentrations of nitric oxide (NO) exhibit antitumor effects [174,175]. The all-synthesized compound showed moderate to potent activity against HeLa cell nuclear extract. Then selectivity was checked for all compounds and showed almost similar selectivity towards HDAC3 comparable to MS275 (compound **3**, **Figure 2.1**) with no significant differences. Among these, compound **61** (IC_{50} = 620 nM) (**Figure 2.14**) showed 2-4-fold better cytotoxicity than MS275 in different cancer cell lines such as in HEL (IC_{50} = 320 nM), HeLa (IC_{50} = 1230 nM), PC-3 (IC_{50} = 2690 nM), HCT116 (IC_{50} = 930 nM), A549 (IC_{50} = 1030 nM). Compound **61** showed potent antitumor activity (tumor growth inhibition: 36%, relative increment ratio: 57%) but not better than MS275 (**3**) (tumor growth inhibition: 31%, relative increment ratio: 64%) when given in the same dose as the mice. It was observed that no significant weight loss when given to the mice suggesting acceptable toxicity.

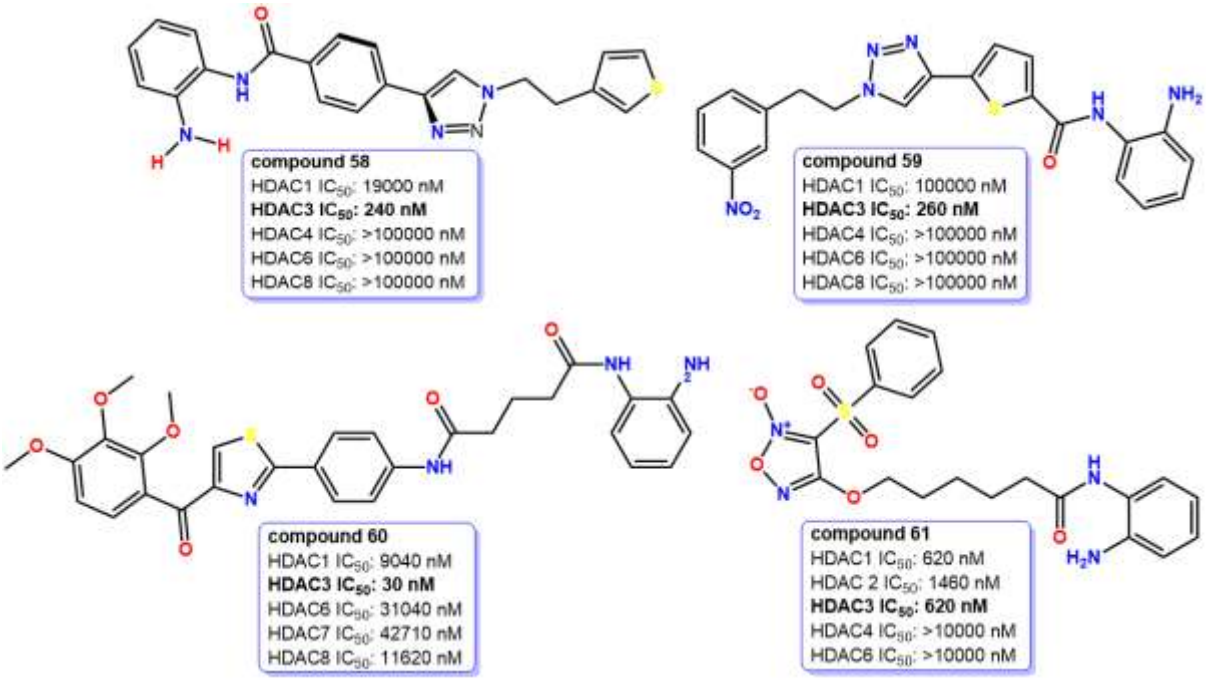

Figure 2.14: Structure of benzamide-based HDAC3 inhibitory activity (compound **58-61**) and their isoform selectivity.

Marson et al. [176] reported some potent chiral histone deacetylase inhibitors containing an oxazolone capping group and N-(2-aminophenyl)-benzamide group. Among those compounds **62** (IC_{50} = 6 nM) (**Figure 2.15**) showed potent HDAC3-CoR2 inhibitory activity and 13-18-fold more potent and selectivity over HDAC1 and HDAC2. The presence of a phenyl ring increases the 5-fold selectivity/potent of HDAC3-CoR2. Compound **63** (**Figure**

2.15) and compound **64** (**Figure 2.15**) having (*R*) and (*S*)-configurations also showed very potent and selective HDAC3 inhibition (IC_{50} = 11 nM, IC_{50} = 35 nM, respectively). Aryl substitution at the oxazoline moieties 4th and 5th position is preferred for inhibiting HDAC3. Compound **65 (Figure 2.15)** containing m-fluorophenyl substitution at the 4th position showed potent HDAC3 inhibition (IC_{50} = 24 nM) with more than 10-fold HDAC3 selectivity over other HDACs.

Ocasio et al. [177] reported a ferrocene-containing HDAC3 selective (pojamide/compound **66**) (**Figure 2.15**) inhibitor. It (IC_{50} = 90 nM) showed more than twelve-fold more potent than other HDACs (HDAC1 IC_{50} = 1100 nM, HDAC2 IC_{50} = 1300 nM, HDAC4, HDAC5, HDAC6, HDAC7, HDAC8 IC_{50} = >30000 nM). It also showed good activity against the HCT116 cancer cell line (GC_{50} = 8600 nM).

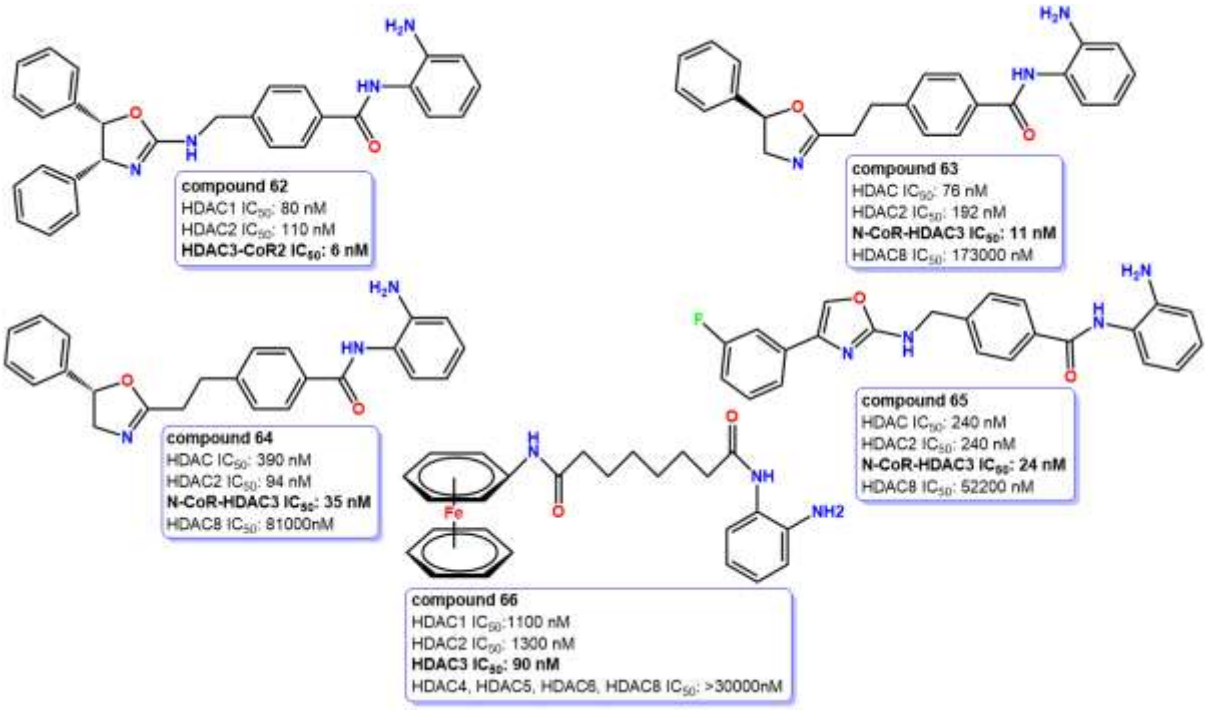

Figure 2.15: Structure of benzamide-based HDAC3 inhibitory activity (compound **62-66**) and their isoform selectivity.

2.1.3. Hydrazide based HDAC3 inhibitors

Wen et al. [178] developed a series of N-(6-mercaptohexyl)-3-substitited-1H-pyrazole-5-carboxamide HDAC inhibitors. Compound **67** (**Figure 2.17**) showed 2-11-fold more potent than the reference compound (vorinostat). Compound **67** exhibited potent and selective HDAC3 inhibitory (IC_{50} = 11 nM) activity over other HDAC. It also showed moderate to good cytotoxicity against various cancer cell lines such as HCT-116 (IC_{50} = 25260 nM), HT-

29 (IC_{50} = 10200 nM), MCF-7 (IC_{50} = 12230 nM), MDA-MB-231 (IC_{50} = >50000 nM), A549 (IC_{50} = 14430 nM), PC-3 (IC_{50} = 11030 nM), AsPC-1 (IC_{50} = 36850 nM), HEK-293 (IC_{50} = 17500 nM).

Hamoud et al. [179] designed and synthesized a series of nicotinamide HDAC3 inhibitors. Most of the compounds showed good HDAC3 inhibitory activity. Among them, compound **68** (**Figure 2.17**) showed excellent HDAC3 (IC_{50} = 694 nM) inhibitory activity and also significant *pan*-HDAC (IC_{50} = 4648 nM) inhibitory activity. In addition, antiproliferative activity was checked in three different cancer cell lines such as B16F10 (IC_{50} = 4660 nM), MCF-7 (IC_{50} = 9450 nM), and A549 (IC_{50} = 4810 nM). It displayed excellent cytotoxicity in different cancer cells. Then a molecular docking was performed of compound **68** to explore the binding affinity of compound **68** with active site residue of HDAC3 (PDB ID: 4A69). It was observed that compound **68** coordinated with zinc ion and carboxamide of the compound interacts with active site residue of HDAC3 such as His134, His135, and gly143. The N-benzoyl hydrazone (as a linker) and a p-methyl phenyl group (as a capping group) make a hydrophobic interaction with His172, and Phe199 respectively in the hydrophobic channel (**Figure 2.16**). This docking study validated the binding affinity of compound **68**.

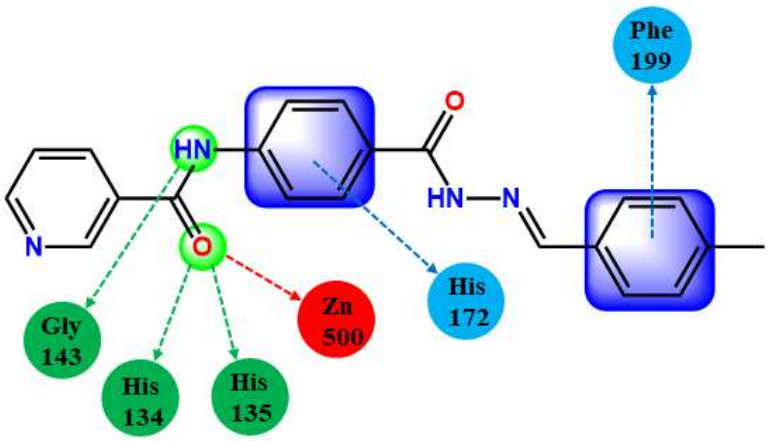

Figure 2.16: Schematic representation of interaction between compound **68** with the active site residue of HDAC3.

In 2015, Wang et al. [180] conducted a high throughput screening (HTS) of 6,22,360 compounds by a luciferase reporter in the colon cancer HCT116 cell line that is controlled by adenovirus (AD) major late promoter (Ad-MLP-Luc). It was observed that Ad-MLP-Luc activity increases with the increase of HDAC*i*. Therefore, HDAC inhibition is the primary mechanism for reporter activation. Then highly toxic compound was removed by a viability counter-screen assay. After the subsequent assay method, workers got a benzoyl hydrazide

scaffold (UF010/compound **69**) that showed excellent HDAC3 inhibitory activity in the nano-molar range. They also reported compound **69** minimum >2.40 fold more potent HDAC3 (IC_{50} = 190 nM) inhibitory activity than other HDACs (HDAC1 IC_{50}: 460 nM, HDAC2 IC_{50}: 1330 nM, HDAC6 IC_{50} = 9090 nM, HDAC8 IC_{50} = 2830 nM). The benzoylhydrazide scaffold is a selective and potent HDAC3 inhibitor. They identified a lead compound UF010/compound **69**, which inhibits cancer cell proliferation (HCT116 IC_{50} = 11200 nM) by inhibiting activity of the HDAC function but less cytotoxicity than MS-275 (IC_{50} = 2100 nM,), and vorinostat (IC_{50} = 1200 nM).

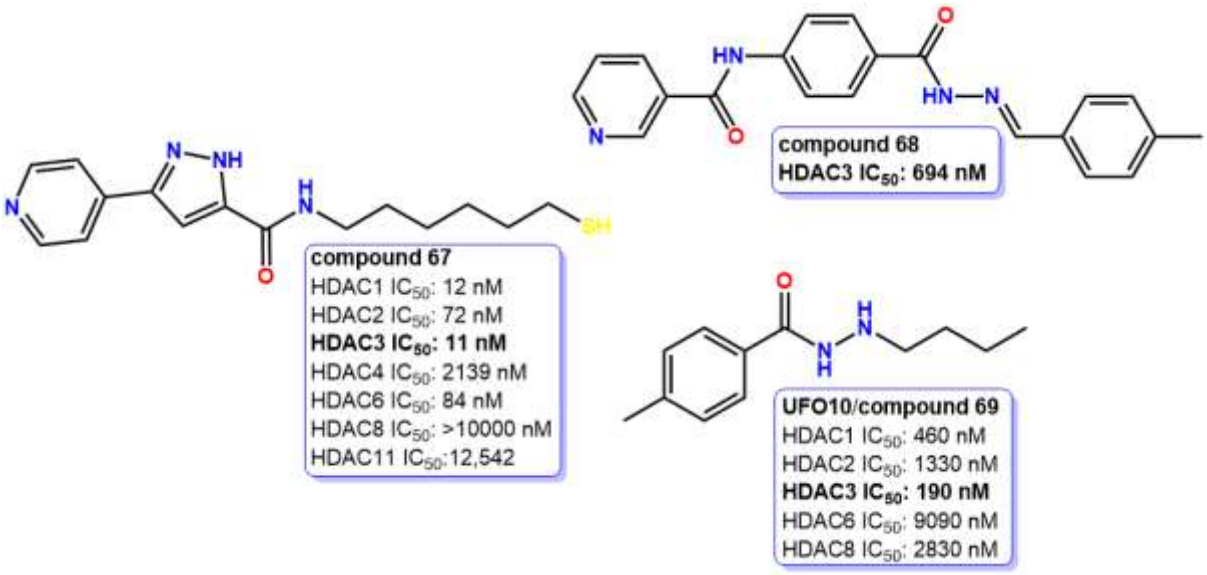

Figure 2.17: Structure of hydrazide-based HDAC3 inhibitory activity (compound **67-69**) and their isoform selectivity.

Pulya and co-workers [181] synthesized hydrazide-based HDAC3 inhibitors. Among these compounds, compounds **70** (IC_{50} = 15 nM) (**Figure 2.18**) and **71** (IC_{50} = 30.67 nM) (**Figure 2.18**) showed minimum 18-fold selectivity over other HDAC and 16.65 and 8.36 times more potent than reference compound UF010 (IC_{50} = 256 nM). It was noticed that the n-propyl group attached to the hydrazide scaffold displayed more HDAC3 inhibitory activity. Compound **70** showed more potent HDAC3 inhibitory activity and comparatively better cytotoxicity against B16F10, A549, MCF-7, and HEK-293 with IC_{50} values of 7210 nM, 19870 nM, 12840 nM, and 1920 nM. Further, **70** tested against normal human cancer cell line (HEK-293), human corneal epithelial (HCEC), and Raw 264.7. Interestingly, it showed less cytotoxicity toward normal cancer cell lines. Then docking study was performed for the selected compound. The amide group connected to the carbonyl group makes a chelate with zinc ion through a salt bridge formation and the other amide group of the hydrazide

connected with Tyr298 residue through hydrogen bonding formation. Moreover, the diphenylamine moiety of compound **70** and carboxamide benzyl moiety of compound **71** formed hydrogen bonds with Asp93 residue. Additionally, the benzyl group of the carboxamide group of compounds **71** formed π-π stacking interaction with Phe200 whereas, the benzene ring in diphenylamine of compound **70** does not participate in π-π stacking interaction with Phe200 and His172 (**Figure 2.18**) but compound **71** less active compared to the compound **70**. Thus, it may concluded that bulky, flexible elongated are not suitable for the activity and may unfavorable steric hindrance to the active site.

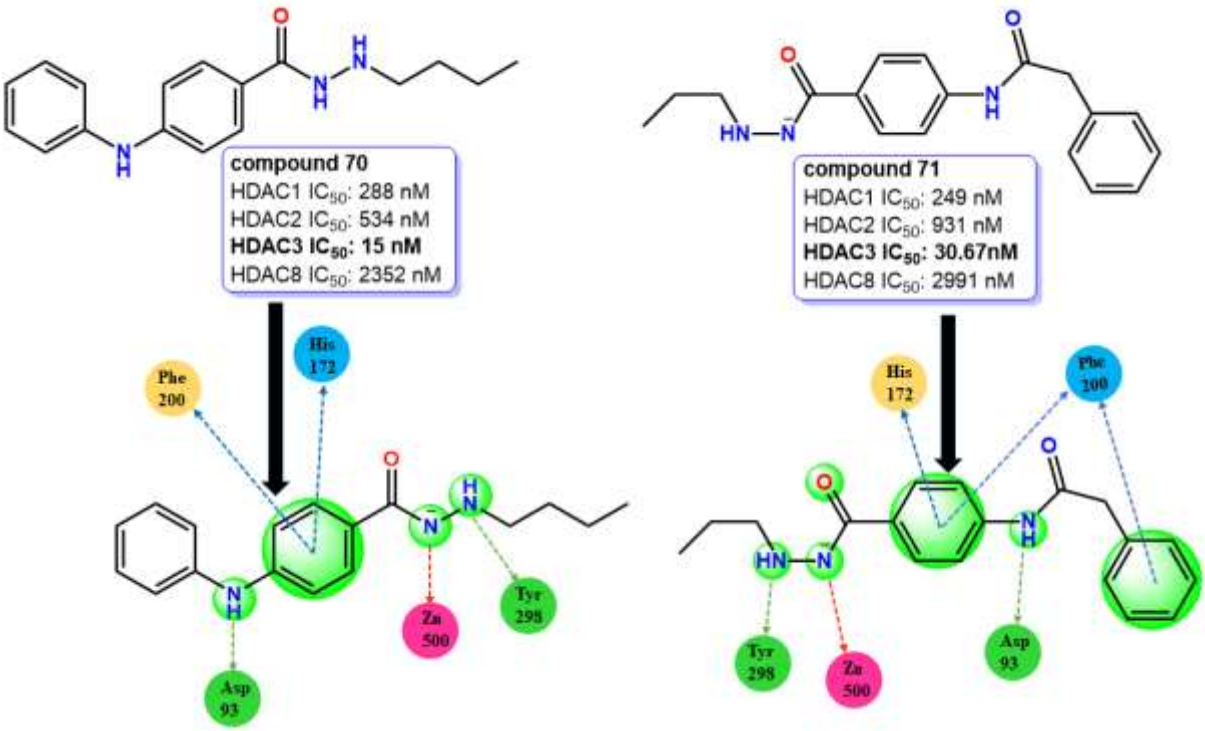

Figure 2.18: Structure of hydrazide-based HDAC3 inhibitory compounds **70** and **71** with potent HDAC inhibitory activity and their interaction in the active site of the HDAC3 enzyme (PDB ID: 4A69).

Jiang et al. reported [182] hydrazide-based HDAC inhibitors by modification (cyclization) of cinnamide, which was previously reported [183,184] hydrazide-based compounds (compounds **72**, and **73**) (**Figure 2.19**) using Michael reaction. It was found that compound **72**, a cinnamide derivative with an n-propylhydrazide moiety, had the strongest HDAC3 inhibition (IC_{50} = 0.95 nM), as well as selectivity over HDAC1 and 2. However, the cinnamide derivative with n-butylhydrazide moiety (compound **74**) exhibits a 4-fold lower HDAC3 inhibitory activity (IC_{50} = 3.67 nM). When cinnamide moiety was replaced with a phenyl group, the HDAC3 inhibitory activity was once again reduced in comparison to

compound **72**, but these molecules (compounds **75** and **76**) were still very potent and selective HDAC3 inhibitors. This cinnamide was modified because it acts as a "Michael receptor" that reacts with the thiol group of the cysteine in the active site of the protein and shows promiscuous cellular response (cells respond to multiple different signaling molecules or stimuli). The reported compound **77** (IC_{50} = 0.44 nM) (**Figure 2.19**), was >2 times more potent HDAC3 inhibitory activity than compound **72** (IC_{50} = 0.95 nM). Compound **77** showed 112% bioavailability which is five times more potent than compound **72**. Compound **73** also showed 78.9% tumor growth inhibition (TGI), demonstrating it's an excellent and efficient treatment of acute myeloid leukemia.

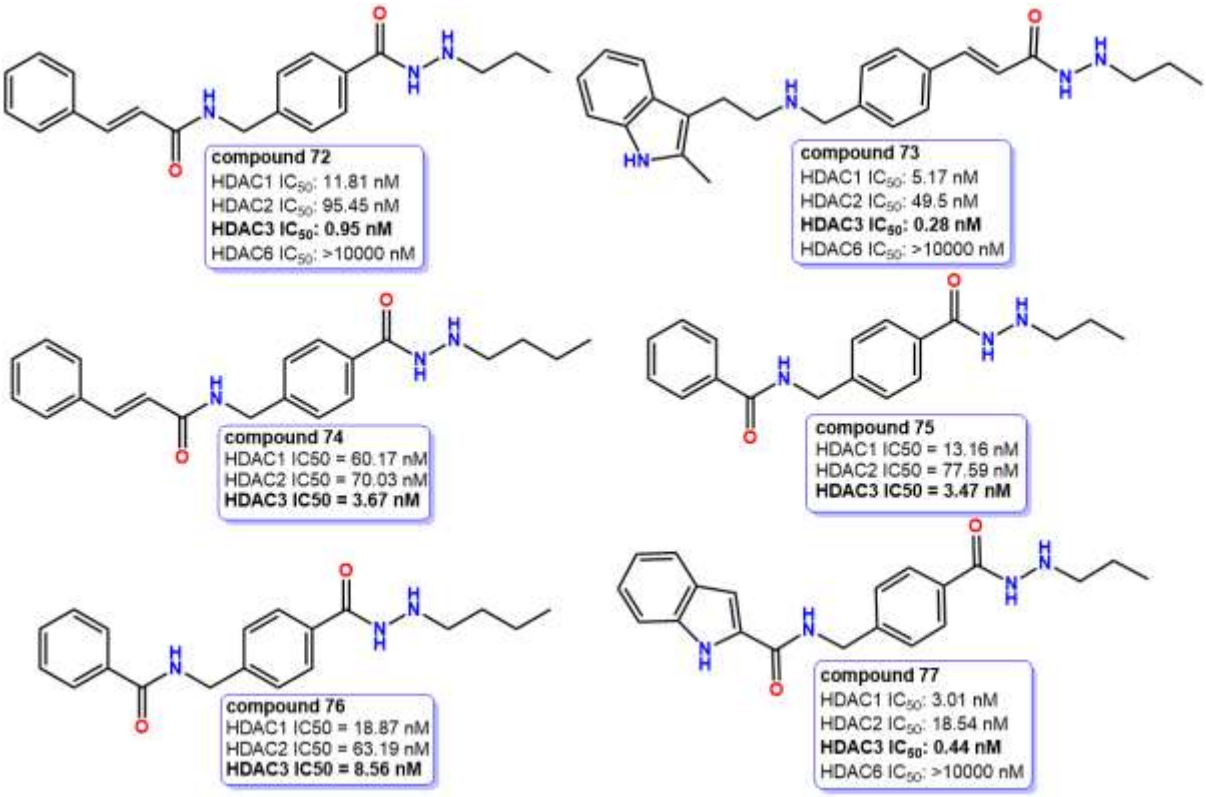

Figure 2.19: Structure of hydrazide-based HDAC3 inhibitory activity (compound **72-77**) and their isoform selectivity.

2.1.4. Thiol based HDAC3 inhibitors

Gong et al. [185] designed and synthesized a series of bis thiazole-based hydroxamic acids as novel HDAC inhibitors which showed potent HDAC3 inhibitory activity. Compound **78** (**Figure 2.20**) showed good HDAC3 inhibitory activity (IC_{50} = 25.84 nM). so, it has been demonstrated that the trifluoromethyl ketone compound showed good HDAC3 inhibitory activity. Similarly, the substitution of left thiazole with methyl or cyclohexyl increases the potency (compound **79, 80, Figure 2.20**) of the compound-like compound **78**. Furthermore,

compound **78** was identified as having potent antiproliferative activity and it showed 1.5-5-fold more antiproliferative activity than SAHA compound in different cancer cell lines such as MM.1S (IC_{50} = 390 nM), RPMI 8226 (IC_{50} = 85 nM), NCI-H929 (IC_{50} = 1230 nM), LPI (IC_{50} = 370 nM), Mino (IC_{50} = 120 nM), Jeko-1 (IC_{50} = 64 nM).

Yao et al. [186] reported some novel cyclic depsipeptide histone deacetylase inhibitors. Compound **81** showed excellent HDAC3 inhibitory activity than other HDACs. Compound **81** exhibited 3-fold HDAC1 (IC_{50} = 2.78 nM) selectivity than HDAC3 (IC_{50} = 7.67 nM) but 5-fold more selectivity than HDAC2 (IC_{50} = 45 nM). But acetyl and octanyl groups in compound **82** and **83**, instead of free thiol, makes the compound more stable and increases the membrane permeability. Results in increased antiproliferative activity. Compounds **82** (IC_{50} = 6.99 nM) and **83** (IC_{50} = 11.02 nM) exhibit excellent anticancer activity in human prostate carcinoma cells (Du145).

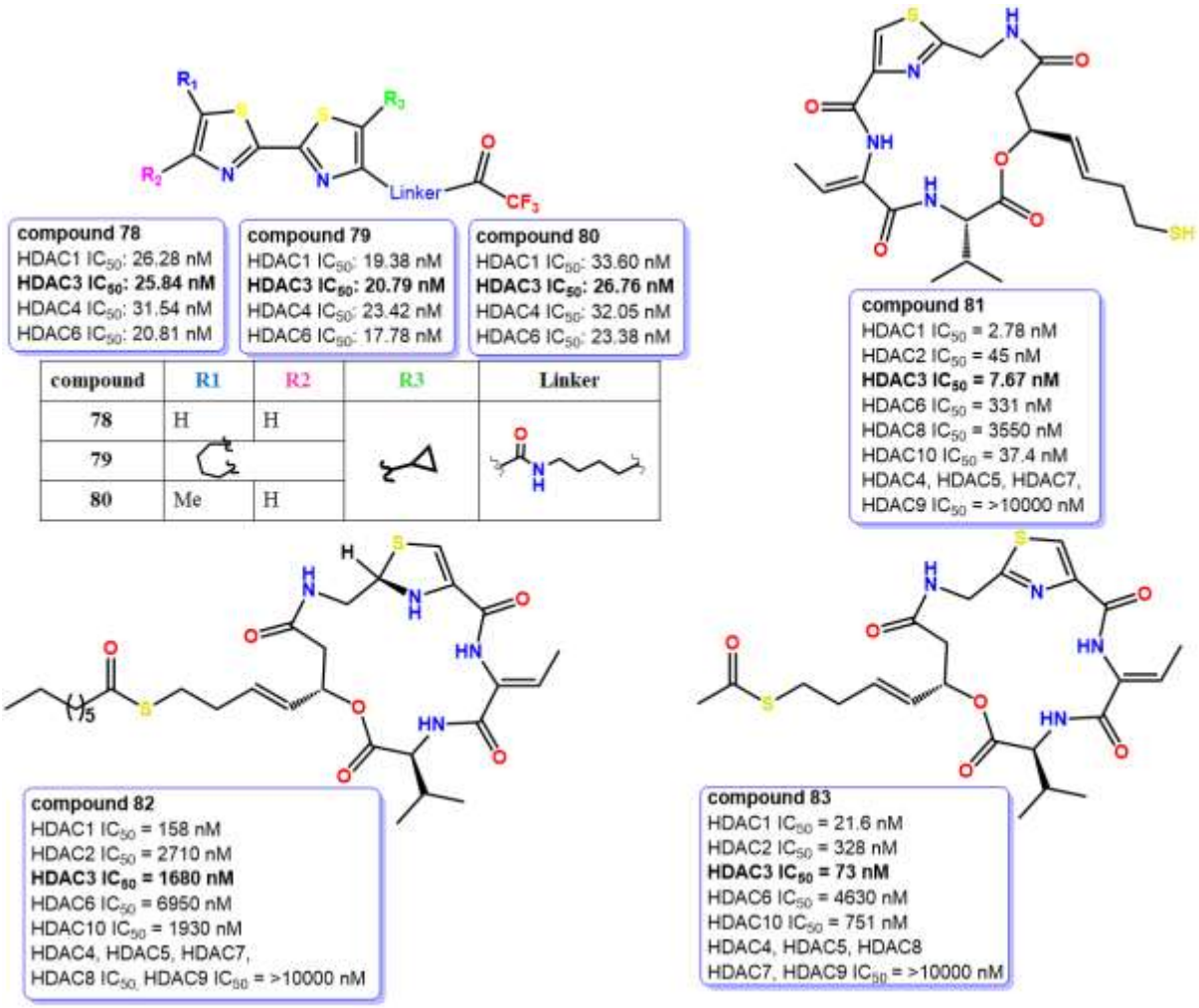

Figure 2.20: Structure of thiol-based HDAC3 inhibitory activity (compound **78-83**) and their HDAC isoform selectivity.

Li et al. [187] reported a new series of largazole analogs. Compound **84** (IC_{50} = 31 nM) (**Figure 2.21**) containing tetrazole ring exhibited more potent and selective HDAC3 inhibitory activity over other HDACs. HDAC3 maintains a minimum 3-fold selectivity over other HDACs.

Guerra-Bubb et al. [188] reported an isosteric thiazole-oxazole largazole analog containing a free thiol group (compound **85, Figure 2.21**). It exhibited potent and selective HDAC3 inhibitory activity (IC_{50} = 7.2 nM). However, it showed less activity (IC_{50} = 6200 nM) against MM1.S multiple myeloma cell line.

The largazole (compound **86**) analogs were tested against the HCT116 colorectal cancer cell line by Almaliti and co-workers [189]. All of these substances demonstrated positive cytotoxicity. The most effective cytotoxic compound was compound **87**, which also showed better potency and selectivity towards HDAC3 (IC_{50} = 27 nM) over HDAC6 but non-selectivity towards HDAC1 (IC_{50} = 21 nM) and HDAC2 (IC_{50} = 28 nM).

Xu et al. [190] reported largazole (compound **88**) and trans-cyclooctane largazole (compound **89**) thiol analogs. Both these compounds showed excellent potency towards HDAC3. Then compound **89** was tested to check the capability to enrich HDACs from cells. Unfortunately, compound **89** was unable to enrich in HDAC3.

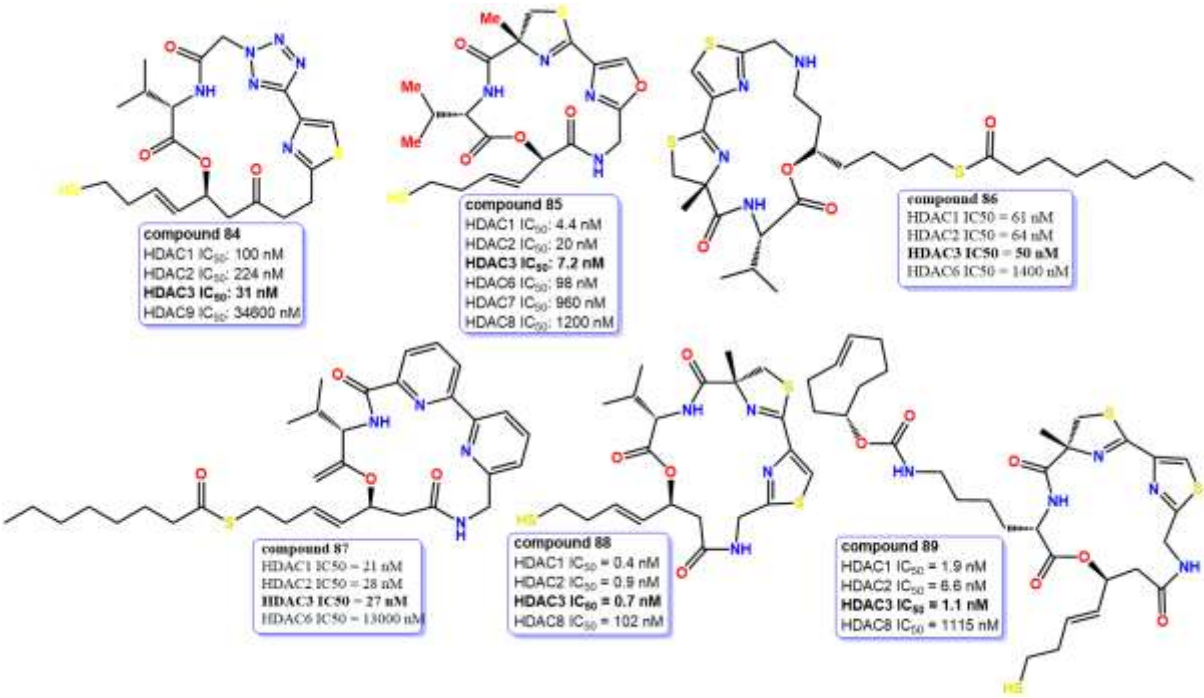

Figure 2.21: Structure of thiol-based HDAC3 inhibitory activity (compound **84-89**) and their isoform selectivity.

2.2. An Overview of QSAR modeling study performed on HDAC3 inhibitors

Drug discovery and development of new compound entities take an average of 10-15 years and require a huge cost [191,192]. The drug discovery process involves several stages such as

(a) Target identification: finding and identification of targets and their function associated with several diseases [193].

(b) Target validation: a process that compares drug targets to others based on their specific disease after binding of chemical compounds [194].

(c) Lead identification: discovery of a chemical compound that may have the potential to treat disease [195].

(d) Lead optimization: identified drug development candidate from biologically active hit and developed into safe and effective medicine [196]. Therefore, computer-aided drug design (CADD) plays an important role in the development of new drugs in a more cost-effective way and in minimizing failure in the final stage of drug discovery. In modeling approaches are categorized into ligand-based drug design (LBDD) and structure-based drug design (SBDD). LBDD consists of collecting a diverse set of molecules with diverse structures with known biologically active compounds to develop predictive models, whereas in structure-based drug design, the 3D structure of the target molecule (receptor/enzyme) is considered for the identification of potential hit/ligand compound, followed by synthesis, testing, and optimization. In previous, several HDAC3-related structural and ligand-based drug designs have been performed. In this section, year-wise work related to HDAC3 has been summarized. Amin et al. [197] reported a set of benzamide-based HDAC3 inhibitors on designing potential HDAC3 selective inhibitors for improve memory and learning on knowledge of reported QSAR models such as 3D QSAR (CoMFA and CoMSIA), as well as Bayesian classification studies to know the important physicochemical features for benzamide based HDAC3 inhibitor. In this study, authors considered 113 diverse benzamide-based HDAC3 inhibitors from different published papers for molecular modeling study. It has been observed that all the models are statistically significant. In CoMFA and CoMSIA models, Q^2 and R^2 were found to be 0.525, 0.531, and 0.870, 0.865, respectively. Then, the generated model is validated by a test set molecule. The R^2_{pred} for the CoMFA and CoMSIA showed 0.589 and 0.546 respectively. Further, 3D-QSAR observation on important structural features regulating HDAC3 inhibitory activity validated by the Bayesian classification study showed *ROC* scores for both training and test sets of 0.811 and 0.825, respectively. The

authors concluded that structural and physiochemical features might be useful for designing more selective and potent benzamide-based HDAC3 inhibitors (**Figure 2.22**).

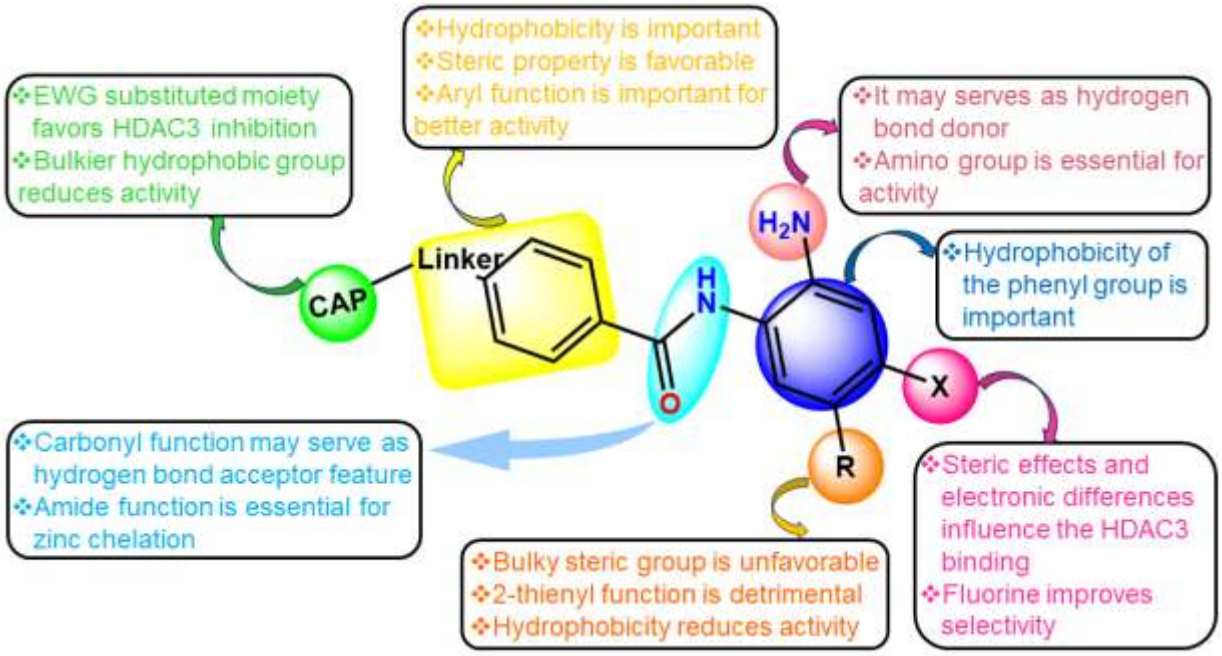

Figure 2.22: Structural features requirements for benzamide-based HDAC3 inhibitors.

Li and co-workers [198] have developed a machine learning-based HDAC3*i*-Finder to screen potent HDAC3 inhibitors. In this study, 1639 HDAC3 inhibitors were taken from the ChEMBL database. After data curation 1098 compounds were retained and three chemical features (two-dimensional Mordred descriptors, MACCS keys, and Morgan2 fingerprints) for each compound were calculated. Further, five machine learning classifiers (KNN, SVM, RF, XGBoost, and DNN) were performed on each feature set. A total of 15 models were generated. Among them, XGBoost_morgan2 was the best based on high *ROC* enrichment ($ROCE_{0.5\%}$ = 41.02. After the developed model XGBoost_morgan2 performed better than the other model used to screen the PubChem library and eight unique HDAC3 inhibitors were identified indicating a higher rate (*i.e.*, 0.27%) than the HTS (*i.e.*, 0.15%) and showing potential to discover new scaffold.

In 2022, Kumbhar and coworkers [11] published an article on HDAC3 to the finding of novel leads as potent inhibitors using pharmacophore-based virtual screening and MD simulation. The Hypo1 pharmacophore model showed an excellent correlation (R^2) of 0.99 and lowest *RMSD* of 0.37 and a significant cost value. Then, the model is validated by Fischer's randomization and test set prediction with a good correlation coefficient (R^2) of 0.970. Then, Hypo1 was used to screen the 418625 hit compounds obtained from different sources (Maybridge, Asinex, NCI, and Chembridge). Further hit compounds were tested using Lipinski's rule, ADMET property. Finally, 174 hit compounds were obtained. Docking of 174 compounds was performed to the

active site of HDAC3 (PDB ID: 4A69) using "Gold" software. HDAC3 has sequence similarity with HDAC8 [61]. The binding mode of interaction was compared with TSA because molecular interaction is similar to acetate ion. Then, the GOLD score of TSA was a cut-off for screening the compounds. The Chemscore value was found to be -37.15 and the lower value was selected as a cut-off to screen the hit compound. Finally, the selected best compounds were used for the docking study. Therefore, three hit compounds (compound **90**-**92**) interact with active site residue His and Tyr which were supported by the pharmacophore model (**Figure 2.23**) and coordinated with Zn^{2+} were selected for MD simulation studies to determine the binding mode and time-dependent behavior of hits in the active site pocket of HDAC3. The interaction profile suggested that hydrogen bond acceptor (HBA), hydrophobicity (HYP), and ring aromaticity (RA) are essential chemical features for HDAC3 inhibition, and the screened hit compounds may act as potent HDAC3 inhibition.

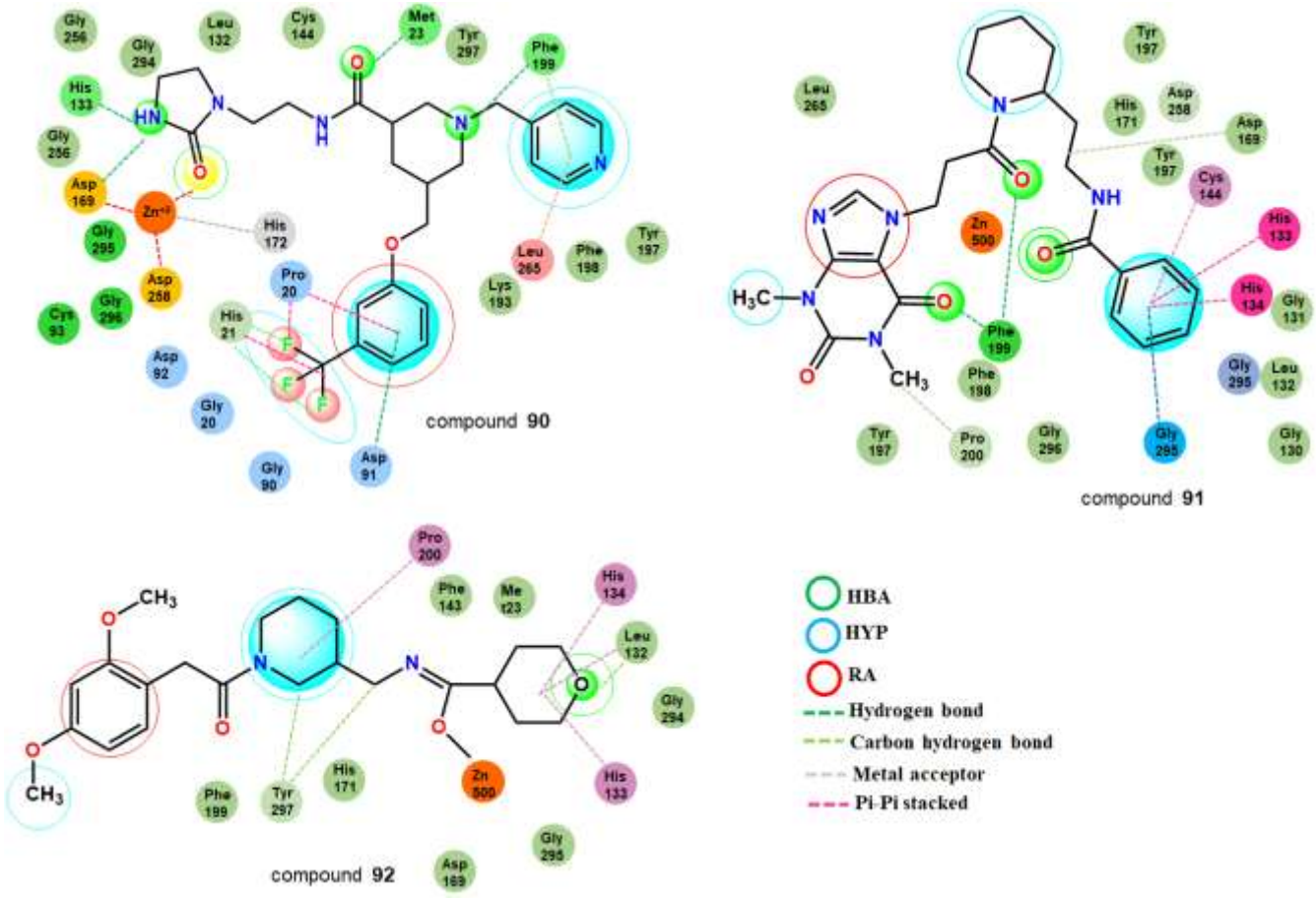

Figure 2.23: Schematic representation of intermolecular interactions of three Hit compounds (compound **90**, **91**, and **92**) and mapped to the best pharmacophore model.

In 2023, Bulbul et al. [199] reported a combined structure and ligand-based prediction models such as pharmacophore model, atom-based QSAR model, molecular docking, and MD simulation for the

design of alkyl hydrazide-based HDAC3 inhibitors as novel anticancer agents. Pharmacophore model generated using 30 compounds having IC_{50} value less than 100 nM with the help of PHASE module in Schrodinger software. A total of 38 pharmacophore hypotheses were generated. Then, these generated pharmacophore models were judged by the SURVIVAL score. The best pharmacophore hypothesis with seven pharmacophoric features (ADDDHRR) showed the highest survival score (6.923) than the inactive score (1.688) means that the selected pharmacophore can discriminate between *active* and *inactive* molecules. After the mapping of the best compound **93** in the generated pharmacophore, it was worth noting that carbonyl oxygen of the hydrazide acts as a hydrogen bond acceptor, two nitrogen atoms act as a hydrogen bond donor, the alkyl chain serves as a hydrophobic feature and two aromatic ring system acts as an aromatic feature. Hence, this selected feature is important for an inhibitor to interact with the HDAC3 active site. Then the best pharmacophoric features were used to align all training set compounds (39 compounds) for the generation of the atom-based 3D-QSAR model. Atom-based 3D-QSAR expressed a good correlation (R^2) of 0.95, and a cross-validated correlation (Q^2) of 0.88. This atom-based 3D-QSAR technique revealed three-dimensional non-covalent protein-ligand interactions namely, hydrogen bond acceptor, donor, hydrophobic, and negative and positive ionic interactions. After detailed analysis, it was concluded that the presence of heptyl alkyl chain, meta-substitution on phenyl linker, and thiophene ring decreases HDAC3 inhibitory activity, whereas, the hydrazide group attached with propyl alkyl chain is favored for HDAC3 inhibitory activity. This work assessed several QSAR models using ligand-based and structure-based techniques to understand the SAR of alkyl hydrazides developed as HDAC3 inhibitors. Then, the binding mode of interaction and free energies of binding were determined as the most potent compound **93** and compound **94** using molecular docking (**Figure 2.24**) and MD simulation to develop potent HDAC3 inhibitors. It showed that hydrazide of both of the compounds forms a hydrogen bond with His135, His134, and Tyr298 at the catalytic pocket of HDAC3 enzyme and also chelates with zinc ion in a bidentate way through nitrogen and carbonyl oxygen. The aromatic linker group engages in π-π interactions with Phe144 and Phe200. The cap group forms hydrophobic contacts with His22 and Pro23 as well as hydrogen bond interactions with Asp93 residues at the surface of HDAC3. The docking result revealed that the substitution of the propyl/butyl chain by any other group caused a substantial drop in HDAC3 activity. A tighter or narrower foot pocket area is produced as a result of the Tyr107 residue pushing Leu133. Hence, the longer chain shows steric hindrance with Met24 and Leu133, which lowers HDAC3 activity. The docking results of both compounds were verified by 100 ns MD simulation. The MD simulations of both compounds revealed that Met 24 and Leu133 are gatekeepers in the foot pocket of HDAC3. Additionally, in 100 ns MD simulation, the alkyl hydrazides maintained their bidentate chelation to the zinc ion.

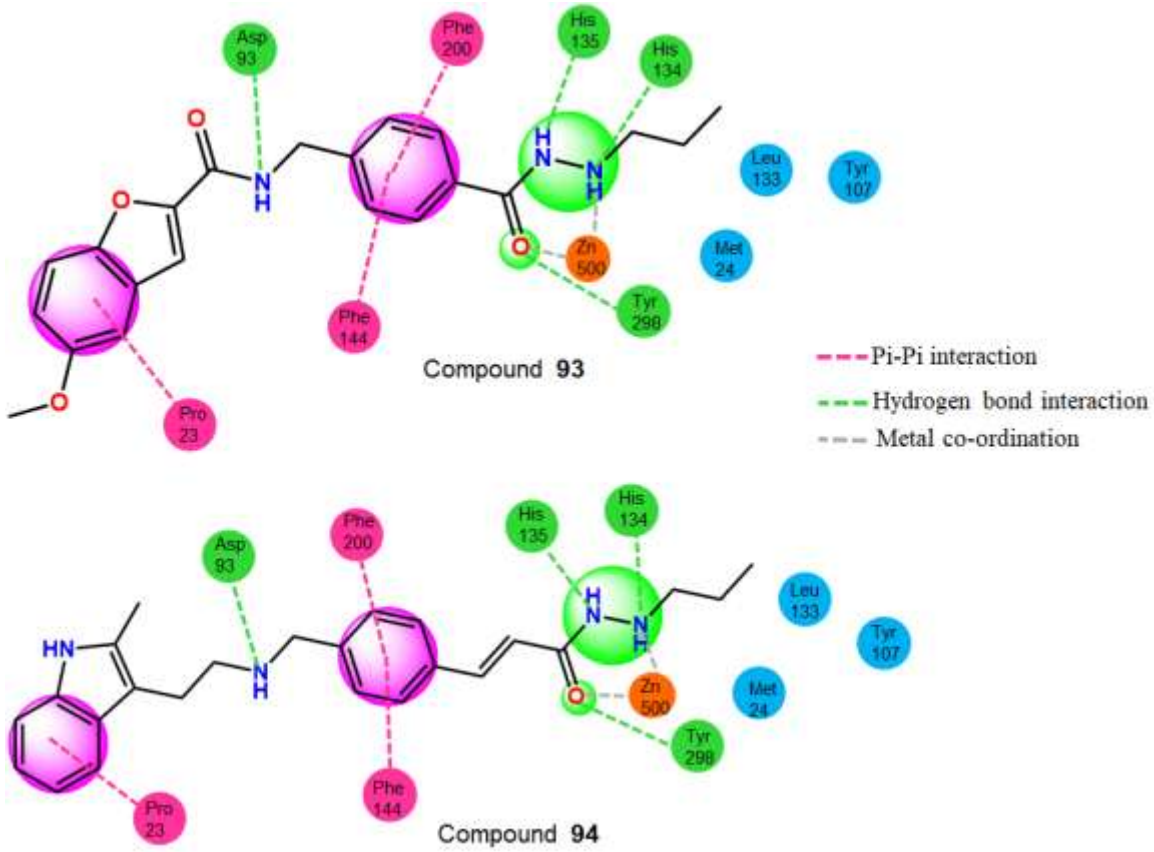

Fig. 2.24: Schematic representation of docking position of compound **93** and **94.**

In 2017, Hu and co-workers [200] developed a virtual screening pipeline (Hypo1_FRED_SAHA-3) to screen chemical libraries from different sources to enrich potential hit compounds. In this study ligand-based virtual screening (common feature pharmacophore model) and structure-based virtual screening (flexible docking) were performed on MUBD-HDAC3 (containing 39 diverse HDAC3i). In structure-based virtual screening, three docking programs such as Libdock, GOLD, and FRED were performed. It was observed that $ROCE_{0.5\%}$ and $ROCE_{1\%}$ (30.90 and 25.66, respectively) of FRED were much higher than the other docking and it was the best docking to find active ligands. In addition, the authors assumed that the ligand-induced-fit protein model may be beneficial to reach better HDAC3 inhibitors. Therefore, flexible ligand docking was performed for five HDAC3*i* [15K (compound **62**), 8d (compound **11**), R306465 (compound **12**), SAHA (compound **8**), MS-275 (compound **3**)] and excluded those complexes that did not form any bond with Zn^{+} ion, amionoanilide or hydroxamic acid and a hydrophobic group of the five-ligand placed between Phe200 and Phe144. Such information generated common features of pharmacophore models for ligand-based virtual screening (LBVS). Finally, 42 ligand-induced fit model was validated. SAHA-3 ligand-induced fit model had the highest overall enrichment factor ($ROCE_{0.5\%}$, $ROCE_{1\%}$, and *ROCE AUC*) and it was chosen as the best

model. Then pharmacophore model was generated using five ligands and hypo1 was selected as the best model based on the rank score 46.740. This model was used to screen the MUBD HDAC3. By using these three models, authors developed a versatile pipeline *i.e.*, Hypo1_FRED_SAHA3 to screen chemical libraries from different sources to enrich potential HDAC3 hit compounds.

Hu and co-workers [200] previously published a paper describing a virtual screening pipeline named "Hypo1_FRED_SAHA3" through which potentially hit compounds can be identified. In this study Xie et al., [201] explored practical-based virtual screening by using this pipeline, also a knowledge-based pose filter. Afterward, 11 diverse compounds were tested to determine for their inhibitory effects on HDAC3. It was seen that compound **95** showed 63.5% inhibition of HDAC3 at 10 μM concentration. Then workers searched the derivative/isoform of compound **95**. Five substructures met the criteria for substructure search. Among these five, compound **96** (IC_{50} = 1300 nM) showed 4.5-fold more potent HDAC3 inhibitory activity than compound **95** (IC_{50} = 6100 nM). The docking result of compound **95** revealed that the 2-hydroxyl group of benzene and the carbonyl group of benzamide coordinated with zinc metal ion. Along with the capping group (phthalimide) carbonyl group and the hydroxyl group of benzene form a hydrogen bond with the Asp259, His134 and Asp170 residue of the HDAC3 active site. The benzene ring of the benzamide was sandwiched between Phe1444 and Phe200 by forming π- π stacking interactions (**Figure 2.25**). In compound **96**, the capping group (quinoline) was located in Pro23, His22, and Phe144 may form π-π interaction (**Figure 2.25**). In conclusion, N-(2-hydroxyphenyl) benzamide scaffold was required for potent HDAC3 activity but itself not biologically active. The introduction of the capping group (e.g., phenyl) may be beneficial for activity. Further, the process was continued to find out the hit compound of the similar chemical type **95**.

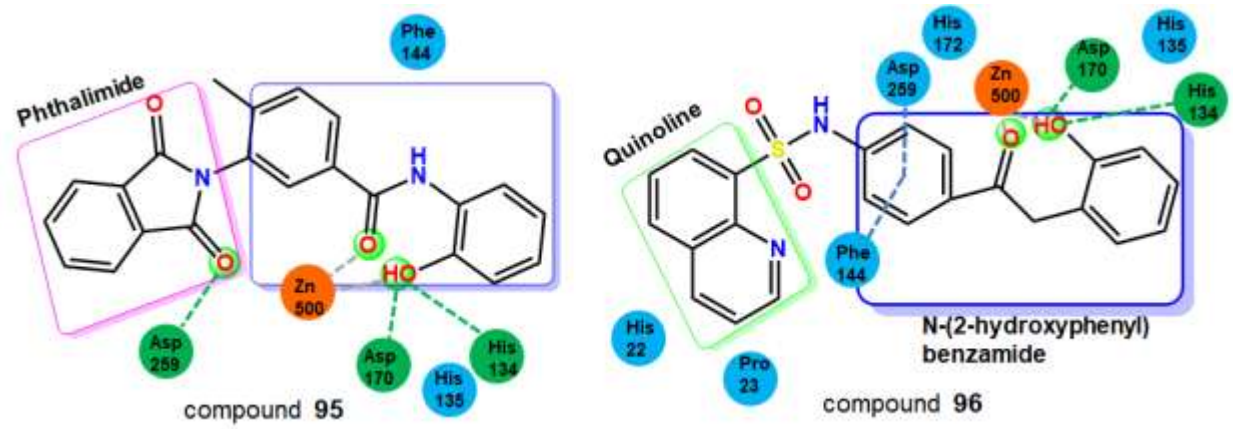

Figure 2.25: Schematic representation of compound **95** and compound **96** with their 2D representation docking image.

Chapter 3: Rational behind Study

HDAC3 is an enzyme that belongs to the histone deacetylase family, which regulates gene expression by removing acetyl groups from histone proteins. HDAC3 is involved in many biological processes such as apoptosis, cell cycle progression, lipid metabolism, and cardiac rhythm, etc. HDAC3 is a member of the class 1 HDACs, which are mainly located in the nucleus and cytoplasm, in addition, it requires nuclear receptor co-repressor (NCoR) and silencing mediated retinoid and thyroid hormone receptor (SMRT) for this activity. This complex is crucial to trigger the hypoacetylation of histone tail for transcriptional repression in different cancers including leukemia and lymphoma [202,203]. HDAC3 deacetylate histone as well as non-histone proteins such as p53, BCL6, NF-kB, and PPARy, thereby affecting the transcription factor. HDAC3 is involved in the development of several diseases such as cancer, kidney diseases, neurodegenerative diseases, lipid metabolism etc. Cancer cells frequently have dysregulated HDAC3 expression or activity, which results in abnormal gene expression and resistance to apoptosis. HDAC3 inhibitors have demonstrated promising anticancer effects by triggering cell cycle arrest, apoptosis, differentiation, and autophagy in numerous cancer models. HDAC3 inhibitors can also influence how well T-cells, macrophages, microglia, and dendritic cells operate, which can impact the immune system. HADAC3 also plays a critical role in gene regulation during development and differential processes. Studies have demonstrated that its importance in embryonic development and tissue-specific gene expression [204]. Moreover, HDAC3 inhibitors have been reported to protect against kidney injury, diabetic nephropathy, retinal degeneration, and cognitive impairment by reducing inflammation, oxidative stress, fibrosis, and neuronal loss. Therefore, HDAC3 is an important epigenetic regulator of gene expression and a potential therapeutic target for various diseases. It has been found that HDAC3 is intricately linked to several pathophysiological conditions. HDAC3 is a prospective target for several disorders. Therefore, there is still a selective HDAC3 inhibitor in demand. Therefore, the development of potential and effective HDAC3 inhibitors is one of the most important ways to treat this pathophysiological condition related to HDAC3.

Here several quantitative structure activity relationships (QSAR) have been conducted on HDAC3 inhibitors to find the importance of structural fingerprints and features for the development of potential HDAC3 inhibitors for the treatment of HDAC3 related different diseases.

Chapter 4: Materials and Methods

4.1. Dataset preparation and descriptor calculation

A series of 115 with diverse chemical scaffolds of HDAC3 inhibitors were collected from the binding DB database (https://www.bindingdb.org) for the modeling study. Primarily, duplication check of 115 compounds was carried out using the '*Prepare ligands for QSAR*' module in Discovery Studio (DS) 3.0 [205]. It was interesting to note that no duplicate molecule present in the dataset. A set of 2327 descriptors were calculated for each molecule using PaDEL descriptor software. Then, the following stage of dataset pre-treatment was subjecting the chemicals to the removal of irrelevant and highly correlated descriptors with a variance cut-off of 0.0001 and intercorrelation cut-off of 0.99, respectively using DTC software [206]. Then subsequent analysis was performed.

4.2. Classification-based QSAR method

Classification-based QSAR study is a popular method to classify the compound into active or inactive. A threshold value of activity scale (IC_{50} = 5000 nM) was chosen as the benchmark to separate compounds in the dataset into two classes: active (IC_{50} = <5000 nM), and inactive (IC50 = >5000 nM) HDAC3 inhibitors. According to this discrimination, 36 compounds (IC_{50} ranging from 1.4 nM to 4940 nM) were considered active compounds, while the remaining 79 compounds in the dataset (IC_{50} ranging from 5170 - >30,000 nM) were classified as inactive compounds. The SMILES notation of all 115 compounds is given in **Appendix A1**. Herein, four supervised learning approaches were performed namely Bayesian classification modeling and Recursive partitioning (RP), SARpy, and linear discriminant analysis (LDA) were performed to develop classification QSAR models.

4.2.1. Calculation of molecular properties for Bayesian classification and RP studies

In this study, we have used several molecular descriptors likes, ALogP (lipophilicity), number of hydrogen bond donors (nHBD), number of hydrogen bond acceptors (nHBA), molecular weight (MW), number of rotatable bonds (nRB), number of rings (nR), number of aromatic rings (nAR), molecular fractional polar surface area (FPSA) and extended connectivity fingerprint of diameter 6 (ECFP_6) by the "Calculate Molecular Properties" by the module of Discovery studio (DS) 3.0 software [205]. The scitegic's ECFP_6 and FCFP_6 extended connectivity fingerprints were used in this work. The letters F and E stand for functional role code and atom type code, respectively. The functional role code consists of a hydrogen-bond acceptor, hydrogen-bond donor, positively ionized or positively ionizable, negatively ionized or negatively ionizable, aromatic, and halogen. The atom type code is made up of the number of connections to an atom, the element type, the charge, and the atomic mass. The C and P

represent extended connectivity fingerprints and path-based fingerprints, respectively. The fourth character of a fingerprint is written by an underscore and the maximum distance, as reported earlier [207]. They reflect a significantly more comprehensive range of features than predefined ones. These fingerprints do not need to be pre-selected because they are generated directly from the molecules. Hence, novel molecular classes are handled just as simply as common ones.

4.2.2. Bayesian classification study

Based on probability and Bayes theorem, good and bad sub-structural fingerprints were identified in molecules that regulate the HDAC3 inhibitory activity. The Bayesian classification model was developed using the "Create Bayesian Model" protocol of DS 3.0.[26] Different independent properties like ECFP_6, AlogP, MW, nHBD, nHBA, nRB, nR, nAR, and FPSA were used during the development of the Bayesian classification model. The Training set molecules were utilized for model generation, while test sets were employed to validate the generated model. The leave-one-out (LOO) and 5-fold cross-validation were employed for model validation purposes. Moreover, different true positives (TP), true negatives (TN), false positives (FP), false negatives (FN), sensitivity (SE), specificity (SP), accuracy (ACC), precision (PR), positive likelihood ratio (ρ+), negative likelihood ratio (ρ-), and Mathew's correlation coefficient (MCC) were calculated to check the quality of the Bayesian model [208-210].

4.2.3. Recursive Partitioning (RP) study

The RP technique was used to discriminate between active and inactive molecules and analyze significant molecular features for a group of compounds having specific biological activities (IC_{50}). Recursive partitioning helps to generate decision trees that attempt to appropriately classify individuals of the population using a dichotomous split of a dependent variable (biological activity = IC_{50}) and a collection of independent variables (molecular properties), [211] also generate fingerprints by DS 3.0 [205] with minimum samples per node 10, maximum 20 along with "class-based weight" method and "Gini based split" method was used [212]. Molecular properties and fingerprints help us better classify. The best decision tree with two leaves and one structural fragment (FCFP_6) plays a significant role in differentiating between HDAC3 higher active and lower active molecules. The 5-fold cross-validation was used to know whether the developed model is statically significant or not. The model with the highest discriminate capability was chosen for HDAC3 inhibitors [213].

The TP, TN, FP, FN, SE, SP, PR as well as ACC, were used to assess the quality of the Bayesian and RP models, respectively [214]. A statistical analysis based on receiver operating characteristics (ROC) was carried out to assess the performance and predictability of these models [212]. Several other statistical parameters including MCC, PR, ρ+, and ρ- were calculated to assess the quality of the model (**Table 4.1**).

Table 4.1: The mathematical description and significance of statistical validation parameters

Equation No.	Parameter	Description	Equation
1	*SE*	Sensitivity	$SE = \frac{TP}{TP+FN}$
2	*SP*	Specificity	$SP = \frac{TN}{TN+FP}$
3	*ACC*	Accuracy	$ACC = \frac{TP+TN}{TP+TN+FP+FN}$
4	*MCC*	Mathews Correlation Coefficient	$MCC = \frac{(TP*TN)-(FP*FN)}{\sqrt{(TP+FN)(TP+FP)(TN+FN)(TN+FP)}}$
5	*PR*	Precision	$PR = \frac{TP}{(TP+FP)}$
6	*ρ+*	Positive likelihood value	$\rho+ = \frac{Sensitivity}{(1-Specificity)}$
7	*ρ-*	Negative likelihood value	$\rho- = \frac{(1-Sensitivity)}{Specificity}$
8	-	Likelihood ratio	$\text{Likelihood ratio} = \frac{TP}{FP} \text{ X } \frac{negatives}{Positives}$
9	*F1*	Fisher-snedecor parameter	$F1 = \frac{2TP}{(2TP+FP+FN)}$
10	*di*	Distance	$d_i = \sqrt{(1\text{-sensitivity})^2 + (1\text{-specificity})^2}$
11	*ROCED*	ROC graph Euclidean distance	$ROCED = (\lvert d1 - d2 \rvert + 1)\ (d1 + d2)\ (d2 + 1)$
12	*ROCFIT*	ROC graph Euclidean distance	$ROCFIT = \frac{ROCED}{\lambda}$

Where, i = 1 for training set, and i = 2 for test set compounds

Sensitivity (SE**)**, also called true positive rate, means the percentage of active compounds correctly predicted. Specificity (SP) also known as true negative rate, means the percentage of inactive compounds is correctly predicted. Accuracy (ACC) means the total percentage correctly predicted. Positive likelihood value (ρ+) observing a positive test in a condition compared to the other conditions. Negative likelihood value (ρ-) observing a negative test in a condition compared to the other condition.

In this equation (*Eq: 1-7*), TP indicates that active compounds are correctly predicted, TN indicates inactive compounds that are correctly predicted, and FP means a compound that is projected to be active but is not. FN means active compounds that are incorrectly predicted negative.

4.2.4. SARpy analysis

SARpy (SAR in Python) is a Python-based tool for automated structural alert (SA) analysis that extracts relevant fragments from data without any prior knowledge [215]. This software uses string mining to create substructures from SMILES notation of training compounds. The classification based structural analysis is widely used to identify the correlation between a particular molecular structure and its biological activity using three steps:

I. *Fragmentation*: This innovative, recursive approach directly manipulates the SMILES string while taking into account every possible bond breakage combination. This quick method can calculate each substructure in the input set of ligands.

II. *Evaluation*: Once substructures have been collected, the next phase is validated as potential SA in the training set to assess the predictive power of each fragment. First of all, each substructure is matched with the molecular structure in the training set. Fragment matches are divided into two parts by experimental label, either against positive structures, called true positive (TP), or against negative structures, called false positive (FP). It is possible to compute several indicators from these two to evaluate the PR of each probable SA and rank the rulesets using the likelihood ratio (*Eq: 8*) from a large set substructure in predicting the target activity label [216,217]

III. *Extraction*: The ultimate objective is to select a smaller collection of rules from the extensive range of potential alerts that can best predict the target class with the best precision.

Evaluation of the developed models is one of the essential components for the prediction of model performance. The number of TP, TN, FP, and FN were identified, and performance indicators such as SE, SP, ACC, and MCC were also predicted using this information.

4.2.5. Classification-based linear discriminant analysis (LDA) model development

LDA is one of the classification methods for feature selection/extraction and dimension reduction techniques. It is a statistical technique used for the classification of data into two or more classes using linear formalism just like MLR. LDA seeks to find the difference between classes. The discriminant function (DF) equation is given below (*Eq: 13*):

$$DF = C_0 + C_1X_1 + C_2X_2 + C_3X_3.....+ C_nX_n \text{ ……... (13)}$$

Whereas, X_1, X_2, X_3...X_n represents the predictor score of the total n variables and C_1, C_2, ...C_n represents their respective weights [218].

To comprehend the crucial structural requirements for active HDAC3 inhibitors in classification-based QSAR modeling, linear discriminant analysis is carried out. The classification of active and inactive compounds is done initially based on the threshold value (5000 nM) of IC_{50} for our LDA analysis. Descriptors were calculated by PaDEL software to develop the LDA model. Then selected descriptors were used for the development of the LDA model by forward stepwise method keeping the tolerance 0.001 and stepping F-criteria variables inclusion (F inclusion = 4.00) and exclusion (F exclusion = 3.9) using the STATISTICA 7.1 software [219]. The SE, SP, ACC, PR, and F-measures (F1) (*Eq: 9*) are used to assess the LDA model's internal and external predictability. Several statistical tests have been run to validate the performance and classification capability of the created LDA model. Such testing includes Wilk's λ, [220] MCC, [221] canonical indexes (R_c) [222], and ROC curve [223] The Fisher-snedecor parameter (F) was used to choose the significance of potential variables. Another statistic, chi-square (χ^2) [224] was used in the model to test the independence between groups. To get more comprehensible results, we calculated two new additional parameters in this study: the ROC graph Euclidean distance (ROCED) and the ROC graph Euclidean distance corrected using fitness function (ROCFIT) (*Eq: 10-12*) [225].

4.3. Regression-based 2D-QSAR model

4.3.1. Multiple linear regression model (MLR)

The 2D QSAR models are used to investigate the correlation between the activities of molecules and their structures without the 3D conformations of the molecules [226, 227]. Here, forty-four molecules having defined HDAC3 inhibitory activities were taken for regression-based QSAR modeling study. The Java-based software namely "Dataset Division GUI 1.2" is freely available at the DTC Lab software for the division of the dataset [206] into the training (N_{train} = 33) and the test (N_{test} = 11) sets. The training molecules were chosen to develop the multiple regression analysis 2D QSAR model (MLR). Some procedures *i.e.*, genetic algorithm (GA) and stepwise regression methods (S-MLR) were used to select relevant descriptors. Ten descriptors were selected from a large set of descriptors that were responsible for the biological activity with the stepping criterion of F = 4 for inclusion and F = 3.9 for exclusion. The S-MLR was used to eliminate the descriptors containing no

structural variance and lesser importance. The identified descriptors were considered for the best subset method. Several models were generated by multiple linear regression (MLR) with a combination of five descriptors. Out of these, the best model was chosen based on the highest square regression co-efficient (R^2) and leave one out (LOO) cross-validated correlation coefficient (Q^2) and lower mean absolute error of 95% (MAE 95%). A model with the R^2 value of more than 0.7 was chosen as the best one. The 2D QSAR model was then validated by using the best model that was chosen to predict the activities of the corresponding test set compound [228].

4.3.2. Pharmacophore Model

A set of 44 diverse compounds was taken to form the training and the test sets in a manner that would ensure that all compounds were bio-assayed in the same condition. The algorithm needs a small number of compounds (training set) for model generation. This collection of chemicals should have as maximal structural diversity as possible and exhibit a wide variety of activity. The resultant 20 diverse compounds were manually selected (also diversity check by the "Find Diverse Molecule" module in Discovery Studio (D.S 3.0) as the training set from these 44 compounds to generate the pharmacophore model. The training set was taken as an input ligand to create the common feature mapping pharmacophore by using D.S 3.0 [205]. The common feature mapping pharmacophore was carried out using the Hipogen algorithm in D.S 3.0 and conformational models were generated by the "BEST" method with an energy threshold value of 20 kcal/mol. A maximum of 255 conformers were produced for model development. Additionally, the uncertainty value 1.5 and excluded volume 5 were used to generate the pharmacophore model. The predictive 3D QSAR pharmacophore generation was obtained in three phases: constructive phase (extracting the most active compounds and identifying and storing their properties), subtractive (removing the inactive compounds that were not likely to be beneficial by pharmacophore matching), optimization (done after these two previous steps to increase the score and get better results) [229]. The pharmacophore model was generated by using some chemical features such as hydrogen bond acceptor (HBA), hydrogen bond acceptor lipid (HBA_lipid), hydrogen bond donor (HBD), hydrophobic (HYP), and ring aromatic (RA). A good pharmacophore model was selected based on some statistical parameters such as high correlation coefficient (r), lowest total cost, lowest root means square (RMS), maximum fit value as well and total cost should be near to fixed cost and far from null cost.

4.3.3. Molecular docking

The X-ray diffraction structure of HDAC3 (PDB ID: 4A69) was obtained from the protein data bank (PDB) to carry out the molecular docking investigation [230]. First, the protein preparation and improvement using the "Protein Preparation Wizard" of Schrodinger Maestro software [231], the protein's structure was refined, missing hydrogens were added, and states were generated. In this procedure, the constrained minimization of the protein structure using the OPLS3e force field. The receptor grid for the molecular docking investigation was performed using the "Receptor Grid Generation" feature of the Schrodinger Maestro program [231]. However, the molecules were prepared before molecular docking using the "Ligprep" module of the Maestro program.

Chapter 5: Result and Discussion

A pool of 115 compounds that act as an HDAC3 inhibitors were used in various molecular modeling studies. The goal of this study was to construct statistically verified QSAR models for screening and prediction of different HDAC3 inhibitors, as well as explore different structural features for HDAC3 inhibition. In this study, several classifications and regression based QSAR studies were performed in order to identify/detection of crucial features that affect their HDAC3 inhibitory potency, which will assist the development of potent HDAC3 inhibitors in the future.

5.1. Bayesian classification analysis

The Bayesian model was developed by DS 3.0 [205] based on such a descriptor. Statistical results for the training sets are summarized in **Table 5.1,** which showed a high *SE* (0.93), *SP* (0.95), and overall *ACC* (0.94). The Leave one out *ROC* (ROC_{LOO}) was found to be 0.93. Then the model is validated with a test set that comprises 28 molecules. The test set also gave a good *SE* (0.87), *SP* (0.95), and *ACC* (0.93). In terms of *ROC* score of training (ROC_{Train} = 0.90), and test set (ROC_{Test} = 0.94) suggest an excellent external predictivity of the model. The *ROC* curves for both the training and test set were given in **Figure 5.1**. The training set statistics support the model's predictive capabilities (*PR* = 0.89), and the higher value of the parameters indicates the model's reliability and statistically significant. The positive likelihood ratio ($\rho+$ = 18.26) is much larger than the negative likelihood ratio ($\rho-$ = 0.07) (*Eq: 6-7*). Another significant parameter that influences the model's predictability is *MCC* (*Eq: 4*). An *MCC* score of 1.0 suggests flawless prediction, while a value of -1.0 denotes an exceptionally weak model. The *MCC* value of 0.87 in the model created substantially supports the results [208].

Table 5.1: Statistical parameters of the best Bayesian model.

Parameter	Training set	Test set
ROC_{LOO}	0.93	--
ROC_{CV}	0.90	0.94
TP	26	7
FN	2	1
FP	3	1
TN	56	19
SE	0.93	0.87
SP	0.95	0.95

ACC	0.94	0.93
PR	0.89	0.87
MCC	0.87	0.82
$\rho+$	18.21	17.50
$\rho-$	0.07	0.13

Where, TP = True positive; FN = False negative; FP = False positive; TN = True negative

In the same way, statistical parameters are used to validate the test set for the created model. The statistical value and precision (*PR* = 0.87) are closely correlated with the training set values. Although the positive likelihood ratio ($\rho+$ = 17.50) of the test set differs from the training set, it is still a solid result; the negative likelihood ratio ($\rho-$ = 0.13) is also very good, indicating that the test set value is very supportive. The MCC value has been determined to be 0.82. All of these statistical metrics indicate that the created model has a significant ability to predict the test set compound [232]. The higher value of these parameters suggests the significance and good reliability of this model [233].

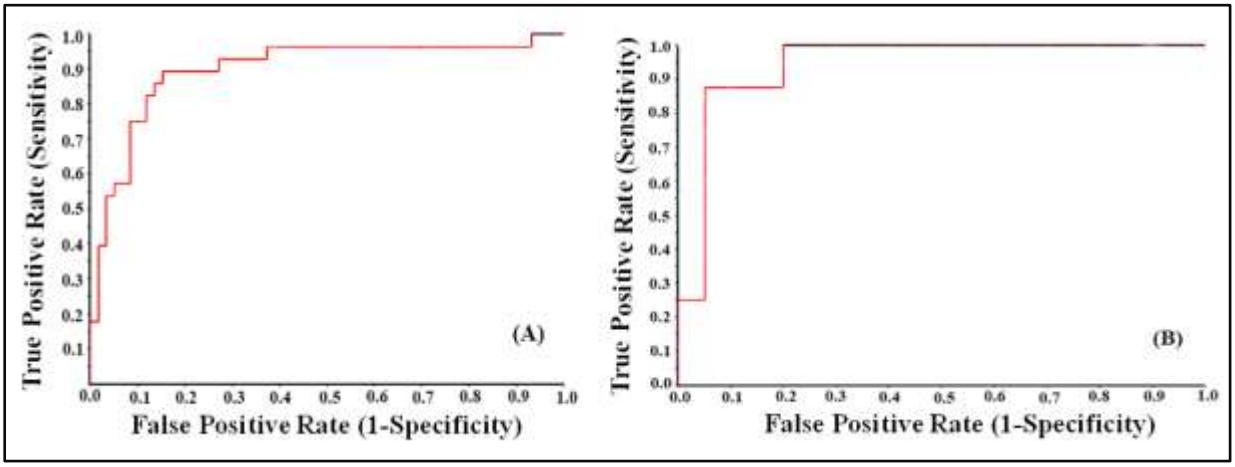

Figure 5.1: Graphical representation of receiver operating characteristics curve (ROC) for (**A**) Training set (**B**) Test set as per Bayesian classification model of HDAC3 inhibitory.

5.1.1. Analysis of fingerprints from the Bayesian classification model

The Bayesian model generates the top 20 good **(G1-G20)** and top 20 bad **(B1-B20)** substructural features/fingerprints or fragments, and these are favorable and unfavorable for HDAC3 inhibitors. These top 20 good (**Figure 5.2**) and top 20 (**Figure 5.3**) bad substructural features are generated from the Bayesian classification study. These good and bad fingerprints are clustered into different groups. One fingerprint from each cluster is given in **Figure 5.4**. Additionally, a total of 20 good (**G1-G20**) and 20 bad (**B1-B20**) substructural fingerprints with positive and negative influences on the HDAC3 inhibitory potency were

given in **Figure 5.5 (A and B)**. First top 20 good substructural features are grouped into four clusters such as (A) cluster 1 (**G1-G5, G10-G12**), (B) cluster 2 (**G13-G17**), (C) cluster 3 (**G18-G20**), and (D) cluster 4 (**G6-G9**). The cluster 1 fingerprint reveals the importance of the hydroxamate group, which interacts with zinc in the active site. Compounds 007, 009, 010, 011, and 013 showed very good HDAC3 inhibitory activity due to the presence of the hydroxamate group. The cluster 2 fingerprints elaborate importance of the thiazole ring as the positive influencer of the HDAC3 inhibition. The thiazole ring-containing compounds can be found in compounds 002 and 004. These are exhibiting good HDAC3 inhibitory activity. Additionally, compounds that contain an amide group exhibit good inhibitory activity against the HDAC3 enzyme. This inhibitory activity can be well described by the presence of a good fingerprint in cluster 3 in the structure of compounds 003 and 004 **[Figure 5.5 (A)].** Other fingerprints in cluster 4 indicate that an amine group also plays a crucial role in HDAC3 inhibition. The compounds 003, 005, 008, and 021 showed good HDAC3 inhibitory activity.

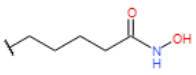 **G1** 22 out of 26 good Score: 0.854	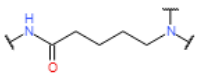 **G2** 21 out of 25 good Score: 0.844	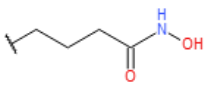 **G3** 23 out of 29 good Score: 0.798	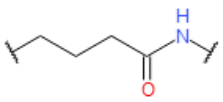 **G4** 23 out of 29 good Score: 0.798	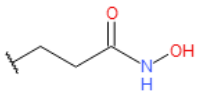 **G5** 23 out of 31 good Score: 0.737
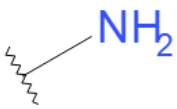 **G6** 6 out of 7 good Score: 0.732	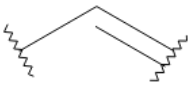 **G7** 3 out of 3 good Score: 0.686	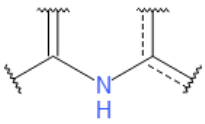 **G8** 3 out of 3 good Score: 0.686	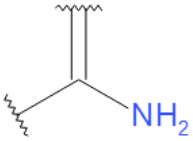 **G9** 3 out of 3 good Score: 0.686	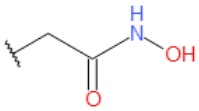 **G10** 23 out of 33 good Score: 0.680
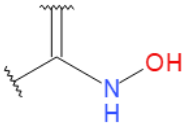 **G11** 24 out of 35 good Score: 0.666	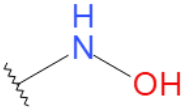 **G12** 24 out of 35 good Score: 0.666	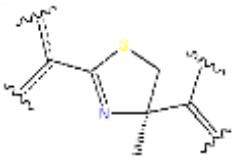 **G13** 2 out of 2 good Score: 0.582	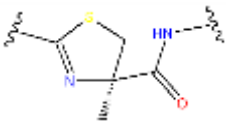 **G14** 2 out of 2 good Score: 0.582	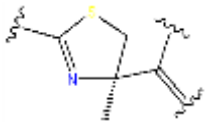 **G15** 2 out of 2 good Score: 0.582

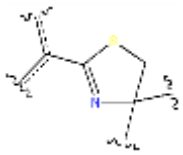 **G16** 2 out of 2 good Score: 0.582	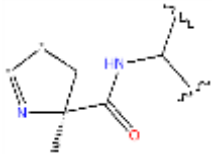 **G17** 2 out of 2 good Score: 0.582	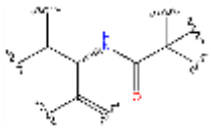 **G18** 2 out of 2 good Score: 0.582	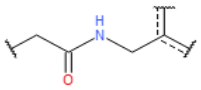 **G19** 2 out of 2 good Score: 0.582	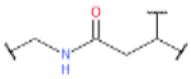 **G20** 2 out of 2 good Score: 0.582

Figure 5.2: The top 20 (G1-G20) good fingerprints for HDAC3 inhibitors obtained from Bayesian classification study.

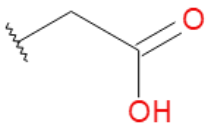 **B1** 0 out of 18 good Score: -1.958	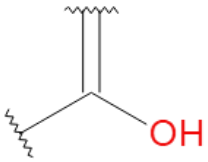 **B2** 0 out of 18 good Score: -1.958	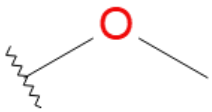 **B3** 0 out of 16 good Score: -1.858	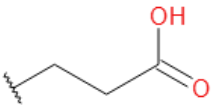 **B4** 0 out of 16 good Score: -1.858	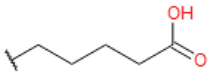 **B5** 0 out of 15 Good Score: -1.804
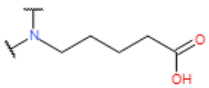 **B6** 0 out of 15 good Score: -1.804	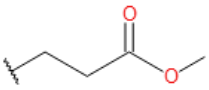 **B7** 0 out of 15 good Score: -1.804	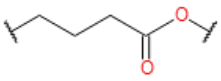 **B8** 0 out of 15 good Score: -1.804	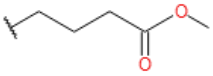 **B9** 0 out of 15 good Score: -1.804	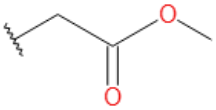 **B10** 0 out of 15 good Score: -1.804
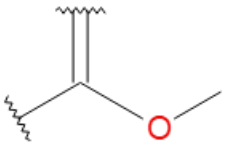 **B11** 0 out of 15 good Score: -1.804	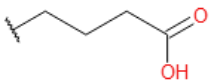 **B12** 0 out of 15 good Score: -1.804	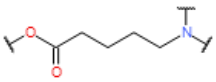 **B13** 0 out of 15 good Score: -1.804	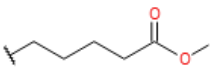 **B14** 0 out of 15 good Score: -1.804	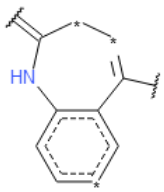 **B15** 1 out of 23 good Score: -1.479
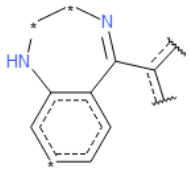 **B16**	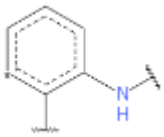	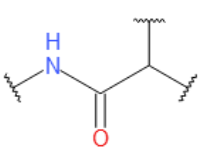 **B18**	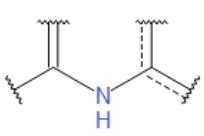 **B19**	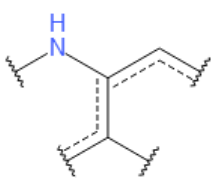 **B20**

1 out of 23 good Score: -1.479	**B17** 1 out of 23 good Score: -1.479	1 out of 23 good Score: -1.479	1 out of 23 good Score: -1.479	1 out of 23 good Score: -1.479

Figure 5.3: Top 20 bad fingerprints (B1-B20) for HDAC3 inhibitors obtained from Bayesian classification study.

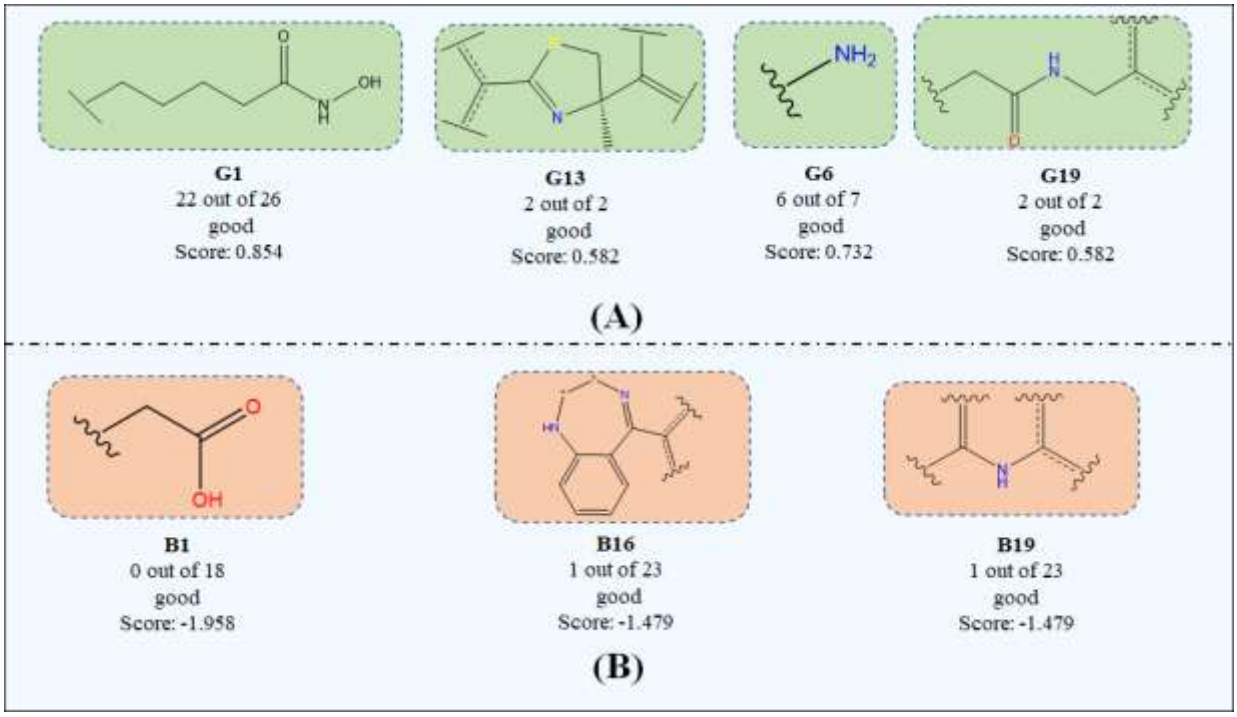

Figure 5.4: **(A)** good molecular fragment **(B)** bad molecular fragment along with Byesian score obtained from Bayesian classification study.

In bad fingerprints, clusters of sub-structural features have a detrimental impact on the suppression of HDAC3. The bad fragments produced by the Bayesian classification model can also be grouped into some clusters similar to the good substructural fingerprint. These clusters are as follows (A) cluster 5 (**B1-B14**), (B) cluster 6 (**B15** and **B16**), (C) cluster 7 (**B17** and **B20**). It can be found that carboxylate moiety negatively affects the inhibition of HDAC3. Moreover, compounds 040, 042, 049, 050, 052, 053, and 064. containing carboxylate group (**B1-B14**) are showing less activity towards HDAC3 activity and also possess weak zinc ion binding ability. Thus, these are not considered better HDAC3 inhibitors than hydroxamate acid moiety. Further, the benzodiazepines ring (**B15, B16**) and aniline-containing compound (**B17-B20**) had shown less activity which can be found in compounds 042, 044, 048, 050, and 051 and their low Bayesian score for HDAC3 inhibitors **[Figure 5.5 (B)]**. From the Bayesian analysis, it is clear that the hydroxamate group with

long-chain carbon (four carbon) linkers is very important for HDAC3 inhibitory activity, whereas carboxylate moiety is against HDAC3 inhibitory activity.

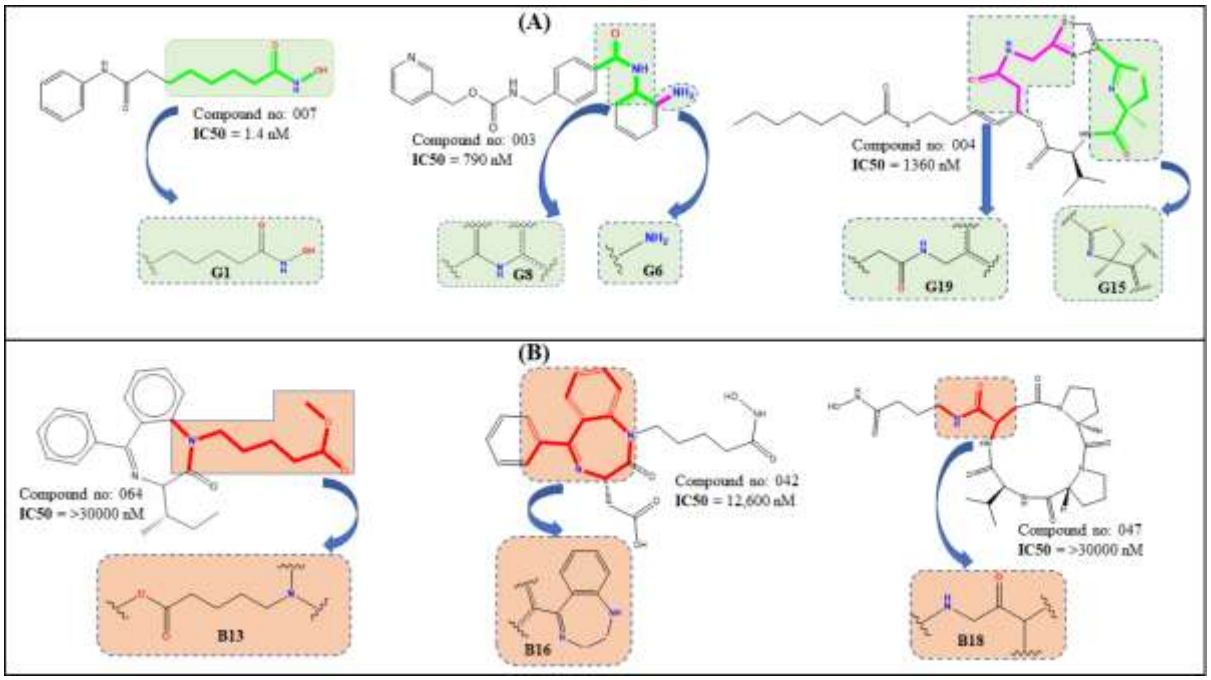

Figure 5.5: Structure of compounds having (A) Good and (B) Bad fingerprints.

5.2. Recursive partitioning (RP) study

The DS 3.0 software was used to create RP models with molecular attributes and fingerprints, especially feature-class fingerprints of diameter 6 (FCFP_6). Two trees were generated from the RP result. The decision *Tree-1* with three leaves (leaf ID: #1, #5, #6) was generated with a single fingerprint depicting the importance of the hydroxamate group with single molecular properties such as molecular fractional polar surface area (MFPSA). The decision *Tree-1* with highest ROC score but the other discrimination ability and predictability of the decision *Tree-1* for the dataset compounds was lower than the *Tree-2*. Thus, decision *Tree-2* with two leaf (leaf ID: #1, #2) was selected for further analysis. The decision *Tree-2* showed ROC_{train} score and ROCcv of 0.86 and 0.89, respectively. The ROC_{test} value was found as 0.91, suggesting significant external predictability of the developed RP model. The result of the best RP model for the training set compounds showed higher degree of statistical significance (SE = 0.78, SP = 0.93, ACC = 0.89, PR = 0.85, F1 = 0.81). The MCC value for the training set compound of 0.73 was close to the perfect classifier value of +1 [**Figur 5.6 (C)**]. On the other hand, the result of the best RP model of the test set compounds showed good statistical significance (SE = 0.87, SP = 0.95, ACC = 0.93, PR = 0.87, F1 = 0.87). The MCC value has also been calculated to be 0.82. All of these statistical metrics indicate that the created model has a significant ability to predict the test set compound. Moreover, higher positive likelihood

(training set ρ+ = 11.59, test set ρ+ = 17.50) and lower negative likelihood (training set ρ- = 0.23, test set ρ- = 0.13) values indicate the better performance of the developed RP model. The decision *Tree-2* was constructed with a single fingerprint depicting the importance of the hydroxamate group with four carbon long chains to classify the dataset into active and inactive compounds [**Figure 5.6 (A)**]. Analysis of the decision *Tree-2* suggested most of the active compounds contain a hydroxamate group with four carbon long chains (FP1). The FP1 containing compound (compound no. 007, 009-012, 014, 016-019, 021, 025-027, 029-031, 033, 034, 036, 038, 039, 041, 042 and 044) is denoted as leaf id: #1. The compounds having FP1 fingerprint are very good active compounds. Thus it may be postulated that compounds with an FP1 fingerprint are positively correlated with HDAC3 inhibitory activity, as suggested by the Bayesian classification study. On the other hand, the rest of the molecule does not have FP1 fingerprint and is denoted as leaf id: #2. These molucules were considered inactive compounds. Also, the confusion matrix of the training and test sets for decision *Tree-2* is given in **Figure 5.6 (B)**.

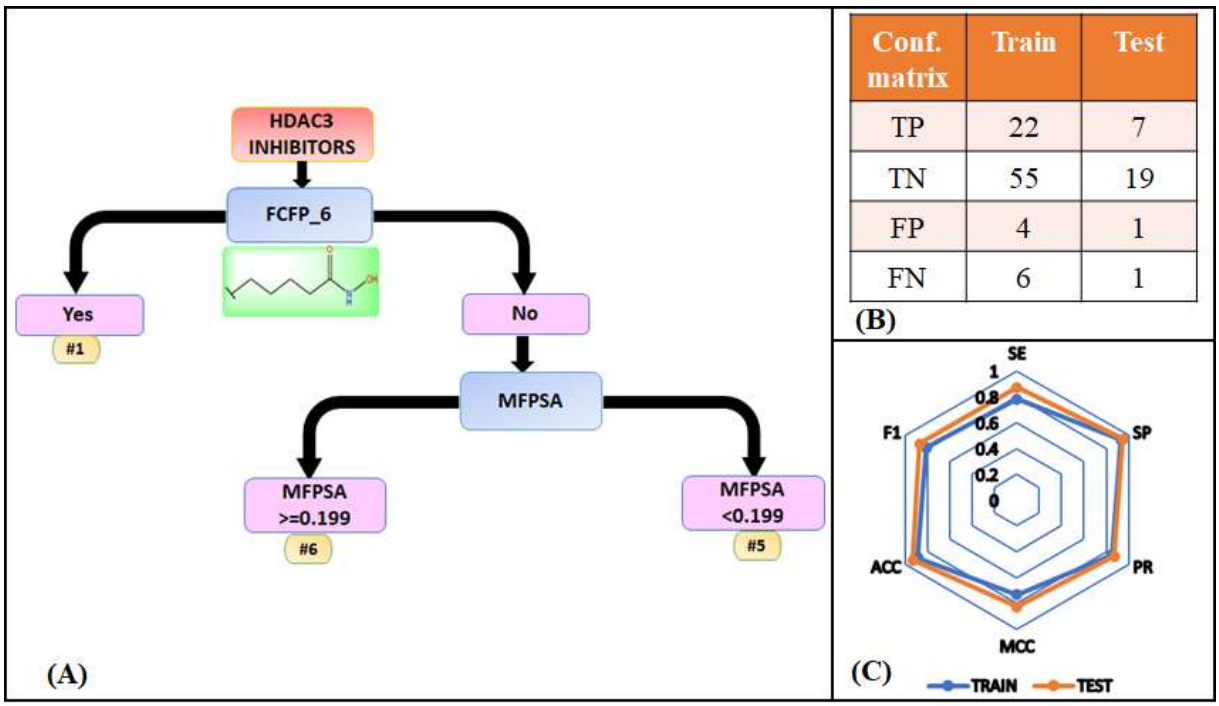

Figure 5.6: (**A**) Schematic representation of decision tree generated from recursive partitioning study, along with the important fingerprint. (**B**) Confusion matrix of the training and test set for decision *Tree-2*. (**C**) Spider plot of statistical performance of decision Tree-2

5.3. SARpy analysis

The potential SA analysis of the fragment ruleset containing 2-18 atoms was carried out for this data set using the SARpy tool. The SA search for molecules of the active class was carried out with "OPTIMAL" single alert precision. The SARpy analysis was able to deliver

the crucial structural alerts as active rulesets in SMILES notation. The active ruleset was generated from their respective training set. The predictive performance of the active ruleset was verified by using their respective test set. The SARpy analysis of this dataset provided two structural alerts along with their likelihood ratio (LR) values as the active ruleset for the dataset is provided in **Figure 5.7**. The SARpy analysis delivers SE, SP, and ACC of 0.89, 0.90, and 0.90 for the training set population. The external validation using the test set shows SE, SP, and ACC of 0.88, 0.95, and 0.93. Furthermore, the MCC value was also calculated, providing an MCC score (*Eq: 4*) of 0.77 and 0.82 for both the training and test sets. It demonstrates that the classifier performance well in the identification of structural features from the dataset. Two structural alerts are provided by the SARpy analysis, which serves as the active ruleset. The SA: C(=O)(CCCC)NO [LR = 7.73] indicates the presence of a hydroxamate group with a saturated four-carbon long chain as a positive structural alert for HDAC3 inhibition which was also suggested by Bayesian classification and recursive partitioning studies. Meanwhile, the hydroxamate group with long-chain carbon plays a crucial role in HDAC3 inhibition. Also, another SA: CC(C(=O))C [LR=inf] indicates the positive influence of iso-butyraldehyde for the activity. The SA, CCCCC(=O)NO identified by SARpy analysis is present in HDAC3 inhibitors (compound no. 007, 010, 011, 013, 014, 015, 017, 018, 020-022, 024-029, 031, 033-035, 038, 039, 042, and 044). Additionally, compounds 002, 004, and 006 with the SA, CC(C(=O))C, have HDAC3 inhibitory activity. Additional information is given in **Appendix A2-A3.**

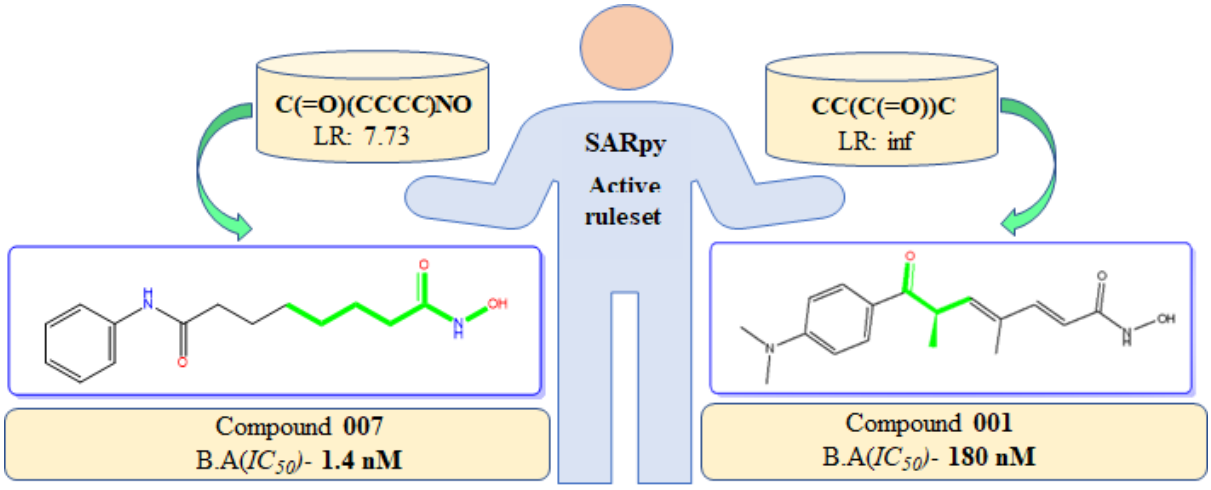

Figure 5.7: SARpy active ruleset and some compound possessing structural alerts (SAs)

5.4. Classification-based linear discriminant analysis (LDA) model

A total pool of 115 diverse molecules was divided into training and test sets, both including higher active and lower active HDAC3 inhibitors. The training set (discrimination set)

consisted of Twenty-seven compounds from the higher active group and 60 compounds from the lower active group. Similar to this, nine of the twenty-eight test set chemicals are more active, while the other nineteen are less active. Seven variables were obtained in the best discrimination function. All the variable information is given in **Table 5.2.** The best discrimination is represented in *Eq: 9* with seven variables.

DF= -75.38 + 4.39 * *maxHBint9* + 16.77 * *minHCsatu* + 10.67 * *nHBint10* + 94.29 * *maxaasC* + 7.87 * *PubchemFP392* – 4.97 * *naaaC* – 33.53 * *PubchemFP590* ……. **(14)**

n_{Train} = 87, *wilk's* λ = 0.138, χ^2 = 161.02**,** R_c = 0.928, F (6,80) = 70.11, p < 0.000, $AUROC_{Train}$ = 0.99, MCC_{Train} = 0.95, n_{Test} =28, $AUROC_{Test}$ = 0.988, MCC_{Test} = 0.82, *ROCED* = 0.209, *ROCFIT* = 1.519

The best discrimination function is obtained with seven variables such as *maxHBint9*, *minHCsatu*, *nHBint10*, *maxaasC*, *PubchemFP392*, *naaaC*, and *PubchemFP590*. These descriptors were found to be important for better discriminant analysis. The developed LDA model is within the acceptable criteria. It showed a good chi-square (χ^2) value of 161.02, suggesting significant independence between the two groups. The discrimination set illustrates the following result: canonical index (R_c) of 0.92, squared Mahalanobis distance of 27.80. The TP, TN, FP, FN, SE, SP, ACC, PR, MCC, and F1 are given for both training and test sets in **Table 5.3**. The ROC plots for the LDA model (*Eq.* 14) are represented in **Figure 5.8**. The LDA showed a perfect SE, SP, PR, ACC, and F1 for both the training and test sets. Additionally, the MCC score also calculated for both the training and test set were found to be 0.95 and 0.82, respectively, demonstrating that *Eq: 9* is capable of non-random prediction. Furthermore, additional material such as classification function grouping LDA, Chi-square and discriminant function analysis are provided in **Table 5.4-5.6.**

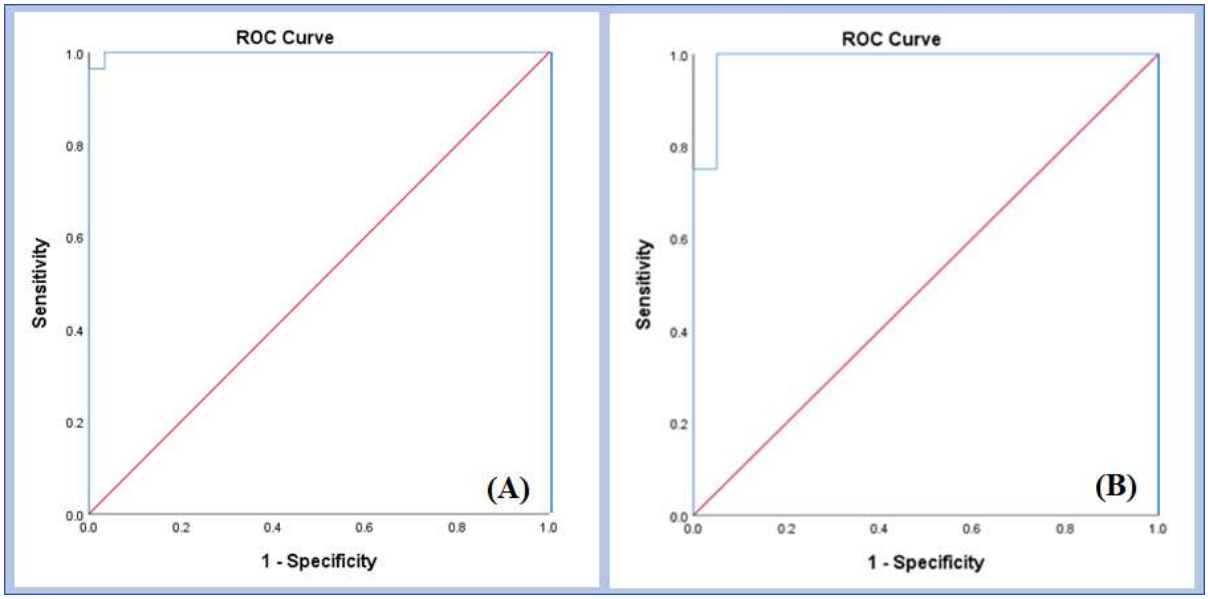

Fig. 5.8. LDA ROC curve for both **(A)** training and **(B)** test set.

Table 5.2: Descriptors found to be important in LDA model for classification of HDAC3 inhibitors

Sl. No.	Descriptors	Definition	Type	Contribution
1	maxHBint9	Maximum E-state descriptors of strength for potential hydrogen bonds of path length 9.	Electro topological descriptors	positive
2	minHHCsatu	Minimum atom type H E-state: H on C bonded to unsaturated C	Electro topological descriptors	Positive
3	nHBint10	Count of E-state descriptors of strength for potential Hydrogen bonds of path length 10	Electro topological descriptors	Positive
4	maxaasC	Maximum atom E-state: C	Atom type electro topological descriptors	Positive
5	pubchemFP392	N(~C)(`~C)(~H)	--	Positive
6	PubchemFP590	C-C:C-O-[#1]	--	Negative
7	naaaC	Count of atom type E-state –C:	Electro topological descriptors	Negative

Table 5.3: Statistics of training and test set during LDA model development.

Model	Dataset	ROC	TP	TN	FP	FN	SE	SP	PR	AC	F1	MCC

LDA	**Train**	0.99	28	57	2	0	1.00	0.97	0.93	0.98	0.96	0.95
	Test	0.99	7	19	1	1	0.87	0.95	0.87	0.93	0.87	0.82

Table 5.4: Classification function grouping LDA model.

Classification function grouping: BINARY		
Descriptors	G_1:0 P= 0.50000	G_2:1 P= 0.5000
maxHBint9	1.5985	4.3961
minHCsatu	36.4564	16.7789
PubchemFP590	-7.4102	-33.5325
nHBint10	6.5876	10.6703
maxaasC	70.4702	94.2914
naaaC	1.2125	-4.9738
PubchemFP392	3.2896	7.8787
constant	-48.8656	-75.3887

Table 5.5: Chi – square with successive roots removed

Chi – square Tests with successive Roots removed					
Eigen value	Canonical R(Rc)	Wilk's lambda	Chi- square.	Df	P - value
6.212	0.928	0.138	161.026	7	0.00

Table 5.6: Discriminant function analysis summary

Descriptors	Discriminant function analysis summary No. of vars in model: 6; Grouping BINARY (2grps) Wilk's lambda: 0.2863, F (6,80) = 33.23, p<0.0000					
	Wilk's Lambda	Partial Lambda	F removed (1,80)	p- value	Toler.	1 – Toler. (R-sqr.)
maxHBint9	0.709	0.195	325.042	0.000	0.459	0.540
minHCsatu	0.174	0.796	20.210	0.000	0.774	0.225
PubchemFP590	0.171	0.808	18.746	0.000	0.784	0.215
nHBint10	0.177	0.778	22.418	0.000	0.702	0.297
maxaasC	0.183	0.754	25.753	0.000	0.602	0.397
naaaC	0.160	0.864	12.360	0.000	0.851	0.148
PubchemFP392	0.158	0.876	11.131	0.001	0.751	0.248

5.4.1. Discussion of LDA model descriptors

The LDA model reflected the importance of seven independent descriptors such as ***maxHBint9***, ***minHCsatu***, ***PubchemFP392***, ***nHBint10***, ***maxaasC***, ***PubchemFP590***, and ***naaaC***. The first five descriptors are positively contributing, and the last two are negatively contributing to HDAC3 inhibitory activity.

maxHBint9 is the maximum E-state descriptor of strength for potential hydrogen bonds of path length 9 [234]. The positive contribution of ***maxHBint9*** indicated that compounds with adjacent highly electronegative groups might be able to form a higher number of hydrogen bonds as favorable interactions that were responsible for the enhancement of HDAC3 inhibitory activity (Compounds 002, 003, 004, 005, 007, 009, 011, 021). Nevertheless, it is observed that these compounds possess keto, hydroxyl, and amide groups that are supposed to form hydrogen bonding interactions at the HDAC3 active site.

minHCsatu is a 2D electro-topological state (E-state indices) atom type descriptor which accounts for the minimum atom type H E-sate: H on C bonded to unsaturated C. E-state indices encode, in the context of the topological nature of the molecule, the inherent electronic state of each atom as it is disrupted by the electronic impacts of all other atoms and influenced activity positively. This implies increases in the value of these descriptors augment the value of the activity in the same direction (Compounds 010, 019, 033, and 034) [235]

nHBint10 is an electro-topological descriptor: count of E-state descriptors of strength for potential hydrogen bonds of path length 10. It indicates the presence of hydrogen bonds within the structures. This descriptor is positively correlated with HADC3 inhibitory activity means biological activity will be increased with an increase in hydrogen bonds within structures (Compounds no. 002, 003, 004, 007, 009, and 032).

maxaasC is the maximum atm type E-state:c belonging to the atom type electro-topological state descriptor [236] is positively correlated with HDAC3 inhibitory activity, indicating that the performance of the inhibitory activity can be improved by increasing the number of carbon atoms (Compounds 001, 002, 004, 005, 009, 011, 012, and 017).

PubchemFP392 (N(~C)(~C)(~H)) is positive contribution to the HDAC3 inhibition. Furthermore, the abovementioned features belong to N-methylmethanamine, which is a precursor for HDAC3 inhibition (Compound 001, 003, 004, 007, 008).

PubchemFP590 (C-C:C-O-[#1]) is negatively correlated with biological activity. It was observed that prop-1-en-1-ol containing compound (Compound 039) has less inhibitory activity towards HDAC3 as compared to the others.

naaaC (count of atom-type E-State: ::C:) [237] which describes the number of ring connections in carbons in fused rings and their sum, respectively. This descriptor has a negative contribution to HDAC3 inhibition. Compounds like 008,022, and 046 showed lower HDAC3 inhibition due to the presence of a fused ring system (like indole). These observations indicate that indole-containing compounds will have lower HDAC3 inhibition.

5.5. 2D QSAR regression-based study

Among all models generated using the MLR method, the best model was selected based on some basic criteria, these are following:

(1) Minimum number of descriptors,
(2) Higher value of R^2, Q^2, Q2F2 metrics and Q2f1/R^2_{pred} and
(3) Model prediction quality in terms of mean absolute error (MAE)

The best MLR model was obtained from 33 compounds with 5 descriptors. The final model is given below.

pIC_{50} = -1.04273(+/-1.32776) - 1.61704 (+/-0.26676) *PubchemFP569* - 0.64701 (+/-0.13942) *PubchemFP20* + 6.59216 (+/-0.99861) *GATS1m* + 4.19044 (+/-0.90618) *GATS3s* - 0.03639 (+/-0.02361) *AATSC2m* …… **(15)**

$N_{training}$ = 33, R^2 = 0.846, R^2_{adj} = 0.818, Q^2_{LOO} = 0.791, $R^2_{m\ (training\ LOO)}$ = 0.712, $\Delta R^2_m\ (LOO)$ = 0.133, $MAE_{train\ (95\%)}$ = 0.211, *SEE* = 0.322, *PRESS* = 2.38, *F (5, 27)* = 29.80

N_{test} = 11; R^2 = 0.843, R^2_{pred} / *Q2f1* = 0.790, $R^2_{m\ (test)}$ = 0.692, *Q2f2* = 0.767, $MAE_{test\ (95\%)}$ = 0.274, $Q2f1/R^2_{pred}$ = 0.790, cR^2_p = 0.775, prediction quality of (train) = good; prediction quality (test) = good; Golbraikh and Tropsha acceptable model criteria's: passed (**Table 5.7**).

Table 5.7: Golbraikh and Tropsha criteria for MLR model

Parameter	Threshold Value	MLR model
Q^2	$Q^2 > 0.5$	0.791
R^2	$R^2 > 0.6$	0.843
$\lvert r_0^2 - r'^2_0 \rvert$	$\lvert r_0^2 - r'^2_0 \rvert < 0.3$	0.031
k	$0.85 < k < 1.15$	0.974
K'	$0.85 < k' < 1.15$	1.023
$(r^2 - r_0^2)/r^2$	$(r^2 - r_0^2)/r^2 < 0.1$	0.037

$(r^2-r'_0{}^2)/r^2$	$(r^2-r'_0{}^2)/r^2 < 0.1$	0.00007

Where, Q^2 is the cross validated Correlation Coefficient, R^2 coefficient of determination between the observed vs predicted response values of the test set compounds.

The r_0^2 and $r'_0{}^2$ represent the corresponding values for regression through the origin and observed vs predicted activities respectively. The slope of the regression linear through the origin are assigned by ***k*** and ***k'***.

It is interesting to note that *Eq. 1* explained 81.80% and predicted 79.10% variance of the HDAC3 inhibitory activity. The R^2_{pred} of the test set compound was found to be 0.790. The correlation matrix, *t*-values, *p*-level, and *VIF* are given in **Figure 5.9** and **Table 5.8** respectively. The additional parameters in *Eq. 1* including R^2_{adj} = 0.818, Q^2_{LOO} = 0.791, $R^2_{m\ (training\ LOO)}$ = 0.712, $R^2_{m\ (test)}$ = 0.692, Q2f2 = 0.767 respectively, show that this model is reliable and robust because their values are within the acceptable limit (> 0.5). The degree of freedom (F = 29.80) and standard error of the estimate (SEE = 0.322) values in *Eq. 1* are the larger and the lower respectively. Also, the model exhibits the higher leave-one out cross-validated R^2 (Q^2_{LOO} = 0.791), $R^2_{m\ (training\ LOO)}$ = 0.712, $\Delta R^2_{m\ (LOO)}$ = 0.133 respectively indicating the model's strong internal predictability. Also, the higher projected R^2_{pred} = 0.790, $R^2_{m\ (test)}$ = 0.692, and the lower mean absolute error of the test set ($MAE_{test\ (95\%)}$ = 0.274) show the models have excellent external predictability. Then the developed model was checked by the Y-randomization test. This test was performed by scrambling each data of the Y-column without changing other column of the training set compounds 50 times. Every time this generated a new model with concerning the R^2 and Q^2_{LOO} values. Calculation of the average value of R^2 ($R^2avg.$: 0.164) and Q^2_{LOO} (Q^2_{LOO} *avg.*: 0.339) which are not closer to the actual model. It means the model is not generated by chance. The higher value of the coefficient of determination (cR^2_p = 0.775) indicates that the model is non-random, statistically significant, and not derived by chance. Furthermore, this MLR model also passed the Golbraikh and Tropsha acceptable criteria, given in **Table 5.7**. Additional information such as MLR training and test set molecule observed and predicted activities were given in **Tables 5.9** and **5.10**.

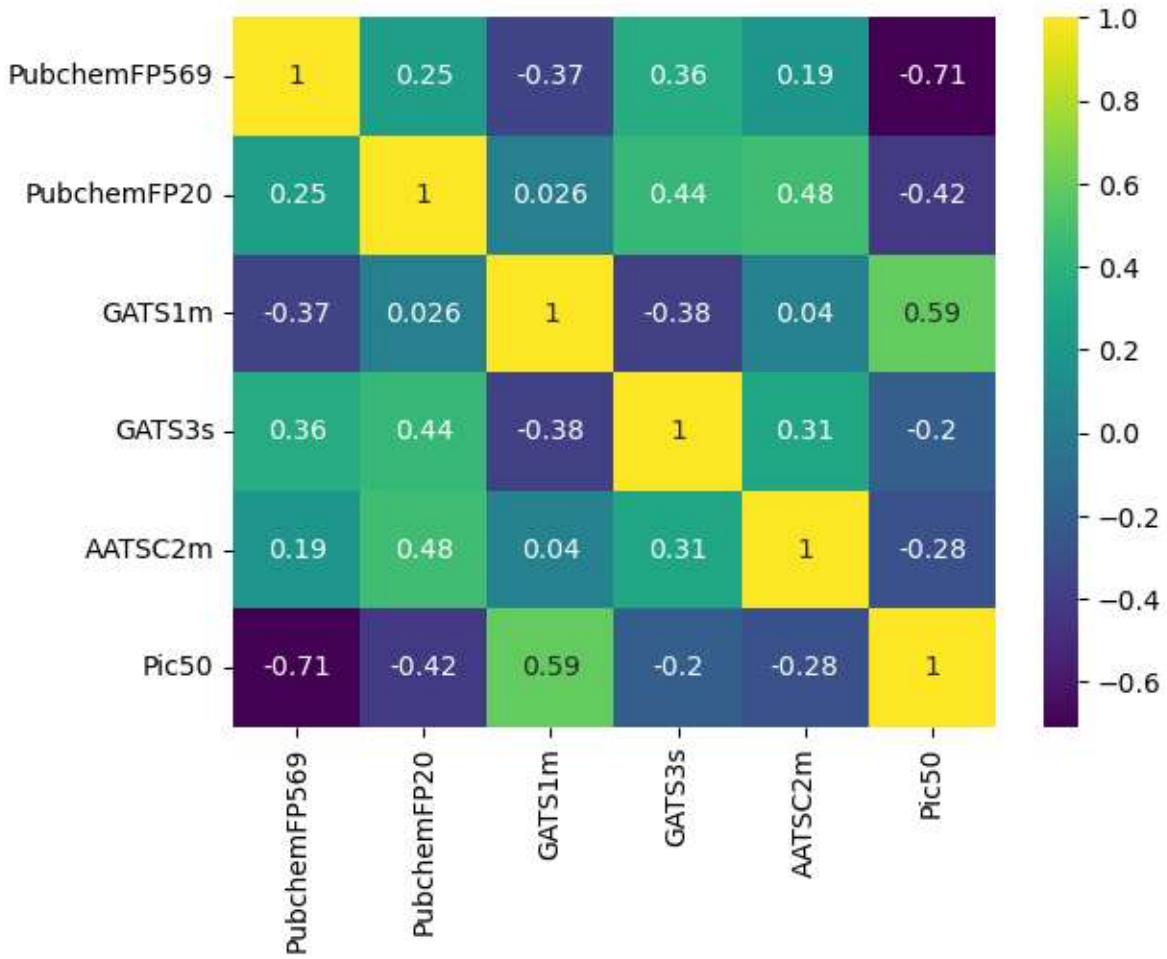

Figure 5.9: Schematic representation of correlation heatmap.

Table 5.8: The *t*-value, *p*-level and *VIF* of the Eq. 15 for the HDAC3 inhibitors

Variable	*t-value*	*p-level*	*VIF* (*variance inflation factor*)
Constant	-0.78	0.43	560.54
PubchemFP569	-6.06	0.00	1.28
PubchemFP20	-4.64	0.00	1.54
GATS3s	6.60	0.00	1.37
GATS1m	4.62	0.00	1.58
AATSC2m	-1.54	0.13	1.33

Table 5.9: MLR training set molecules observed activity and predicted activity with descriptors.

Name	PubchemFP569	PubchemFP20	GATS1m	GATS3s	AATSC2m	*Observed* pIC_{50}	Predicted pIC_{50}
2	1	1	0.771459	0.997081	3.750493	6.3279	5.68624
3	1	0	0.770033	0.868978	-1.57592	6.10237	6.116558
4	1	1	0.802756	0.9343	3.657996	5.86646	5.753178
5	1	0	0.724947	0.903993	-3.30075	5.4045	6.164645
6	1	1	0.843948	0.862007	1.159128	4.86328	5.899073
7	0	0	0.922785	0.862472	-3.38633	8.85387	8.596947
8	0	0	0.899068	0.568242	-0.89801	7.22185	7.478773
9	1	0	0.855174	0.780002	-4.69303	6.74473	6.3542
10	1	0	0.893909	0.823103	-0.63014	6.65758	6.714424
11	1	0	0.796399	0.778267	-6.67777	6.36653	6.016737
12	1	0	0.80277	0.783433	-2.05734	6.3098	5.965152
13	1	0	0.870163	0.760027	0.620038	6.24413	6.237995
14	1	1	0.877613	0.824206	2.41544	6.22915	5.802119
15	1	0	0.851778	0.760162	0.875675	6.22185	6.094137
16	1	0	0.790174	0.794629	-1.51998	6.18046	5.91611
17	1	0	0.824986	0.78774	2.865329	6.12494	5.946856
18	1	1	0.800953	0.856319	-1.78605	6.08092	5.568893
19	1	1	0.846818	0.90692	2.587003	6.07058	5.971874
21	1	0	0.910083	0.735515	-0.90806	6.02228	6.542713
22	1	0	0.785634	0.791112	-1.29506	5.99568	5.872759
23	1	1	0.843089	0.904771	3.245245	5.98716	5.916886
25	1	1	0.861663	0.887931	2.597749	5.91721	6.008829
28	1	0	0.81185	0.775416	0.042211	5.74473	5.957216
29	1	1	0.815656	0.881731	-0.59365	5.7122	5.793684
30	1	0	0.779005	0.775069	-1.81549	5.59346	5.806856
34	1	1	0.861321	0.792838	6.798622	5.36754	5.475147
35	1	1	0.788675	0.869546	-1.8229	5.36552	5.634082
36	1	1	0.810703	0.74427	-2.15554	5.30627	5.215455
38	1	1	0.794484	0.832884	3.536239	5.28316	5.293137
39	1	1	0.802213	0.802425	-1.49017	5.27654	5.415848
40	1	1	0.758659	0.759221	-0.94288	5.05998	4.867745
43	1	0	0.547326	0.918665	1.596234	4.69897	4.819665
44	1	1	0.797849	0.904431	-0.50471	5.50864	5.787895

Table 5.10: MLR test set molecules actual activity and predicted activity with descriptors.

Name	PubchemFP569	PubchemFP20	GATS1m	GATS3s	AATSC2m	Actual pIC_{50}	Predicted pIC_{50}
1	0	0	0.899567	0.799019	3.565818	7.69897	8.105816
20	1	1	0.81612	0.815871	-1.40673	6.04096	5.543256
24	1	0	0.870163	0.743173	0.620038	5.98716	6.168126
26	1	0	0.805758	0.797121	-1.9631	5.87943	6.063641
27	1	1	0.829402	0.863787	-0.42061	5.74473	5.795715
31	1	1	0.801681	0.752389	-1.71092	5.59007	5.193129
32	1	1	0.779299	0.935245	-1.80951	5.49349	5.81542

33	1	1	0.827232	0.92293	3.597021	5.38195	5.883028
37	1	1	0.797849	0.910121	-1.77908	5.28651	5.831314
41	1	1	0.784803	0.771357	-1.72846	4.98338	5.161988
42	1	1	0.739286	0.780738	-0.91917	4.89963	4.871793

5.5.1. Interpretation of 2D-QSAR model

It was observed that *Eq. 01* show different descriptors like *PubchemFP569*, *PubchemFP20*, *AATSC2m*, *GATS1m*, *GATS3s*, play an important role in predicting HDAC3 inhibitory activity. From these descriptors first two descriptors (*GATS1m* and *GATS3s*) are positively contributing, whereas the last three descriptors (*PubchemFP569*, *PubchemFP20*, and *AATSC2m*) are negatively contributing to HDAC3 inhibitory activity. These descriptors symbols, definitions and contributions are given in **Table 5.11**.

Table 5.11: Descriptors symbol, definition and contribution for selected descriptors in 2D-QSAR regression model.

2D-QSAR REGRESSION MODEL DESCRIPTORS				
Sl.no	**Descriptors**	**Definition**	**Block**	**Contribution**
1	GATS3s	Geary autocorrelation of lag 3 weighted by I-state	2D autocorrelations	Positive
2	GATS1m	Geary autocorrelation-lag 1 weighted by mass	2D autocorrelations	Positive
3	PubchemFP569	N-C-C-N	----	Negative
4	PubchemFP20	> = 4 o	----	Negative
5	AATSC2m	Average centered Boto-Moreau autocorrelation of lag2/ weighted by mass/average atomic topological state connectivity index of order 2 weighted by mass	----	Negative

The order of contribution of each descriptor towards the activity is as follows:

GATS1m > GATS3s > PubchemFP569 > PubchemFP20 > AATSC2m

GATS1m is a Geary auto-correlation lag-1/weighted by atomic masses belonging to the 2D auto-correlation descriptors [238]. These descriptors describe the specific atomic properties of a molecule. The higher value is obtained when pairs of atoms in a molecule at a specified

topological distance (lag value) present the difference in the selected atomic property. Larger differences in an atomic weight at a topological distance 1 tend to favor HDAC3 inhibitory activity. ***GATS1m*** is positively correlated to HDAC3 inhibitory activity means the biological activity will be increased if the ***GATS1m*** descriptor value increases. The highest ***GATS1m*** value is observed for molecules (compounds. 7, 8, 10, and 21) with very good activities, whereas compound 43 is observed with the lower activity for their lowest ***GATS1m*** value.

GATS3s is an autocorrelated 2D descriptor, which corresponds to Geary autocorrelation - lag 3 / weighted by I-state, representing 2D Autocorrelation descriptors [239]. This set of descriptors is a part of the Geary autocorrelation of topological structures and represents the topology at the molecular level or at least in some of its component portions that depend on physicochemical qualities with the weighting component incorporated in descriptors. ***GATS3s*** descriptors are in positive correlation with HDAC3 inhibitory activity. It indicates that active molecules (compounds 2, and 19) will possess higher values of these descriptors, compared to the less active molecules (compounds 21, 28, 30, 36, and 40) which possess the lower value of these descriptors.

The rest of the descriptors such as ***PubchemFP569***, ***PubchemFP20***, and ***AATSC2m*** are negatively correlated with the biological activity means the presence of this fingerprint descriptor may decrease the HDAC3 inhibitory activity. The negative coefficient of ***PubchemFP569*** suggests that the presence of ethane 1,2 diamine in the molecule may be unfavorable for HDAC3 inhibition. Compounds 7 and 8 are showing good inhibitory activity due to the absence of this fingerprint, while the rest of the molecules (compounds 2-6, 9-19, 21-23, and 43-44) with ethane 1,2 diamine are less effective to the HDAC3 inhibition. Similarly, ***PubchemFP20*** (4-O) is negatively correlated with the biological activity. It was observed that 4-oxygen-containing molecules (compounds 4, 6, 14, 18, 19, 38, and 44) are have less inhibitory activity towards HDAC3 as compared to the other molecules (compounds 7, 8, 9, 10, 11). [240]

AATSC2m is the average centered Boto-Moreau autocorrelation of lag2/ weighted by mass/average atomic topological state connectivity index of order 2 weighted by mass [241]. This ***AATSC2m*** descriptor is calculated by summing the all-topological distance between pairs of atoms in a molecule that are separated by two bonds, taking into account the, mass of each atom. This provides information about connectivity and size, which can be useful in predicting the biological activity of the compound. This descriptor has a negative

contribution suggesting that increasing the value of this descriptor decreases the value of the activity (compounds 4, 6, 23, 25, 34, and 43). Also, the value of these descriptors suggests that smaller molecules or simple molecules may have the higher biological activity of the molecule (compounds 7, 9, and 11). These five descriptors and their contribution to some compounds are shown in **Figure 5.10**.

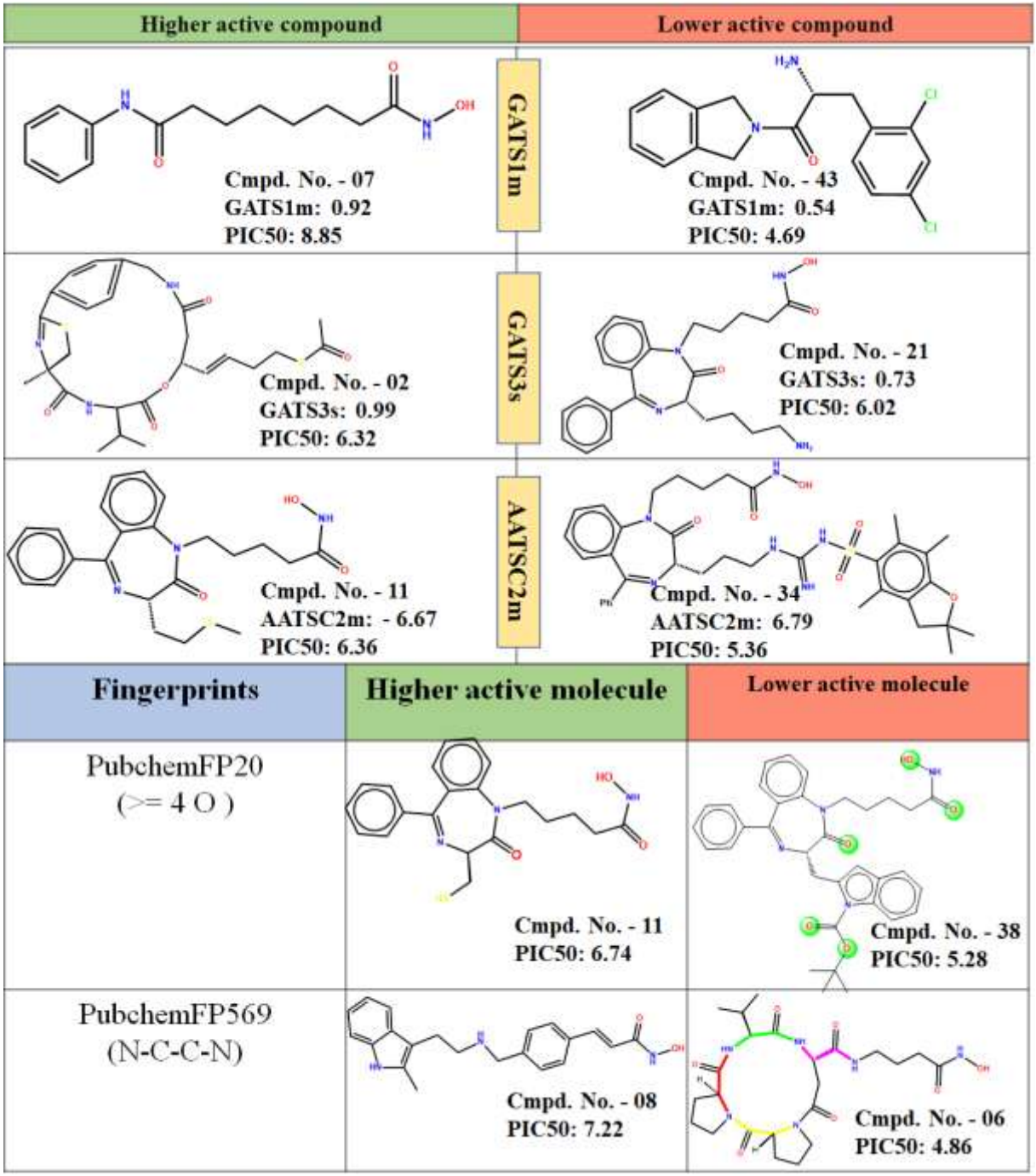

Figure 5.10. Descriptors and their contributions with their pIC_{50}

The experimental pIC_{50} values (X-axis) and the projected (predicted) pIC_{50} values (Y-axis) for the training and test sets in the scatter plot are shown in **Figure 5.11**. The training and test

sets are uniformly distributed along the diagonal line, according to a visual assessment of the scatter plot. This means a low level of error between the training and test set data

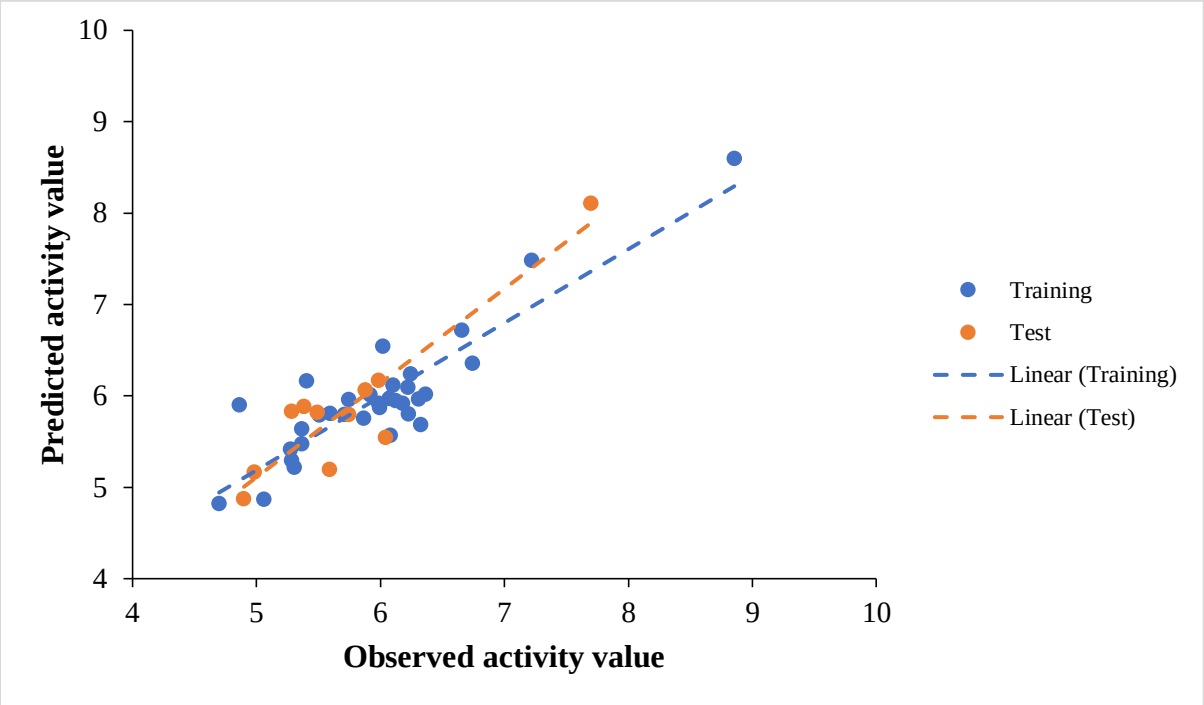

Figure 5.11: Scatter plot of training and test set

5.6. Pharmacophore modeling study and validation

3D-QSAR pharmacophore model was generated using the Hypogen algorithm in D.S 3.0 [1] to construct a pharmacophore model by utilizing some chemical features such as hydrogen bond acceptor (HBA), hydrogen bond donor (HBD), hydrogen bond acceptor_lipid (HBA_lipid), ring aromaticity (RA), hydrophobicity (HYP) and excluded volume (EV). These chemical features were chosen using mapping based on the chemical features found in the molecules of the training set. The active properties were chosen based on the pIC50 values of the various compounds in the training set. The conformation of the training set molecules was generated using the "Best" conformation generation with minimum interference distance (2.97Å), energy threshold (20 kcal/mol and weight variation (0.302) taken as default value. The maximum excluded value was set as five. The uncertainty value was set to 1.5. The best model was generated by constraints a number of features such as uncertainty value and weight variation. The best quality hypothesis was selected on some statistical parameter as well as the Debnath analysis [242]. The top 10 hypotheses from training set were generated and their corresponding statistical parameters were employed to select the optimal pharmacophore model. The best model (HYPO1) was comprised of four features along with five excluded volumes (EV). The best pharmacophore HYPO 1 model

was chosen due to its higher correlation coefficient (0.99), the lowest RMS (0.77), and higher cost difference (null cost - total cost = 280.01) which may indicate correlation probability between the observed and predictive activity is > 95%. In the present study, the total cost, fixed cost and, null cost for HYPO1 is 72.91, 65.41 and, 352.92 respectively. Hence, a meaningful pharmacophore model is cosigned by a difference of 287.51 bits between fixed cost and null cost. Additionally, the generated hypothesis of the total cost is somewhat closer to the fixed cost value [243, 244]. The configuration cost (16.950) and error cost (53.28) are the two additional cost parameters of the pharmacophore model. These are also used to determine the quality of the pharmacophore model. The configurational cost should be less than 17 and also dependent on the complexity of the pharmacophore model space. The error cost depends on RMS deviation which is the deviation between predicted and observed activity data. The configuration cost of the HYPO1 model was 16.950, which was used to predict the activity value of all training set compounds. All the result of the pharmacophore hypothesis was given in tabulated format in **Table 5.12.**

Table 5.12: Results of pharmacophore hypotheses generated using training set molecule.

Hypo[a]	Total cost	Error cost	RMS	*r*	Features[b]
1	**72.916**	**53.284**	**0.771**	**0.990**	**HBA, HBA_L, HYP, RA, 5EV**
2	73.543	53.971	0.814	0.989	HBA_L, HBA_L, HYP, RA, 4EV
3	80.025	60.609	1.152	0.978	HBA, HBA_L, HYP, RA, 3EV
4	81.625	62.991	1.251	0.974	HBA, HBA, HYP, RA, 5EV
5	82.404	47.336	1.241	0.974	HBA, HBD, HYP, RA, 4EV
6	85.708	47.336	1.380	0.968	HBA, HBA_L, HYP, RA, 4EV
7	88.028	65.040	1.330	0.970	HBA, HBA_L, HYP, RA, 1EV
8	88.920	47.336	1.472	0.963	HBA_L, HBD, HYP, RA, 3EV
9	89.810	47.336	1.542	0.960	HBA, HBD, HYP, RA, 5EV
10	90.145	47.336	1.566	0.959	HBA_L, HBA, HYP, RA, 3EV

[a]Hypotheses: Null cost = 352.921; Fixed cost = 65.412; Configuration cost = 16.950. All cost units are in bits. HBA: hydrogen bond acceptor; HBA_L: hydrogen bond acceptor lipid; HBD: hydrogen bond donor; HYP: hydrophobicity; RA: ring aromatic; EV: excluded volume.

Hence, HYPO 1 is the best model for HDAC3 inhibitor and further it is considered for the validation. The best HYPO 1 was constructed with HBA, HBA_L, one HYP, one RA, and five EVs. The HBA and HBA_L features are located at a minimum distance of 4.125 Å. The HBA_L and HYP are located within a distance of 7.193 Å. The HYP features maintains the distance of 7.454 Å and 4.608 Å from RA and HBA respectively. The HBA_L and RA are situated at the distance of 13.407 Å which was depicted in **Fig. 5.12 (A)**.

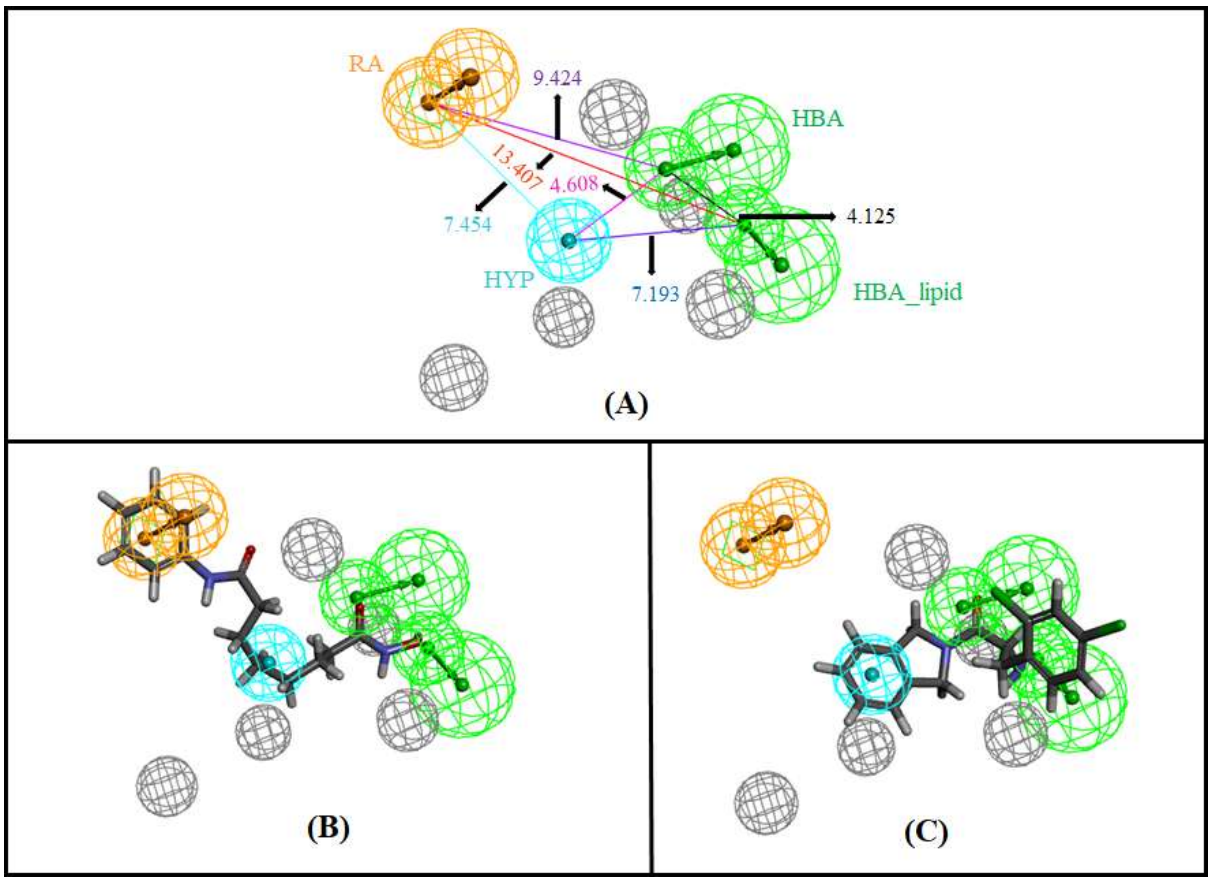

Figure 5.12: **(A)** Pharmacophore features with interference distances (HBA: hydrogen bond acceptor, HBA_L: hydrogen bond acceptor_lipid, HY: hydrophobicity, RA: ring aromaticity), **(B)** Schematic representation of the most active 007 and **(C)** least active 043 compound pharmacophore mapping in 3D space.

Further assessing the model's statistical significance, Fisher randomization method was employed to make sure the pharmacophore model was much better than the 19 random pharmacophore hypotheses obtained from the same pharmacophoric features with a 95% confidence level. The correlation value of HYPO 1 was greater than the other hypotheses generated in a random spreadsheet which indicates that the pharmacophore model is not generated accidentally, it is generated statistically. Also, HYPO 1 had the lowest total cost value in comparison to the other hypotheses in the randomly generated spreadsheets which

means that the hypotheses is not mapping of any inactive molecules. The correlation and cost value of HYPO 1 with nineteen random spreadsheets were given in **Figure 5.13.**

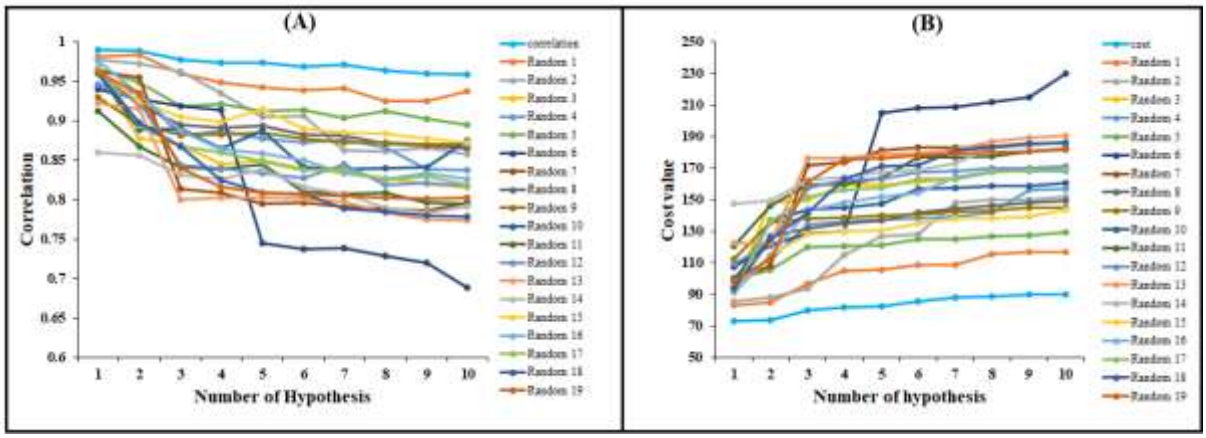

Figure 5.13: A graphical representation of **(A)** correlation and **(B)** cost of HYPO 1and nineteen random spreadsheets generated during Fischer randomization run with 95% confidence level.

The series of active compounds (most active compound **7**) fit into the right place of each pharmacophore attribute but the least compound fits less pharmacophoric feature as depicted in **Figure 5.12 (B** and **C)**. As checked by the **Figure 5.12 (B** and **C)** show that the most active compound **7** strongly mapped to all pharmacophoric features of HYPO 1. Compound **7** pharmacophoric fit value was also good (9.43) and accurately predicted. Also, the mapping of the modeling set components onto the HYPO 1 model using the best fit option was used to assess the predictability of the HYPO 1 model. The pharmacophore fit value along with the estimated activity scale for training set compounds is given in **Table 5.13**.

Table 5.13: Observed activity (nM), activity scale, estimated activity scale and fit value of training set molecules generated on the basis of HYPO 1 model.

Cmpd. No.	[a]Fit value	[b]Mapping [HBA, HBA_lipid, HYP, Ra]	Estimated/predicted activity	Estimated scale	Actual activity	Actual scale	[c]Error
1	8.41	[2 1 20 6]	28	+++	20	+++	1.4
4	6.65	[10 * 12 22]	1600	+	1360	+	1.176471
5	6.21	[26 * 23 1]	4400	+	3940	+	1.116751
6	5.59	17 14 2 *]	18000	+	13700	+	1.313869

7	9.43	[17 19 12 1]	2.6	+++	1.4	+++	1.857143
8	8.40	[1 2 22 3]	28	+++	60	+++	-2.14286
11	7.22	[30 * 29 12]	430	+++	430	+++	1
14	7.08	[4 * 6 20]	590	++	590	++	1
16	7.23	[6 * 4 19]	420	+++	660	++	-1.57143
17	7.06	[6 8 17 20]	630	++	750	++	-1.19048
20	6.74	[8 * 28 20]	1300	+	910	++	1.428571
26	6.65	[6 8 * 28]	1600	+	1320	+	1.212121
30	6.55	[45 * 17 26]	2000	+	2550	+	-1.275
33	6.27	[30 * 31 9]	3900	+	4150	+	-1.0641
34	6.37	[3 * 29 22]	3000	+	4290	+	-1.43
35	6.24	[27 28 * 12]	4100	+	4310	+	-1.05122
36	6.25	[6 28 * 19]	4100	+	4940	+	-1.20488
38	6.16	[37 39 * 25]	5000	+	5210	+	0.959693
39	5.98	[6 34 * 19]	7500	+	5290	+	1.417769
43	5.61	[13 22 19 *]	18000	+	20000	+	-1.11111

[a]Fit value: fit value is calculated by geometry fittings between hypothesis and compound

+++ = value less than equal to 500 (≤ 500 nM); ++ = value between 501 – 1000 nM (501 ≤ ++ ≤ 1000); + = value greater than equal to 1001 (≥ 1001)

[b]Mapping degree of specific pharmacophore features with specific conformation of the molecule, asterisk (*) indicate no conformation matching with pharmacophore features.

[c]error is calculated divided estimate activity value to actual value, inverse if actual value is greater than the measure activity value. Negative value if actual value greater than estimate value and vice versa.

Based on the activity scale only one best active (+++) compound was predicted as a moderate active (++) compound, one less active (+) compound was overestimated as moderate active (++), otherwise no highly active compound (+++) was predicted as less active compound (+) or vice versa. This indicates that pharmacophore HYPO 1 classifies the training set compound correctly predicted. Further, HYPO 1 model was evaluated by mapping the test set compound onto the HYPO 1 using the "Ligand Pharmacophore Mapping" protocol in D.S 3.0 [34] with maximum omitted features 2 and fitting methods rigid. The pharmacophore fit values along with the estimated activated scale of each test set compound was given in **Table**

5.14. It was shown that HYPO 1 model can estimate the inhibitory activity of compound beyond the training set compounds. However, few compounds from the external set (test set) were either overestimated or underestimated. As checked by the residual value of the external set, compounds 2, 9, 41, and 42 were considered outliers (**Figure 5.14**). After deleting those outliers R^2_{pred} was found to be 0.533 respectively.

Table 5.14: Test set prediction on the basis of best pharmacophore Hypo 1

Compd. no.	[a]Fit value	Actual activity value	Actual activity scale	Estimated activity value	Estimated Activity scale	[b]Error
2	6.07763	470	+++	5989.27	+	12.74313
3	6.94992	790	++	803.678	++	1.017314
9	5.94429	180	+++	8141.69	+	45.23161
10	6.48348	220	+++	2352.45	+	10.69295
12	7.22908	490	+++	422.58	+++	-1.15954
13	6.70241	570	++	1420.98	+	2.492947
15	6.2972	600	++	3612.47	+	6.020783
18	6.64812	830	++	1610.2	+	1.94
19	6.28608	850	++	3706.12	+	4.360141
21	6.27715	950	++	3783.12	+	3.982232
22	7.04399	1,010	+	647.152	++	-1.56068
23	6.92028	1,030	+	860.445	++	-1.19706
24	6.80208	1,030	+	1129.58	+	1.09668
25	6.47857	1,210	+	2379.2	+	1.966281
27	6.47707	1,800	+	2387.44	+	1.326356
28	6.64994	1,800	+	1603.48	+	-1.12256
29	6.35614	1,940	+	3154.02	+	1.625784
31	6.23814	2,570	+	4138.68	+	1.610381
32	6.54272	3,210	+	2052.47	+	-1.56397
37	6.53264	5,170	+	2100.69	+	-2.4611
40	6.04172	8,710	+	6505.43	+	-1.33888
41	6.5514	10,390	+	2011.89	+	-5.1643
42	6.21508	12,600	+	4364.31	+	-2.88705
44	6.47525	3,100	+	2397.46	+	-1.29304

[a]**Fit value**: fit value is calculated by geometry fittings between hypothesis and compound

+++ = value less than equal to 500 (≤ 500 nM); ++ = value between 501 – 1000 nM (501 ≤ ++ ≤ 1000); + = value greater than equal to 1001 (≥ 1001)

[b]**error** is calculated divided estimate activity value to actual value, inverse if actual value is greater than the measure activity value. Negative value if actual value greater than estimate value and vice versa.

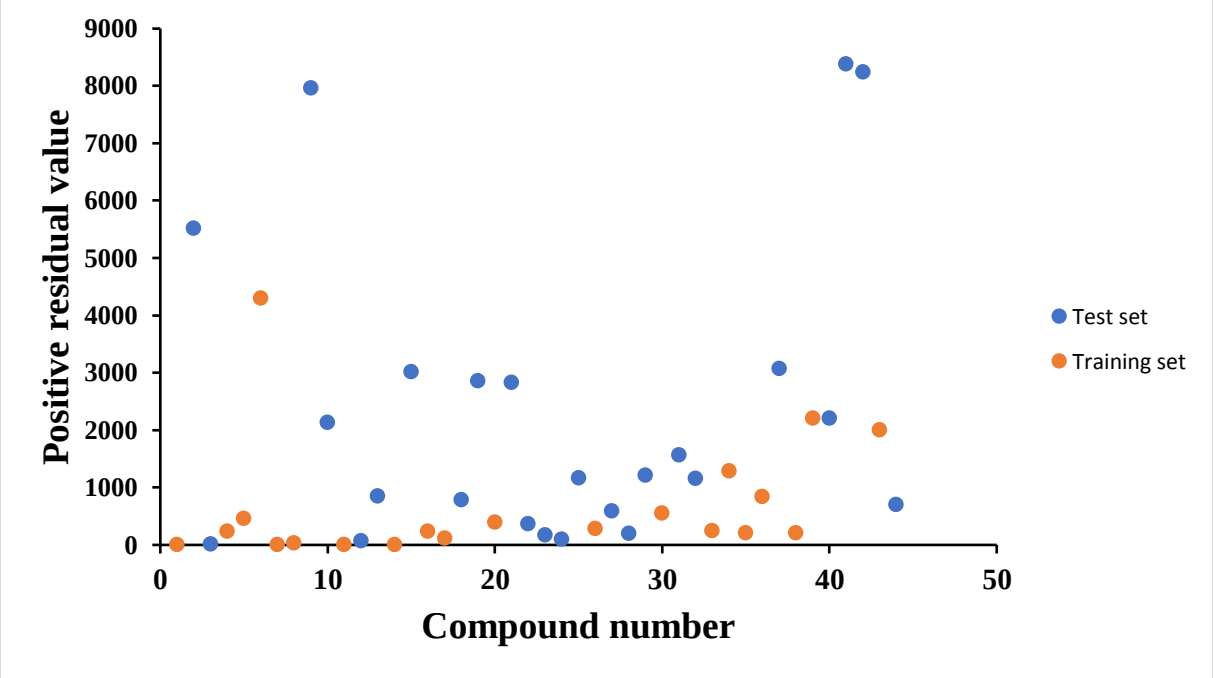

Figure 5.14: Schematic diagram for detecting outlier's compounds

5.7. Molecular docking studies for validation of the outcomes

The molecular docking was performed of some of the best active compounds by Schrodinger software. Only one crystal structure of HDAC3 (PDB ID: 4A69) is available in the protein data bank (PDB). The most active compounds (compounds 001 and 007) were chosen from the dataset for docking studies. After analyzing the complex between crystal structure of HDAC3 and inhibitors, it was observed that the hydroxamate group of both of these compounds formed a strong interaction with the catalytic Zn^{+} ion. Apart from that, the oxygen atom of the hydroxamate group of both these compounds makes a hydrogen bond with Asp259 and Tyr298 residue and coordinates with the Zn^{+} ion from the catalytic pocket of the HDAC3 enzyme. Additionally, the carbonyl oxygen of the hydroxamate moiety of compound 001 and the amide function adjacent to the phenyl group of compounds 007 formed a hydrogen bonding interaction with Tyr298 and Asp93, respectively (**Figure 5.15).** Interestingly, LDA models identified the importance of hydrogen bonds for HDAC3 inhibition. Moreover, the Bayesian, recursive partitioning, and SARpy models identified the importance of hydroxamate groups for HDAC3 inhibitors. Additionally, the benzine ring, and long carbon chain adjacent to the hydroxamate group of compounds 007, participated in two pi-stacking interactions with His22 and Phe200. Compound 001 participated in pi-sigma interaction with Phe200. Analysis of these two substances revealed a nearly identical pattern of binding in which they coordinated closely with the zinc in the catalytic pocket of HDAC3 at a short distance. The 2D structure of ligand-protein interaction of these two compounds is

given in **Figure 5.16**. Therefore, the docking study of these inhibitors proves the importance of structural features obtained by several classification QSAR studies conducted for finding the best structural features to inhibit the HDAC3 enzyme.

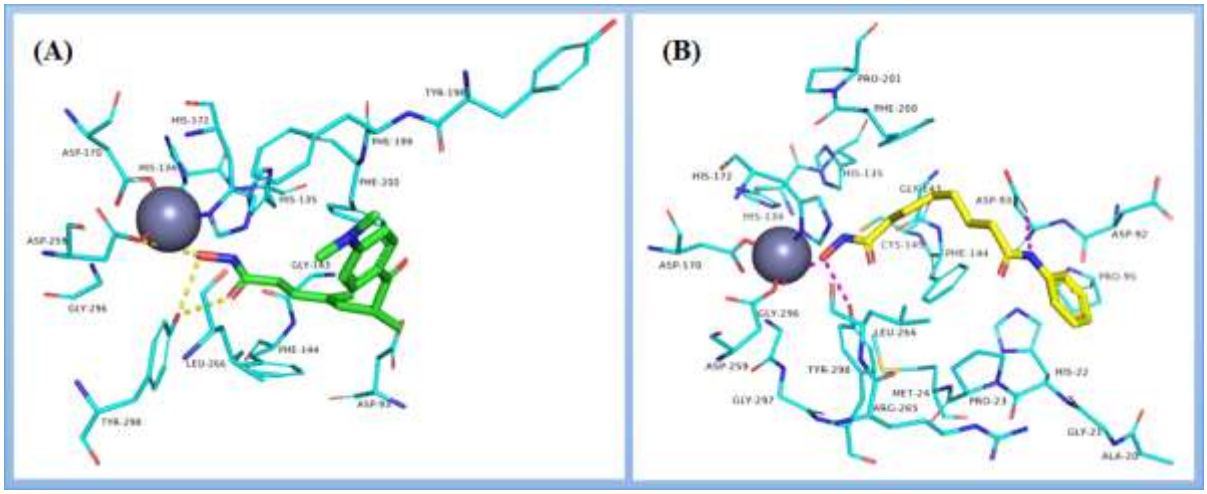

Fig. 5.15. Binding mode of interaction of most active compound **(A)** compound 001 **(B)** compound 007 for most active compound.

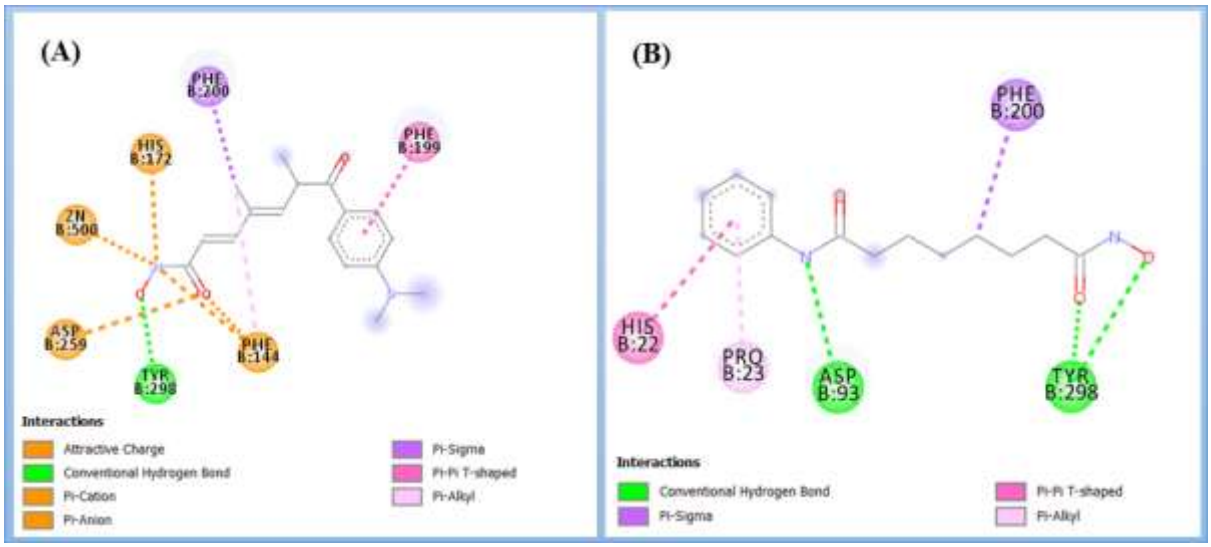

Figure 5.16. 2D representation of ligand-protein interactions of **(A)** compound 001 and **(B)** compound 007.

Chapter 6: Conclusion and Future Perspective

HDAC3 is a member of the histone deacetylase (HDAC) family that remove acetyl groups from histones and other proteins to alter gene expression and protein function. HDAC3 is a unique HDAC with distinct structural and functional features, such as its dependence on co-repressors for catalytic activity and subcellular localization, its interaction with various transcription factors and chromatin modifiers, and its regulation by post-translational modifications, and proteasomal degradation. HDAC3 plays an important role in several biological processes including cell cycle, apoptosis, differentiation, metabolism, and inflammation. Dysregulation of HDAC3 expression or activity has been implicated in the pathogenesis of various diseases, such as cancer, cardiovascular diseases, diabetes, neurodegenerative diseases, and kidney diseases. A variety of HDAC3 inhibitors has also been studied regarding their HDAC3 inhibitory potency and selectivity over other HDACs. Hence, inhibition or targeting selective HDAC3 is a great initiation to fight those diseases with fewer side effects due to its selectivity. In this context, several QSAR modeling studies have been performed which were used to find out important structural features of these compounds with highly effective HDAC3 inhibitors. The hydroxamate group with a long chain plays a crucial role in HDAC3 inhibitors which were suggested by all classification studies and also adjudicated by ligand-protein interaction. This hydroxamate group makes a strong bond with Tyr298 residue at the enzyme active site. Nevertheless, thiazole and iso-butyraldehyde were also important structural features responsible for effective HDAC3 inhibitory activity. It was observed that the carboxamide linker group negatively correlated with biological activity that decreased the inhibitory activity of the molecule. Moreover, the zinc-binding group (hydroxamate) with a longer chain suggested by Bayesian classification, RP, and SARpy studies was found to coordinate with the catalytic zinc of HDAC3, which was significant for HDAC3 inhibitors. Thiol, lysine, and arginine moieties also play crucial for HDAC3 inhibitors. It was noticed that the 2D-QSAR equation by multiple linear regression techniques gave a high correlation with a significant positive GATS1m and GATS3s descriptor. The 3D-QSAR model showed that the position of HBA, HBA_L, HBD, and RA features are important at specific distances to enhance the activities of molecules against HDAC3.

Nonetheless, from this study, it is quite clear that the development of selective HDAC3-specific inhibitors is required for the treatment of HDAC3-related pathophysiological conditions including cancer. Therefore, this study of HDAC3 inhibitors can be useful for the development of such specific inhibitors that can be utilized effectively for the treatment of

HDAC3-associated pathophysiology. In this context, it was noticed that very less computational/other methods have been applied to existing HDAC3 inhibitors. Moreover, the lack of selective and active HDAC3 inhibitors may also hinder the discovery of novel therapeutic candidates. HDAC3 inhibitors have demonstrated promising therapeutic effects in preclinical and clinical studies for a variety of diseases. However, given the structural variety and functional complexity of HDAC3, it is difficult to develop strong and selective HDAC3 inhibitors. Two main approaches have been used to design HDAC3 inhibitors: LBDD and SBDD. The goal of ligand-based drug design is to develop new substances with higher potency, selectivity, and pharmacokinetics properties by focusing on the chemical characteristics and structure of known ligands (molecules that bind to the target protein). The investigation of current HDAC3 inhibitors and their structure-activity relationships (SARs) can be used in the context of HDAC3 inhibition to pinpoint crucial structural elements that affect their binding and activity. Using this knowledge, new drug candidates can be created that are more potent and selective against HDAC3. On the other hand, structure-based drug design uses the three-dimensional structure of the target protein (e.g., HDAC3) to give an idea for novel inhibitors. Researchers can determine potential binding sites and interactions between the protein and small compounds by examining the three-dimensional structure of HDAC3. Using this knowledge, it is, therefore, possible to build or improve drugs that can bind to HDAC3 and interact with certain amino acid residues to block the enzymatic functions. The future perspective of ligand-based and structure-based drug design for HDAC3 inhibition is promising. The accuracy and effectiveness of these methods will be improved by the ongoing developments in computational techniques for the development of new drug candidates. Furthermore, artificial intelligence machine learning techniques can accelerate the drug discovery process by predicting the binding affinity of potential HDAC3 inhibitors. Additionally, the combination of ligand-based and structure-based drug design, known as hybrid methods, can leverage the strengths of both strategies to design more potent and selective HDAC3 inhibitors. Overall, a multidisciplinary strategy combining computational modeling, structural biology, and experimental validation will be used in drug design for HDAC3 inhibition in the future. These methods have a great deal of promise for the development of novel HDAC3 inhibitors with enhanced therapeutic effects to treat a range of disorders, including cancer and other diseases. Therefore, not only the LBDD and SBDD strategies but also the intuitive design methodologies may also be useful for the finding of new HDAC3-related drugs. There have been several studies done on the molecular mechanism of HDAC3 inhibitors. These investigations are still going on. However, there is a

lack in the discovery of novel potential and HDAC3-selective inhibitors. In a nutshell, this perspective offers a full understanding of both the function of HDAC3 in several diseases and a wide range of selective HDAC3 inhibitors. Hopefully, this will be helpful for researchers to find potential HDAC3 selective inhibitors.

References

References

[1] https://www.who.int/newsroom/factsheets/detail/cancer#:~:text=breast%20(2.26%20million%20cases)%3B,prostate%20(1.41%20million%20cases)%3B (Accessed on 03 May 2023)

[2] H. Wang, C. Fu, J. Du, H. Wang, R. He, X. Yin, H. Li, X. Li, H. Wang, K. Li, L. Zheng, Enhanced histone H3 acetylation of the PD-L1 expression in drug-resistant cancer cells, J. Exp. Clin. cancer Res. 39 (2020) 1-16. doi: 10.1186/s13046-020-1536-x.

[3] https://www.cancer.gov/about-cancer/causes-prevention/risk (accessed on 28th Aug 2023)

[4] https://www.cancer.gov/about-cancer/causes-prevention (accessed on 28th Aug 2023)

[5] C. de Castro Sant'Anna, A.G.F. Junior, P. Soares, F. Tuji, E. Paschol, L.C. Chaves, R.R. Burbano, Molecular biology as a tool for the treatment of cancer, Clin. Exp. Med. 18 (2018) 457-464. doi: 10.1007/s10238-018-0518-1.

[6] J.J. Wang, K.F. Lei, F. Han, F. Tumor microenvironment: Recent advances in various cancer treatments, Eur. Rev. Med. Pharmacol. Sci. 22 (2018) 3855-3864. doi: 10.26355/eurrev_201806_15270.

[7] A. Beddok, Y. Kirova, F. Laki, F. Reyal, A. Vincent Salomon, V. Servois, A. Fourquet, The place of the boost in the breast cancer treatment: State of art, Radiother. Oncol. 170 (2022) 55-63. doi: 10.1016/j.radonc.2022.03.010.

[8] M.J. Elliott, B. Wilson, D.W. Cescon, Current treatment and future trends of immunotherapy in breast cancer, Curr. Cancer Drug Targets, 22 (2022) 667-677. doi: 10.2174/1568009622666220317091723.

[9] A. Skelly, A. O'Donovan, Recognizing Frailty in Radiation Oncology Clinical Practice: Current Evidence and Future Directions, Semin. Radiat. Oncol. 32 (2022) 115-124. doi: 10.1016/j.semradonc.2021.11.010.

[10] M. Mottamal, S. Zheng, T.L. Huang, and G. Wang, Histone deacetylase inhibitors in clinical studies as templates for new anticancer agents, Molecules 20 (2015) 3898-3941. doi: 10.3390/molecules20033898.

[11] N. Kumbhar, S. Nimal, S. Barale, S. Kamble, R. Bavi, K. Sonawane, and R. Gacche, Identification of novel leads as potent inhibitors of HDAC3 using ligand-based pharmacophore modeling and MD simulation, Sci. Rep. 12 (2022) 1-21. doi: 10.1038/s41598-022-05698-7.

References

[12] B. C. Smith, and J.M. Denu, Chemical mechanisms of histone lysine and arginine modifications, Biochim. Biophys. Acta. Gene Regul. Mech. 1789 (2009) 45-47. doi: 10.1016/j.bbagrm.2008.06.005.

[13] T.Y. Kim, Y.J. Bang, and K.D. Robertson, Histone deacetylase inhibitors for cancer therapy, Epigenetics 1 (2006) 15-24. doi: 10.4161/epi.1.1.2644.

[14] R. Sangwan, R. Rajan, and P.K. Mandal, HDAC as onco target Reviewing the synthetic approaches with SAR study of their inhibitors, Eur. J. Med. Chem. 158 (2018) 620-706. doi: 10.1016/j.ejmech.2018.08.073.

[15] S.S. Soflaei, A.A. Momtazi-Borojeni, M. Majeed, G. Derosa, P. Maffioli, and A. Sahebkar, Curcumin: a natural pan-HDAC inhibitor in cancer, Curr. Pharm. Des. 24 (2018) 123-129. doi: 10.2174/1381612823666171114165051.

[16] S.Y. Park, J.S. Kim, A short guide to histone deacetylases including recent progress on class II enzymes, Exp. Mol. Med. 52 (2020) 204-212. doi: 10.1038/s12276-020-0382-4.

[17] P.A. Marks, The clinical development of histone deacetylase inhibitors as targeted anticancer drugs, Expert. Opin. Investig. Drugs, 19 (2010) 1049-1066. doi: 10.1517/13543784.2010.510514.

[18] S.G. Gray, T.J. Ekström, The human histone deacetylase family, Exp. Cell. Res. 262 (2001) 75-83. doi: 10.1006/excr.2000.5080.

[19] E. Verdin, F. Dequiedt, H.G. kasler, Class II histone deacetylases: versatile regulators, Trends Genet. 19 (2003) 286-293. doi: 10.1016/S0168-9525(03)00073-8.

[20] E. Seto, M. Yoshida, Erasers of histone acetytlation: the histone deacetylase enzymes, Cold Spring Harb Perspect Biol. 6 (2014) a018713. doi: 10.1101/cshperspect.a018713.

[21] G. Blander, L. Guarente, The Sir2 family of protein deacetylases, Annu. Rev. Biochem. 73 (2004) 417-435. doi: 10.1146/annurev.biochem.73.011303.073651.

[22] L. Tong, H. Liang, H. Zhuang, C. Liu, Z. Zhang, The relationship between HDAC3 and malignant tumors: a mini review, Crit. Rev. Eukaryot. Gene Expr. 30 (2020) 279-284. doi: 10.1615/CritRevEukaryotGeneExpr.2020034380.

[23] https://www.uniprot.org/uniprotkb/Q13547/publications. (Accessed on 20 June 2023)

[24] I. Bauer, D. Varadarajan, A. Pidroni, S. Gross, S. vergeiner, B. Faber, S. Graessle, A class 1 histone deacetylase with potential as an antifungal target, MBio 7 (2016) e00831-16. doi: 10.1128/mbio.00831-16.

[25] D.M. Vigushin, R.C. Coombes, Histone deacetylase inhibitors in cancer treatment, Anti-cancer drugs 13 (2002) 1-3. doi: 10.1097/00001813-200201000-00001.

[26] J. Tauton, C.A. Hassig, S.L. Schreiber, A mammalian histone deacetylase related to the yeast transcriptional regulator Rpd3, Science 272 (1996) 408-411. doi: 10.1126/science.272.5260.408.

[27] S. Emiliani, W. Fischle, C.V. Lint, Y. Al-Abed, E. Verdin, Characterization of a human RPD3 ortholog, HDAC3, Proc. Natl. Acad. Sci. 95 (1998) 2795-2800. doi: 10.1073/pnas.95.6.27.

[28] N.R. Bertos, A.H. Wang, X.J. Yang, Class II histone deacetylases: structure, function, and regulation, Biochem. cell Biol. 79 (2001) 243-252. doi: 10.1139/o01-032.

[29] R.A. Mathias, A.J. Guise, I.M. Cristea, Post-translational modifications regulate Class IIa histone deacetylase (HDAC) function in health and disease*[S], Mol. Cell. Proteom. 14 (2015) 456-470. doi: 10.1074/mcp.O114.046565.

[30] W. Fischle, V. kiermer, F. Dequiedt, E. verdin, The emerging role of class II histone deacetylases, Biochem. Cell. Biol. 79 (2001) 337-348. doi: 10.1139/o01-116.

[31] J. Wang, T.H. Kim, M.Y. Ahh, J. Lee, J.H. Jung, B.M. Lee, K.S. Yoon, S. Yoon, H.S. Kim, Sirtinol, a class III HDAC inhibitor, induces apoptotic and autophagic cell death in MCF-7 human breast cancer cells, Int. J. Oncol. 41 (2012) 1101-1109. doi: 10.3892/ijo.2012.1534.

[32] S. Michan, D. Sinclair, Sirtuins in mammals: insights into their biological function, Biochem. J. 404 (2007) 1-13. doi: 10.1042/BJ20070140.

[33] J.M. Mariadason, HDACs AND HDAC inhibitors in colon cancer, Epigenetics 3 (2008) 28-37. doi: 10.4161/epi.3.1.5736.

[34] Y. Núñez- Álvarez, M. Suelves, HDAC11: a multifaceted histone deacetylase with proficient fatty deacylase activity and its roles in physiological processes, FEBS. J. 289 (2022) 2771-2792. doi: 10.1111/febs.15895.

[35] S. Bhaskara, Histone deacetylase 11 as a key regulator of metabolism and obesity, EBioMedicine 35 (2018) 27-28. doi: 10.1016/j.ebiom.2018.08.008.

[36] M. Haberland, R.L. Montgomery, E.N. Olson, The many roles of histone deacetylases in development and physiology: implications for disease and therapy, Nat. Rev. Genet. 10 (2009) 32-42. doi: 10.1038/nrg2485.

[37] R. Sarkar, S. Banerjee, S.A. Amin, N. Adhikari, and T. Jha, Histone deacetylase 3 (HDAC 3) inhibitors as anticancer agents: A review, Eur. J. Chem. 192 (2020) 112171. doi: 10.1016/j.ejmech.2020.112171.

References

[38] Y. Ma, J. Duan, and X. Hao, Down-regulated HDAC3 elevates microRNA-495-3p to restrain epithelial-mesenchymal transition and oncogenicity of melanoma cells via reducing TRAF5, J. Cell. Mol. Med. 24 (2020) 12933-12944. doi: 10.1111/jcmm.15885.

[39] J. Li, M. Hu, N. Liu, H. Li, Z. Yu, Q. Yan, M. Zhou, Y. Wang, Y. Song, G. Pan, and F. Liang, HDAC3 deteriorates colorectal cancer progression via microRNA-296-3p/TGIF1/TGFβ axis, J. Exp. Clin. Cancer Res. 39 (2020) 1-13. doi: 10.1186/s13046-020-01720-w.

[40] D.Q. Chen, C. Yu, X.F. Zhang, Z.F. Liu, R. Wang, M. jiang, H. Chen, F. Yan, M. Tao, L.B. Chen, and H. Zhu, HDAC3-mediated silencing of miR-451 decreases chemosensitivity of patients with metastatic castration-resistant prostate cancer by targeting NEDD9, Ther. Adv. Med. Oncol. 10 (2018) 1758835918783132. doi: 10.1177/1758835918783132.

[41] M. Li, C. Long, G. Yang, Y. Luo, and H. Du, MiR-26b inhibits melanoma cell proliferation and enhances apoptosis by suppressing TRAF5-mediated MAPK activation, Biochem. Biophys. Res. Commun. 471 (2016) 361-367. doi: 10.1016/j.bbrc.2016.02.021.

[42] C. Liu, L. Liu, J. Shan, J. Shen, Y. Xu, Q. Zhang, Z. Yang, L. Wu, F. Xia, P. Bie, Y. Cui, X. Zhang, X. Bian, C. Qian, Histone deacetylase 3 participates in self-renewal of liver cancer stem cells through histone modification, Cancer Lett. 339 (2013) 60-69. doi: 10.1016/j.canlet.2013.07.022.

[43] T. Harda, H. Ohguchi, Y. Grondin, S. Kikuchi, M. Sagawa, Y.T. Tai, R. Mazitschek, T. Hideshima, K.C. Anderson, HDAC 3 regulates DNMT1 expression in multiple myeloma: therapeutic implications, Leukemia 31 (2017) 2670-2677. doi: 10.1038/leu.2017.144.

[44] J. Minami, R. Suzuki, R. Mazitschek, G. Gorgun, B. Ghosh, D. Cirstea, and K.C. Anderson, Histone deacetylase 3 as a novel therapeutic target in multiple myeloma, Leukemia 28 (2014) 680-689. doi: 10.1038/leu.2013.231.

[45] P. Karagianni, and J. Wong, HDAC3: taking the SMRT-N-CoRrect road to repression, Oncogene 26 (2007) 5439-5449. doi: 10.1038/sj.onc.1210612.

[46] N. Adhikari, S.A. Amin, P. Trivedi, T. Jha, and B.Ghosh, HDAC3 is a potential validated target for cancer: An overview on the benzamide-based selective HDAC3 inhibitors through comparative SAR/QSAR/QAAR approaches, Eur. J. Med. Chem. 157 (2018) 1127-1142. doi: 10.1016/j.ejmech.2018.08.081.

References

[47] C. Angiolilli, P.A. Kabala, A.M. Grabiec, I.M. Van Baarsen, B.S. Ferguson, S. Garcia, B.M. Fernandez, T.A. McKinsey, P.P. Tak, G. Fossati, and P. Mascagni, Histone deacetylase 3 regulates the inflammatory gene expression programme of rheumatoid arthritis fibroblast-like synoviocytes, Ann. Rheum. Dis. 76 (2017) 277-285. doi: 10.1136/annrheumdis-2015-209064.

[48] B.C. Meier, and B.K. Wagner, Inhibition of HDAC3 as a strategy for developing novel diabetes therapeutics, Epigenomics 6 (2014) 209-214. doi: 10.2217/epi.14.11.

[49] M.A. Hoeksema, M.J. Gijbels, J. van den Bossche, S. Van der Velden, A. Sijm, A.E. Neela, T. Seijkens, J.L. Stöger, S. Meiler, M.C. Boshuizen, and G.M. Dallinga-Thie, Targeting macrophage Histone deacetylase 3 stabilizes atherosclerotic lesions, EMBO Mol. Med. 6 (2014) 1124-1132. doi: 10.15252/emmm.201404170.

[50] S.R. D'Mello, Histone deacetylase-3: Friend and foe of the brain, Exp. Biol. Med. 245 (2020) 1130-1141. doi: 10.1177/15353702209282.

[51] K. Huber, G. Doyon, J. Plaks, E. Fyne, J.W. Mellors, N. Sluis-Cremer, Inhibitors of histone deacetylases: correlation between isoform specificity and reactivation of HIV type 1 (HIV-1) from latently infected cells, J. Biol. Chem. 286 (2011) 22211-22218. doi: 10.1074/jbc.M110.180224.

[52] L. Zhang, W. Cao, Histone deacetylase 3 (HDAC3) as an important epigenetic regulator of kidney diseases, J. Mol. Med. 100 (2022) 43-51. doi: 10.1007/s00109-021-02141-8.

[53] L. Zeng, G. WangD. Ummarino, A. Margariti, Q. Xu, Q. Xiao, W. Wang, Z. Zhang, X. Yin, M. mayr, G. Cockerill, Histone deacetylase 3 unconventional splicing mediates endothelial-to-mesenchymal transition through transforming growth factor β2, J. Biol. Chem. 288 (2013) 31853-31866. doi: 10.1074/jbc.M113.463745.

[54] Y.D. Wen,V. perissi, L.M. Stastzewski, W.M. Yang, A. Krones, C.K. Glass, M.G. Rosenfeld, E. Seto, The histone deacetylase-3 complex contains nuclear receptor corpressors, Proc. Natl. Acd. Sci. 97 (2000) 7202-7207. doi: 10.1073/pnas.97.13.7202.

[55] T. Tabata, K. Kokura, P. Ten Dijke, S. Ishii, Ski co-repressor complexes maintain the basal repressed state of the TGF- β target gene, SMAD7, via HDAC3 and PRMT5, Genes Cells 14 (2009) 17-28. doi: 10.1111/j.1365-2443.2008.01246.x.

[56] P.J. Watson, L. Fairall, G.M. Santos, J. WR Schwabe, Structure of HDAC3 bound to co-repressor and inositol tetraphosphate, Nature 481 (2012) 335-340. doi: 10.1038/nature10728.

References

[57] V.R. RUSSANOVA, T. HIRAI, N.Y. QIN, B. HOWARD, Stable histone deacetylase complexes distinguished by the presence of SANT domain proteins CoREST/kiaa0071 and Mta-LI, J. Bioi. Chern. 276 (2001) 6817-24. doi: 10.1074/jbc.M007372200.

[58] Y. Zhang, H.H. Ng, H. Erdjument-Bromage, P. Tempst, A. Bird, D. Reinberg, Analysis of the NuRD subunits reveals a histone deacetylase core complex and a connection with DNA methylation, Genes Dev. 13 (1999) 1924-1935. doi: 10.1101/gad.13.15.1924.

[59] T. Heinzel, R.M. Lavinsky, T.M. Mullen, M. Söderstrom, C.D. Laherty, J. Torchia, W.M. Yang, G. Brard, S.D. ngo, J.R. Davie, E. Seto, R.N. Eisenman, D.W. rose, C.K. Glass, M.G. Rosenfeld, A complex containing N-CoR, mSin3 and histone deacetylase mediates transcriptional repression, Nat. 387 (1997) 43-48. doi:10.1038/387043a0.

[60] M.G. Guenther, O.R.R. Barak, M.A. Lazar, The SMRT and N-CoR corepressors are activating cofactors for histone deacetylase 3, Mol. Cell. Biol. 21 (2001) 6091-6101. doi: 10.1128/MCB.21.18.6091-6101.2001.

[61] J.R. Somoza, R.J. Skene, B.A. katz, C. Mol, J.D. Ho, A.J. Jennings, C. Luong, A. Arvai, J.J. Buggy, E. Chi, J. Tang, Structural snapshots of human HDAC8 provide insights into the class I histone deacetylases, Structure, 12 (2004) 1325-1334. doi: 10.1016/j.str.2004.04.012.

[62] P.J. Watson, L. Fairall, G.M. Santos, J.W. Schwabe, Structure of HDAC3 bound to co-repressor and inositol tetraphosphate, Nature, 481 (2012) 335-340. doi: 10.1038/nature10728.

[63] N. Wanner, W. Bechtel-Walz, Epigenetics of kidney disease, Cell Tissue Res. 369 (2017) 75-92. doi: 10.1007/s00441-017-2588-x.

[64] H.R. kim, B.Y. Nam, D.W. Kim, M.W. Kang, J.H. Han, M.j. lee, D.H. shin, F.M. Doh, H.M. Koo, K.I. Ko, C.H. kim, Circulating α-klotho levels in CKD and relationship to progression, Am. J. Kidney Dis. 61 (2013) 899-909. doi: 10.1007/s00109-021-02044-8.

[65] L. Zhang, W. Cao, Histone deacetylase 3 (HDAC3) as an important epigenetic regulator of kidney diseases, J. Mol. Med. 100 (2022) 43-51. doi: 10.1007/s00109-021-02141-8.

[66] P. Corrales, A. Izquierdo-Lahuerta, G. Medina-Gómez, Maintenance of kidney metabolic homeostatis by PPAR gamma. Int. J. Mol. sci. 19 (2018) 2063. doi: 10.3390/ijms19072063.

[67] F. Chen, Q. Gao, A. Wei, X. Chen, Y. Shi, H. Wang, W. Cao, Histone deacetylase 3 aberration inhibits Klotho transcription and promotes renal fibrosis, Cell Death Differ. 28 (2021) 1001-1012. doi: 10.1038/s41418-020-00631-9.

[68] L.L. Brilli, L.M. Swanhart, MP. de Caestecker, N.A. Hukriede, HDAC inhibitors in kidney development and disease, Pediatr. Nephrol. 28 (2013) 1909-1921. doi: 10.1007/s00467-012-2320-8.

[69] N. Mishra, C.M. Reilly, D.R. Brown, P. Ruiz, G.S. Gilkeson, Histone deacetylase inhibitors modulate renal disease in the MRL-lpr/ipr mouse, J. Clin. Invest. 111 (2003) 539-552. doi: 10.1172/JCI16153.

[70] T.L. Cha, M.J. Chuang, S.T. Wu, G.H. Sun, S.Y. Chang, D.S. Yu, S.M. Huang, S.K.H. Huan, T.C. Cheng, T.T. Chen, P.L. Fan, Dual degradation of aurora A and B kinases by the histone deacetylase inhibitor LBH589 induces G2-M arrest and apoptosis of renal cancer cells, Clin. cancer. Res. 15 (2009) 840-850. doi: 10.1158/1078-0432.CCR-08-1918.

[71] H.K. Kwon, S.H. Ahn, S.H. Park, J.H. Park, J.W. Park, H.M. Kim, S.K. Park, K. Lee, C.W. Choi, G. Han, A novel γ-lactam-based histone deacetylase inhibitor potently inhibits the growth of human breast and renal cancer cells, Biol. Pharm. Bull. 32 (2009) 1723-1727. doi: 10.1248/bpb.32.1723.

[72] L.P. Jiang, X.H. Yu, J.Z. Chen, M. Hu, Y.K. Zhang, H.L. Lin, W.Y. Tang, P.P. He, X.P. Ouyang, Histone Deacetylase 3: A Potential Therapeutic Target for Atherosclerosis, Aging Dis. 13 (2022). doi: 10.14336/AD.2021.1116.

[73] S.A. Manea, M.L. Vlad, I.M. Fenyo, A.G. Lazar, M. Raicu, H. Muresian, M. Simionescu, A. Manea, Pharmacological inhibition of histone deacetyalse reduces NADPH oxidase expression, oxidative stress and the progression of atherosclerotic lesions in hypercholesterolemic apolipoprotein E-deficient mice; potential implications for human atherosclerosis, Redox Biol. 28 (2020) 101338. doi: 10.1016/j.redox.2019.101338.

[74] https://medlineplus.gov/download/genetics/gene/abca1.pdf (Accessed on 20 July 2023)

[75] https://medlineplus.gov/genetics/gene/abca1/ (Accessed on 25 July 2023).

[76] https://www.ncbi.nlm.nih.gov/gene?Db=gene&cmd=showDetailView&TermToSearch=9619 (Accessed on 01 august 2023).

[77] T. Engel, G. Bode, A. Leuken, M. Knop, F. Kannenberg, J.R. Nofer, G. Assmann, U. Seedorf, Expression and functional characterization of ABCG1 splice variant ABCG1 (666), FEBS lett. 580 (2006) 4551-4559. doi: 10.1016/j.febslet.2006.07.006.

[78] W. Huang, J. Zhou, G. Zhang, Y. Zhang, H. Wang, Decreased H3K9 acetylation level of LXRα mediated dexamethasone-induced placental cholesterol transport dysfunction, Biochim. Biophys. Acta Mol. Cell. Biol. Lipids BBA-Mol. Cell Biol. Lipids, 1864 (2019) 158524. doi: 10.1016/j.bbalip.2019.158524.

[79] D. Li, X. Wang, W. Ren J. Ren, X. Lan, F. Wang, H. Li, F. Zhang, Y. Han, T. Song, R. Holmdahl, High expression of liver histone deacetylase 3 contributes to high-fat-diet-induced metabolic syndrome by suppressing the PPAR-γ and LXR-α-pathways in E3 rats, Mol. Cell. Endocrinol. 344 (2011) 69-80. doi: 10.1016/j.mce.2011.06.028.

[80] X.H. Yu, W.Y. Deng, J.J. Chen, X.D. Xu, X.X. Liu, L.Chen, M.W. Shi, Q.X. Liu, M. Tao, K. Ren, LncRNA kcnq1ot1 promotes lipid accumulation and accelerates atherosclerosis via functioning as a ceRNA through the miR-452-3p/HDAC3/ABCA1 axis, Cell Death Dis. 11 (2020) 1043. doi: 10.1038/s41419-020-03263-6.

[81] D. Martin, Y. Li, J. Yang, G. Wang, A. Margariti, Z. Jiang, H. Yu, A. Zampetaki, Y. Hu, Q. Xu, L. Zeng, Unspliced X-box-binding protein 1 (XBP1) protects endothelial cells from oxidative stress through interaction with histone deacetylase 3, J. Biol. Chem. 289 (2014) 30625-30634. doi: 10.1074/jbc.M114.571984.

[82] G. Pizzino, N. Irrera, M. Cucinotta, G. pallio, F. Mannino, V. Arcoraci, F. Squadrito, D. Altavilla, A. Bitto, Oxidative stress: harms and benefits for human health, Oxid. Med. Cell. longev. 2017. doi: 10.1155/2017/8416763.

[83] H. Sies, C. Berndt, D.P. Jones, Oxidative Stress, Annu. Rev. Biochem. 86 (2017) 715-748. doi: 10.1016/j.redox.2015.01.002.

[84] X. Chen, I. Barozzi, A. Termanini, E. Prosperini, A. Recchiuti, J. dalli, F. Mietton, G. Matteoli, S. Hiebert, G. Natoli, Requirement for the inflammatory gene expression program in macrophages, Proc. Natl. Acad. Sci. 109 (2012) E2865-E2874. doi: 10.1073/pnas.11211311.

[85] M. Saraiva, A. O'garra, The regulation of IL-10 production by immune cells, Nat. Rev. Immunol. 10 (2010) 170-181. doi: 10.1038/nri2711.

[86] L. Chen, C. Shang, B. Wang, G. Wang, Z. Jin, F. Yao, Z. Yue, L. Bai, R. Wang, S. Zhao, E. Liu, W. Wang, HDAC3 inhibitor suppresses endothelial-to-mesenchymal transition via modulating inflammatory response in atherosclerosis, Biochem. Pharmacol. 192 (2021) 114716. doi: 10.1016/j.bcp.2021.114716.

[87] J.C. Ozougwu, K.C. Obimba, C.D. Belonwu, C.B. Unakalamba, The pathogenesis and pathophysiology of type 1 and type 2 diabetes mellitus, J. Physiol. Pathophysiol. 4 (2013) 46-57. doi: 10.5897/JPAP2013.0001.

[88] B.C. Meier, B.K. Wagner, Inhibition of HDAC3 as a strategy for developing novel diabetes therapeutics, Epigenomics, 6 (2014) 209-214. doi: 10.2217/epi.14.11.

[89] X. Jiang, X. ye, W. Guo, H. Lu, Z. Gao, Inhibition of HDAC3 promotes ligand-independent PPARγ activation by protein acetylation, J. Mol. Endocrinol. 53 (2014) 191. doi: 10.1530/JME-14-0066.

[90] D.P. Christensen, M. Dahllöf, M. Lundh, D.N. Rasmussen, M.D. Nielsen, N. Billestrup, L.G. Grunnet, T. Mandrup-Poulsen, Histone deacetylase (HDAC) inhibition as a novel treatment for diabetes mellitus, Mol. Med. 17 (2011) 378-390. doi: 10.2119/molmed.2011.00021.

[91] B.C. Meier, B.K. Wagner, Inhibition of HDAC3 as a strategy for developing novel diabetes therapeutics, Epigenomics 6 (2014) 209-214. doi: 10.2217/epi.14.11.

[92] D.D. Yao, L. Yang, Y. Wang, C. Liu, Y.J. Wei, X.B. Jia, W. Yin, L. Shu, Geniposide promotes beta-cell regeneration and survival through regulating β-catenin/TCF7L2 pathway, Cell Death Dis. 6 (2015) e1746-e1746. doi: 10.1038/cddis.2015.107.

[93] F.F. Wagner, M. Lundh, T. Kaya, P. McCarren, Y.L. Zhang, S. Chattopadhyay, J.P. Gale, T. Galbo, S.L. Fisher, B.C. Meier, A. Vetere, An isochemogenic set of inhibitors to define the therapeutic potential of histone deacetylases in β-cell protection, ACS Chem. Biol. 11 (2016) 363-374. doi: 10.1021/acschembio.5b00640.

[94] J. Tian, H. Dang, A. Hu, W. Xu, D.L. Kaufman, Repurposing lesogaberan to promote human islet cell survival and β-cell replication, J. Diabetes Res. (2017). doi: 10.1155/2017/6403539.

[95] A. Fischer, F. Sananbenesi, A. Mungenast, L.H. Tsai, Targeting the correct HDAC (s) to treat cognitive disorders, Trends Pharmacol. Sci. 31 (2010) 605-617. doi: 10.1016/j.tips.2010.09.003.

[96] S.C. McQuown, M.A. Wood, HDAC3 and the molecular brake pad hypothesis, Neurobiol. Learn. Mem. 96 (20111) 27-34. doi: 10.1016/j.nlm.2011.04.005.

[97] S.C. McQuown, R.M. Barrett, D.P. Matheos, R.J. post, G.A. Rogge, T. Alenghat, S.E. Mullican, S. Jones, J.R. Rusche, M.A. Lazar, M.A. Wood, HDAC3 is a critical negative regulator of long-term memory formation, J. Neurosci. 31 (2011) 764-774. doi: 10.1523/JNEUROSCI.5052-10.2011.

[98] K.J. Janczura, C.H. Volmer, G.C. Sartor, S.J. Rao, N.R. Ricciardi, G. Lambert, S.P. Brothers, C. Wahlestedt, Inhibition of HDAC3 reverses Alzheimer's disease-related pathologies in vitro and in the 3xTg-AD mouse model, Proc. natl. Acad. Sci. 115 (2018) E11148-E11157. doi: 10.1073/pnas.18054361.

[99] H.K. Choi, Y. Choi, H. kang, E.J. lim, S.Y. Park, H.S. Lee, J.M. Park, J. Moon, Y.J. Kim, I. Choi, E.H. joe, PINK1 positively regulates HDAC3 to suppress dopaminergic neuronal cell death, Hum. Mol. Genet. 24 (2015) 1127-1141. doi: 10.1093/hmg/ddu526.

[100] H. Jia, Y. Wang, C.D. Morris, V. Jacques, J.M. Gottesfeld, J.R. Rusche, E.A. Thomas, The effects of pharmacological inhibition of histone deacetylase 3 (HDAC3) in Huntington's disease mice, PLoS One 11 (2016) e0152498. doi: 10.1371/journal.pone.0152498.

[101] J.L. Kwapis, Y. Alaghband, A.J. López, J.M. Long, X. Li, G. Shu, K.K. Bodinayake, D.P. Matheos, P.R. Rapp, M.A. Wood, HDAC3-mediated repression of the Nr4a family contributes to age-related impairments in long-term memory, J. Neurosci. 39 (2019) 4999-5009. doi: 10.1523/JNEUROSCI.2799-18.2019.

[102] K.A. Han, W.H. Shin, S. Jung, W. Seol, H. Seo, C. Ko, K.C. Chung, Leucine-rich repeat kinase 2 exacerbates neuronal cytotoxicity through phosphorylation of histone deacetylase 3 and histone deacetylation, Hum. Mol. Genet. 26 (2017) 1-18. doi: 10.1093/hmg/ddw363.

[103] E.A. Bates, M. Victor, A.K. Jones, Y. Shi, A.C. Hart, Differential contributions of Caenorhabditis elegans histone deacetylases to huntingtin polyglutamine toxicity, J. Neurosci. 26 (2006) 2830-2838. doi: 10.1523/JNEUROSCI.3344-05.2006.

[104] K. Hecklau, S. Mueller, S.P. Koch, M.H. Mehkary, B. Kilic, C. Harms, P. Boehm-Stum, F. Yildirim, The effects of selective inhibition of histone deacetylase 1 and 3 in Huntington's disease mice, Front. Mol. Neurosci. 14 (2021) 616886. doi: 10.3389/fnmol.2021.616886.

[105] D.A. Rodrigues, P.D.S. Pinheiro, F.S. Sagrillo, M.L. Bolognesi, C.A. Fraga, Histone deacetylases as targets for the treatment of neurodegenerative disorders: Challenges and future opportunities, Med. res. Rev. 40 (2020) 2177-2211. doi: 10.1002/med.21701.

[106] S.A. Amin, N. Adhikari, S. Kotagiri, T. Jha, B. Ghosh, Histone deacetylase 3 inhibitors in learning and memory processes with special emphasis on benzamides, Eur. J. Med. Chem. 166 (2019) 369-380. doi: 10.1016/j.ejmech.2019.01.077.

[107] Y. Li, C. Liu, G. Wang, H. Wang, X. Liu, C. Huang, Y. Chen, L. Fan, L. Zhou, A. Tong, HDAC3 inhibitor (BRD3308) modulates microglial pyroptosis and neuroinflammation through PPARγ/NLRP3/GSDMD to improve neurological function after intraventricular hemorrhage in mice, Neuropharmacology (2023) 109633. doi: 10.1016/j.neuropharm.2023.109633.

[108] S. Ahmad Ganai, M. Ramadoss, V. Mahadevan, Histone Deacetylase (HDAC) Inhibitors-emerging roles in neuronal memory, learning, synaptic plasticity and neural regeneration, Curr. Neuropharmacol. 14 (2016) 55-71. doi: 10.2174/1570159x13666151021111609.

[109] L. Ning, X. Rui, W. Bo, G. Qing, The critical roles of histones deacetylase 3 in the pathogenesis of solid organ injury, Cell Death Dis. 12 (2021) 734. doi: 10.1038/s41419-021-04019-6.

[110] F. Loi, L.A. Córdova, J. Pajarinen, T.H. Lin, Z. Yao, S.B. Goodman, Inflammation, fracture and bone repair Bone, 86 (2016) 119-130. doi: 10.1016/j.bone.2016.02.020.

[111] E.W. Bradley, L.R. Carpio, A.J. Wijnen, M.E. McGee-Lawrence, J.J. Westendorf, Histone Deacetylases in Bone Development and Skeletal Disorders, Physiol. Rev. 95 (2015) 1359-1381. doi: 10.1152/physrev.00004.2015.

[112] L. Zeng, G. Wang, D. Ummarino, A. Margariti, Q. Xu, Q. Xiao, W. Wang, Z. Zhang, X. Yin, M. Mayr, G. Cockerill, Histone deacetylase 3 unconventional splicing mediates endothelial-to-mesenchymal transition through transforming growth factor β2, J. Biol. Chem. 288 (2013) 31853-31866. doi: 10.1074/jbc.M113.463745.

[113] C. Underhill, M.S. Qutob, S.P. Yee, J. Torchia, A novel nuclear receptor corepressor complex, N-CoR, contains componenets of the mammalian SWI/SNF complex and the corepressor KAP-1, J. Biol. Chem. 275 (2000) 40463-40470. doi: 10.1074/jbc.M007864200.

[114] J. Li, J. Wang, J. Wang, Z. Nawaz, J.M. Liu, J. Qin, J. Wong, Both corepressor proteins SMRT and N-CoR exit in large protein complexes containing HDAC3, EMBO J. 19 (2000) 4342-4350. doi: 10.1093/emboj/19.16.4342.

[115] S.H. Kim, J.W. Lee, K.G. Choi, H.W. Chung, H.W. Lee, A 6-month longitutional study of bone mineral density with antiepileptic drug monotherapy, Epilepsy Behav. 10 (2007) 291-295. doi: 10.1016/j.yebeh.2006.11.007.

[116] H. Tsukahara, K. Kimura, Y. Todoroki,Y. Ohshima, M. Hiraoka, Y. Shigematsu, Y. Tsukahara, M. Miura, M. Mayumi, Bone mineral status in ambulatory pediatric

patients long-term anti-epileptic drug therapy, Pediatr. Int. 44 (2002) 247-253. doi: 10.1046/j.1442-200X.2002.01561.x.

[117] S.M. Senna, S. Kantor, I.J. Poulton, M.J. Morris, N.A. Sims, T.J. O'Brien, J.D. Wark, Adverse effects of valporate on bone: defining a model to investigate the pathophysiology, Epilepsia 51 (2010) 984-993. doi: 10.1111/j.1528-1167.2009.02516.x.

[118] M.E. McGee-Lawrence, A.L. McCleary-Wheeler, F.J. Secreto, D.F. Razidlo, M. Zhang, B.A. Stensgard, X. Li, G.S. Stein, J.B. Lian, J.J. Westendorf, Suberoylanilide hydroxamic acid (SAHA; vorinostat) causes bone loss by inhibiting immature osteoblasts, Bone 48 (2011) 1117-1126. doi: 10.1016/j.bone.2011.01.007.

[119] M.D. Cantley, D.P. Fairlie, P.M. Bartold, K.D. Rainsford,G.T. Le, A.J. Lucke, C.A. Holding, D.R. Haynes, Inhibitors of histone deacetylases in class I and class II suppress human osteoclasts in vitro, J. Cell Physiol. 226 (2011) 3233-3241. doi: 10.1002/jcp.22684.

[120] K.L. Culley, The role of histone deacetylases in cartilage gene regulation and chondroprotection, Doctoral disserttion, 2010, University of East Anglia.

[121] W.P. Chen, J.P. Bao, P.F. Hu, J. Feng, L.D. Wu, Alleviation of osteoarthritis by Trichostatin A, a histone deacetylase inhibitor, in experimental osteoarthritis, Mol. Biol. Rep. 37 (2010) 3967-3972. doi: 10.1007/s11033-010-0055-9.

[122] W.P. Chen, J.P. bao, J.L. Tang, P.F. Hu, L.D. Wu, Trichostatin A inhibits expression of cathepsins in experimental osteoarthritis,Rheumatol. Int. 31 (2011) 1325-1331. doi: 10.1007/s00296-010-1481-7.

[123] Y.H. Huh, J.H. Ryu, J.S. Chun, Regulation of type II collagen expression by histone deacetylase in articular chondrocytes, J.Biol. Chem. 282 (2007) 17123-171231. doi: 10.1074/jbc.M700599200.

[124] X. Wang, Y. Song, J.L. Jacobi, R.S. Tuan, Inhibition of histone deacetylases antagonized FGF2 and IL-1beta effects on MMP expression in human articular chondrocytes, Growth Factors 27 (2009) 40-49. doi: 10.1080/08977190802625179.

[125] S. Xu, K. De Veirman, H. Evans, G.C. Santini, I. Vande Broek, X. Leleu, A. De Becker, B. Van Camp, P. Crocher, K. Vanderkerkan, I. Van Riet, Effect of the HDAC inhibitor vorinostat on the osteogenic differentiation of mesenchymal stem cells in vitro and bone formation in vivo, Acta. Pharmacol. Sin. 34 (2013) 699-709. doi: 10.1038/aps.2012.182.

[126] M. Ho, T. Chen, P. Dowling, T. Hideshima, L. Zhang, E. Morelli, G. Camci-Unal, Y.T. Tai, K. Wen, M. Samur, R.L. Schlossman, R. Mazitschek, E.L. Kavanagh, S. Lindsay, T. Harada, A. McCann, K.C. Anderson, P. O'Gorman, G. Bianchi, Targeting histone deacetylase 3 (HDAC3) in the bone marrow microenvironment inhibits multiple myeloma proliferation by modulating exosomes and IL-6 trans-signaling, Leukemia 34 (2020) 196-209. doi: 10.1038/s41375-019-0493-x.

[127] T. Lawrence, The nuclear factor NF-kappaB pathway in inflammation, Cold Spring Harb. Perspect. Biol. 1 (2009) 1-10. doi: 10.1101/cshperspect.a001651.

[128] C. Gasparini, M. Feldmann, NF-κB as a target for modulating inflammatory responses, Curr. Pharm. Des. 18 (2012) 5735-5745. doi: 10.2174/138161212803530763.

[129] M. Herkenham, P. Rathore, P. Brown, S.J. Listwak, Cautionary notes on the use of NF-κB p65 and p50 antibodies for CNS studies, J. Neuroinflammation 8 (2011) 1-14. doi: 10.1186/1742-2094-8-141.

[130] N.G. Leus, M.R. Zwinderman, F.J. Dekker, Histone deacetylase 3 (HDAC 3) as emerging drug target in NF-κB-mediated inflammation, Curr. Opin. Chem. Biol. 33 (2016) 160-168. doi: 10.1016/j.cbpa.2016.06.019.

[131] N.G. Leus, P.E. van der Wouden, T. van den Bosch, W.T.R. Hooghiemstra, M.E. Ourailidou, L.E. Kistemaker, R. Bischoff, R. Gosens, H.J. Haisma, F.J. Dekker, HDAC 3-selective inhibitor RGFP966 demonstrates anti-inflammatory properties in RAW 264.7 macrophages and mouse precision-cut lung slices by attenuating NF-κB p65 transcriptional activity, Biochem. Pharmacol. 108 (2016) 58-74. doi: 10.1016.j.bcp.2016.03.010.

[132] Y. Kim, K. Kim, D. Park, E. Lee, H. Lee, Y.S. Lee, J. Choe, D. Jeoung, Histone deacetylase 3 mediates allergic skin inflammation by regulating expression of MCP1 protein, J. Biol. Chem. 287 (2012) 25844-25859. doi: 10.1074/jbc.M112.348284.

[133] S. Chen, J. Ye, X. Chen, J. Shi, W. Wu, W. Lin, W. Lin, Y. Li, H. Fu, S. Li, Valproic acid attenuates traumatic spinal cord injury-induced inflammation via STAT1 and NF-κB pathway dependent of HDAC3, J. Neuroinflamation 15 (2018) 1-14. doi: 10.1186/s12974-018-1193-6.

[134] S. Chen, H. Wu, D. Kleb, Y. Hong, J. Zhang, Valproic acid: a new candidate of therapeutic application for the acute central nervous system injuries, Neurochem. Res. 39 (2014) 1621-1633. doi: 10.1007/s11064-014-1241-2.

[135] A.J. Wilson, D.S. Byun, N. Popova, L.B. Murray, K. L'italien, Y. Sowa, D. Arango, A. Velcich, L.H. Augenlicht, J.M. Mariadason, Histone deacetylase 3 (HDAC3) and other class 1 HDACs regulate colon cell maturation and p21 expression and are deregulated in human colon cancer, J. Biol. Chem. 281 (2006) 13548-13558. doi: 10.1074/jbc.M510023200.

[136] C.C. Spurling, C.A. Godman, E.J. Noonan, T.P. Rasmussen, D.W. Rosenberg, C. Giardina, HDAC3 overexpression and colon cancer proliferation and differentiation, Mol. Carcinog. 47 (2008) 137-147. doi: 10.1002/mc.20373.

[137] H.Y. Hsieh, H.C. Chuang, F.H. Shen, K. Detroja, L.W. Hsin, C.S. Chen, Targeting breast cancer stem cells by novel HDAC3-selective inhibitors, E. J. Med. Chem. 140 (2017) 42-51. doi: 10.1016/j.ejmech.2017.08.069.

[138] Z. Cui, M. Xie, Z. Wu, Y. Shi, Relationship between histone deacetylase 3 (HDAC3) and breast cancer, Med. Sci. Monit. 24 (2018) 2456. doi: 10.12659/MSM.906576.

[139] G. Hu, N. He, C. Cai, F. Cai, P. Fan, Z. Zheng, X. Jin, HDAC3 modulates cancer immunity via increasing PD-L1 expression in pancreatic cancer, Pancreatology 19 (2019) 383-389. doi: 10.1016/j.pan.2019.01.011.

[140] N. Adhikari, T. Jha, B. Ghosh, Dissecting Histone Deacetylase 3 in Multiple Disease Conditions: Selective Inhibition as a Promising Therapeutic Strategy, J. Med. Chem. 64 (2021) 8827-8869. doi: 10.1021/acs.jmedchem.0c01676.

[141] S. Terracciano, S.Di Micco, G. Bifulco, P. Gallinari, R. Riccio, I. Bruno, Synthesis and biological activity of cyclotetrapeptide analogues of the natural HDAC inhibitor FR235222, Bioorg. Med. Chem. 18 (2010) 3252-3260. doi: 10.1016/j.bmc.2010.03.022.

[142] J. Wang, M. Su, T. Li, A. Gao, W. Yang, L. Sheng, Y. Zang, J. Li, H. Liu, Design, synthesis and biological evaluation of thienopyrimidine hydroxamic acid-based derivatives as structurally novel histone deacetylase (HDAC) inhibitors, Eur. J. Med. Chem. 128 (2017) 293-299. doi: 10.1016/j.ejmech.2017.01.035.

[143] S.W. Zhang, C.J. Gong, M.B. Su, F. Chen, T. He, Y.M. Zhang, Q.Q. Shen, Y. Su, J. Ding, J. Li, Y. Chen, F.J. Nan, Synthesis and in Vitro and in Vivo Biological Evaluation of Tissue-Specific Bisthiazole Histone Deacetylase (HDAC) Inhibitors, J. Med. Chem. 63 (2020) 804-815. doi: 10.1021/acs.jmedchem.9b01792.

[144] J.I. Lai, L.J. Leman, S. Ku, C.J. Vickers, C.A. Olsen, A. Montero, M.R. Ghadiri, J.M. Gottesfeld, Cyclic tetrapeptide HDAC inhibitors as potential therapeutics for spinal

muscular atrophy: Screening with iPSC-derived neuronal cells, Bioorg. Med. Chem. 27 (2017) 3289-3293. doi: 10.1016/j.bmcl.2017.06.027.

[145] Q. Zhu, X. Yu, Q. Shen, Q. Zhang, M. Su, Y. Zhou, J. Li, Y. Chen, W. Lu, A series of camptothecin prodrugs exhibit HDAC inhibition activity, Bioorg. Med. Chem. 26 (2018) 4706-4715. doi: 10.1016/j.bmc.2018.08.008.

[146] X. Zhang, J. Zhang, L. Tong, Y. Luo, M. Su, Y. Zang, J. Li, W. Lu, Y. Chen, The discovery of colchicine-SAHA hybrids as a new class of antitumor agents, Bioorg. Med. Chem. 21 (2013) 3240-3244. doi: 10.1016/j.bmc.2013.03.049.

[147] X. Zhang, B. Bao, X. Yu, L. Tong, Y. Luo, Q. Huang, M. Su, L. Sheng, J. Li, H. Zhu, B. Yang, X. Zhang, Y. Chen, W. Lu, The discovery and optimization of novel dual inhibitors of topoisomerase II and histone deacetylase, Bioorg. Med. Chem. 21 (2013) 6981-6985. doi: 10.1016/j.bmc.2013.09.023.

[148] Y. Luo, H.M. Liu, M.B. Su, L. Sheng, Y.B. Zhou, J. Li, W. Lu, Synthesis and biological evaluation of piperamide analogues as HDAC inhibitors, Bioorg. Med. Chem. 21 (2011) 4844-4846. doi: 10.1016/j.bmcl.2011.06.046.

[149] S. Tapadar, R. He, D.N. Luchini, D.D. Billadeau, A.P. Kozikowski, Isoxazole moiety in the linker region of HDAC inhibitors adjacent to the Zn-chelating group: effects on HDAC biology and antiproliferative activity, Bioorg. Med. Chem. Lett. 19 (2009) 3023-3026. doi: 10.1016/j.bmcl.2009.04.058.

[150] B. Ghosh, W.N. Zhao, S.A. Reis, D. Patnaik, D.M. Fass, L.H. Tsai, R. Mazitschek, S.J. Haggarty, Dissecting structure-activity-relationships of crebinostat: Brain penetrant HDAC inhibitors for neuroepigenetic regulation, Bioorg. Med. Chem. 26 (2016) 1265-1271. doi: 10.1016/j.bmcl.2016.01.022.

[151] Y. Ling, J. Guo, Q. Yang, P. Zhu, J. Miao, W. Gao, Y. Peng, J. Yang, K. Xu, B. Xiong, G. Liu, J. Tao, L. Luo, Q. Zhu, Y. Zhang, Development of novel β-carboline-based hydroxamate derivatives as HDAC inhibitors with antiproliferative and antimetastatic activities in human cancer cells, Eur. J. Med. Chem. 144 (2018) 398-409. doi: 10.1016/j.ejmech.2017.12.061.

[152] Y. Ling, Y. Li, R. Zhu, J. Qian, J. Liu, W. GAo, C. Meng, J. Miao, B. Xiong, X. Qiu, C. Ling, H. Dai, Y. Zhang, Hydroxamic Acid Derivatives of β-Carboline/Hydroxycinnamic Acid Hybrids Inducing Apoptosis and Autophagy through the PI3K/Akt/mTOR Pathways, J. Nat. Prod. 82 (2019) 1442-1450. doi: 10.1021/acs.jnatprod.8b00843.

[153] T. Tashima, H. Murata, H. Kodama, Design and synthesis of novel and highly-active pan-histone deacetylase (pan-HDAC) inhibitors, Bioorg. Med. Chem. 22 (2014) 3720-3731. doi: 10.1016/j.bmc.2014.05.001.

[154] J. Tng, J. Lim, K.C. Wu, A.J. Lucke, W. Xu, R.C. Reid, D.P. Fairlie, Achiral Derivatives of Hydroxamate AR-42 Potently Inhibit Class I HDAC Enzymes and Cancer Cell Proliferation, J. Med. Chem. 63 (2020) 5956-5971. doi: 10.1021/acs.jmedchem.0c00230.

[155] K. Jin, S. Li, X. Li, J. Zhang, W. Xu, X. Li, Design, synthesis and preliminary biological evaluation of indoline-2,3-dione derivatives as novel HDAC inhibitors, Bioorg. Med. Chem. 23 (2015) 4728-4736. doi: 10.1016/j.bmc.2015.05.048.

[156] X. Li, J. Hou, X. Li, Y. Jiang, X. Liu, W. Mu, Y. jin, Y. Zhang, W. Xu, Development of 3-hydroxycinnamamide-based HDAC inhibitors with potent in vitro and in vivo anti-tumor activity, Eur. J. Med. Chem. 89 (2015) 628-637. doi: 10.1016/j.ejmech.2014.10.077.

[157] A.E. Shouksmith, F. Shah, M.L. Grimard, J.M. Gawel, Y.S. Raouf, M. Geletu, A. Berger-Becvar, E.D. de Araujo, H.A. Luchman, W.L. heaton, D. Bakhshinyan, Identification and characterization of AES-135, a hydroxamic acid-based HDAC inhibitor that prolongs survival in an orthotopic mouse model of pancreatic cancer, J. Med. Chem. 62 (2019) 2651-2665. doi: 10.1021/acs.jmedchem.8b01957.

[158] A.E. Shouksmith, J.M. Gawel, N. Nawar, D. Sinha, Y.S. Raouf, S. Bukhari, L. He, A.E. Johns, P. Manaswiyoungkul, O.O. Olaoye, A.D. Cabral, Class I/IIb-selective HDAC inhibitor exhibits oral bioavailability and therapeutic efficacy in acute myeloid leukemia, ACS Med. Chem. Lett. 11 (2019) 56-64. doi: 10.1021/acsmedchemlett.9b00471.

[159] Y. Zhang, P. Yang, C.J. Chou, C. Liu, X. Wang, W. Xu, Development of N-Hydroxycinnamamide-Based Histone Deacetylase Inhibitors with Indole-Containing Cap Group, ACS Med. Chem. Lett. 4 (2013) 235-238. doi: 10.1021/ml300366t.

[160] X. Li, E.S. Inks, x. Li, J. Hou, C.J. Chou, J. Zhang, Y. Jiang, Y. Zhang, W. Xu, Discovery of the first N-hydroxycinnamamide-based histone deacetylase 1/3 dual inhibitors with potent oral antitumor activity, J.Med. Chem. 57 (2014) 3324-3341. doi: 10.1021/jm401877m.

[161] W. Yang, L. Li, X. Ji, X. Wu, M. Su, L. Sheng, Y. Zang, J. Li, H. Liu, Design, synthesis and biological evaluation of 4-anilinothieno [2, 3-d] pyrimidine-based

hydroxamic acid derivatives as novel histone deacetylase inhibitors, Bioorg. Med. Chem. 22 (2014) 6146-6155. doi: 10.1016/j.bmc.2014.08.030.

[162] H. Abdelkarim, R. Neelarapu, A. Madriage, A.S. Vaidya, I. Kastrati, B. Karumudi, Y.T. Wang, T.Y. Taha, G.R. Thatcher, J. Frasor, P.A. Petukhov, Design, Synthesis, Molecular Modeling, and Biological Evaluation of Novel Amine- based Histone Deacetylase Inhibitors, ChemMedChem 12 (2017) 2030-2043. doi: 10.1002/cmdc.201700449.

[163] M.A. Fischer, A.H.M. Mustafa, K. Hausmann, R. Ashry, A.G. Kansy, M.C. Liebl, C. Brachetti, A. Piee-Staffa, M. Zessin, H.S. Ibrahim, T.G. Hofmann, Novel hydroxamic acid derivative induces apoptosis and constrains autophagy in leukemic cells, J. Adv. Res. (2023). doi: 10.1016/j.jare.2023.07.005.

[164] S. Mahboobi, A. Sellmer, M. Winkler, E. Eichhorn, H. Pongratz, T. Ciossek, T. Baer, T. Maier, T. Beckers, Novel chimeric histone deacetylase inhibitors: a series of lapatinib hybrides as potent inhibitors of epidermal growth factor receptor (EGFR), human epidermal growth factor receptor 2 (HER2), and histone deacetylase activity, J. Med. Chem. 53 (2010) 8546-8555. doi: 10.1021/jm100665z.

[165] J.C. Wong, L. Guo, Z. Peng, W. Zhang, N. Zhang, W. Lai, Z. Zhang, C. Zhang, X. Zhang, S. Song, D. Pan, C. Xie, J. Li, Z. Ning, X. Lu, Y. he, L. Chen, Application of p21 and klf2 reporter gene assays to identify selective histone deacetylase inhibitors for cancer therapy, Bioorg. Med. Chem. Lett. 21 (2011) 110-116. doi: 10.1016/j.bmcl.2010.11.063.

[166] F. Hu, C.J. Chou, J.M. Gottesfeld, Design and synthesis of novel hybrid benzamide-peptide histone deacetylase inhibitors, Bioorg. Med. Chem. 19 (2009) 3928-3931. doi: 10.1016/j.bmcl.2009.03.085.

[167] J. Zang, X. Liang, Y. Huang, Y. Jia, X. Li, W. Xu, C.J. Chou, Y. Zhang, Discovery of Novel Pazopanib-Based HDAC and VEGFR Dual Inhibitors Targeting Cancer Epigenetics and Angiogenesis Simultaneously, J. Med. Chem. 61 (2018) 5304-5322. doi: 10.1021/acs.jmedchem.8b00384.

[168] G. Routholla, S. Pulya, T. Patel, N. Adhikari, S.A. Amin, M. Paul, S. Bhagavatula, S. Biswas, T. Jha, B. Ghosh, Design, synthesis and binding mode of interaction of novel small molecule o-hydroxy benzamides as HDAC3-selective inhibitors with promising antitumor effects in 4T1-Luc breast cancer xenograft model, Bioorg. Chem. 117 (2021) 105446. doi: 10.1016/j.bioorg.2021.105446.

[169] Z. Wang, L. Zhao, B. Zhang, H. Jin, L. Ding, N. Wang, S. He, Discovery of novel polysubstituted N-alkyl acridone analogues as histone deacetylase isoform-selective inhibitors for cancer therapy, J. Enzyme inhib. Med. Chem. 38 (2023) 2206568. doi: 10.1080/14756366.2023.2206581.

[170] P. Trivedi, N. Adhikari, S.A. Amin, T. Jha, B. Ghosh, Design, synthesis and biological screening of 2-aminobenzamides as selective HDAC3 inhibitors with promising anticancer effects, Eur. J. Pharm. Sci. 124 (2018) 165-181. doi: 10.1016/j.ejps.2018.08.030.

[171] T. Suzuki, Y. Kasuya, Y. Itoh, Y. Ota, P. Zhan, K. Asamitsu, H. Nakagawa, T. Okamoto, N. Miyata, Identification of highly selective and potent histone deacetylase 3 inhibitors using click chemistry-based combinatorial fragment assembly, PloS One 8 (2013) e68669. doi: 10.1371/journal.pone.0068669.t003.

[172] X. Peng, J. Chen, L. Li, Z. Sun, J. Liu, Y. Ren, J. Huang, J. Chen, Efficient synthesis and bioevaluation of novel dual tubulin/histone deacetylase 3 inhibitors as potential anticancer agents, J. Med. Chem. 64 (2021) 8447-8473. doi: 10.1021/acs.jmedchem.1c00413.

[173] Q. Ding, C. Liu, C. Zhao, H. Dong, Q. Xu, J. Chou, Y. Zhang, Synthesis and biological study of class I selective HDAC inhibitors with NO releasing activity, Bioorg. Chem. 104 (2020) 104235. doi: 10.1016/j.bioorg.2020.104235.

[174] Z. Huang, J. Fu, Y. Zhang, Nitric oxide donor-based cancer therapy: advances and prospects, J. Med. Chem. 60 (2017) 7617-7635. doi: 10.1021/acs.jmedchem.6b01672.

[175] B. Bonavida, Sensitizing activities of nitric oxide donors for cancer resistance to anticancer therapeutic drugs, Biochem. pharmacol. 176 (2020) 113913. doi: 10.1016/j.bcp.2020.113913.

[176] C.M. Marson, C.J. Matthews, S.J. Atkinson, N. Lamadema, N.S.B. Thomas, Potent and selective inhibitors of histone deacetylase-3 containing chiral oxazoline capping groups and a N-(2-aminophenyl)-benzamide binding unit, J. Med. Chem. 58 (2015) 6803-6818. doi: 10.1021/acs.jmedchem.5b00545.

[177] C.A. Ocasio, S. Sansook, R. Jones, J.M. Roberts, T.G. Scott, N. Tsoureas, P. Coxhead, M. Guille, G.J. Tizzaed, S.J. Coles, H. Hochegger, Pojamide: An HDAC3-selective ferrocene analogue with remarkably enhanced redox-triggered ferrocenium activity in cells, Organometallics 36 (2017) 3276-3283. doi: 10.1021/acs.organomet.7b00437.

[178] J. Wen, Y. Bao, Q. Niu, J. Yang, Y. Fan, J. Li, Y. Jing, L. Zhao, D. Liu, Identification of N-(6-mercaptohexyl)-3-(4-pyridyl)-1H-pyrazole-5-carboxamide and its disulfide

prodrug as potent histone deacetylase inhibitors with in vitro and in vivo anti-tumor efficacy, Eur. J. Med. Chem. 109 (2016) 350-359. doi: 10.1016/j.ejmech.2016.01.013.

[179] M.M. Hamoud, S. Pulya, N.A. Osman, Y. Bobde, A.E. Hassan, H.A. Abdel-Fattah, B. Ghosh, A.M. Ghanim, Design, synthesis, and biological evaluation of novel nicotinamide derivatives as potential histone deacetylase-3 inhibitors, New J. Chem. 44 (2020) 9671-9683. doi: 10.1039/d0nj01274b.

[180] Y. Wang, R.L. Stowe, C.E. Pinello, G. Tian, F. Madoux, D. Li, L.Y. Zhao, J.L. Li, Y. Wang, H. Ma, Identification of histone deacetylase inhibitors with benzoylhydrazide scaffold that selectively inhibit class I histone deacetylases, Chem. Biol. 22 (2015) 273-284. doi: 10.1016/j.chembiol.2014.12.015.

[181] S. Pulya, T. Patel, M. Paul, N. Adhikari, S. Banerjee, G. Routholla, S. Biswas, T. Jha, B. Ghosh, Selective inhibition of histone deacetylase 3 by novel hydrazide based small molecules as therapeutic intervention for the treatment of cancer, Eur. J. Med. Chem. 238 (2022) 114470. doi: 10.1016/j.ejmech.2022.114470.

[182] Y. Jiang, J. Xu, K. Yue, C. Huang, M. Qin, D. Chi, Q. Yu, Y. Zhu, X. Hou, T. Xu, M. Li, Potent hydrazide-based HDAC inhibitors with a superior pharmacokinetic profile for efficient treatment of acute myeloid leukemia in vivo, J. Med. Chem. 65 (2021) 285-302. doi: 10.1021/acs.jmedchem.1c01472.

[183] J.J. McClure, C. Zhang, E.S. Inks, Y.K. Peterson, J. Li, C.J. Chou, Development of allosteric hydrazide-containing class I histone deacetylase inhibitors for use in acute myeloid leukemia, J. Med. Chem. 59 (2016) 9942-9959. doi: 10.1021/acs.jmedchem.6b01385.

[184] X. Li, Y. Jiang, Y.K. Peterson, T. Xu, R.A. Himes, X. Luo, G. Yin, E.S. Inks, N. Dolloff, S. Halene, S.S. Chan, Design of hydrazide-bearing HDACIs based on panobinostat and their p53 and FLT3-ITD dependency in antileukemia activity, J. Med. Chem, 63 (2020) 5501-5525. doi: 10.1021/acs.jmedchem.0c00442.

[185] C.J. Gong, A.H. Gao, Y.M. Zhang, M.B. Su, F. Chen, L. Sheng, Y.B. Zhou, J.Y. Li, J. Li, F.J. Nan, Design, synthesis and biological evaluation of bisthiazole-based trifluoromethyl ketone derivatives as potent HDAC inhibitors with improved cellular efficacy, Eur. J. Med. Chem. 112 (2016) 81-90. doi: 10.1016/j.ejmech.2016.02.003.

[186] Y. Yao, Z. Tu, C. Liao, Z. Wang, S. Li, H. Yao, Z. Li, S. Jiang, Discovery of novel class I histone deacetylase inhibitors with promising in vitro and in vivo antitumor activities, J. Med. Chem. 58 (2015) 7672-7680. doi: 10.1021/acs.jmedchem.5b01044.

[187] X. Li, Z. Tu, H. Li, C. Liu, Z. Li, Q. Sun, Y. Yao, J. Liu, S. Jiang, Biological evaluation of new largazole analogues: alteration of macrocyclic scaffold with click chemistry, ACS Med. Chem. Lett. 4 (2012) 132-136. doi: 10.1021/ml300371t.

[188] J.M. Guerra-Bubb, A.A. Bowers, W.B. Smith, R. Paranal, G. Estiu, O. Wiest, J.E. Bradner, R.M. Williams, Synthesis and HDAC inhibitory activity of isosteric thiazoline-oxazole largazole analogs, Bioorg. Med. Chem. Lett. 23 (2013) 6025-6028. doi: 10.1016/j.bmcl.2013.06.012.

[189] J. Almaliti, A.A. Al-Hamashi, A.T. Negmeldin, C.L Hanigan, L. Perera, M.K.H. Pflum, R.A. Casero Jr, L.V. Tillekeratne, Largazole analogues embodying radical changes in the depsipeptide ring: Development of a more selective and highly potent analogue, J. Med. Chem. 59 (2016) 10642-10660. doi: 10.1021/acs.jmedchem.6b01271.

[190] H. Xu, L.R. Roberts, S. Chou, B. Pierce, A. Narayana, L.H. Jones, Quantitative measurement of intracellular HDAC1/2 drug occupancy using a trans-cyclooctene largazole thiol probe, MedChemComm, 8 (2017) 767-770. doi: 10.1039/C6MD00633G.

[191] J.A. DiMasi, R.W. Hansen, H.G. Grabowski, The price of innovation: new estimates of drug development costs, J. Health Econ. 22 (2003) 151-85. doi: 10.1016/S0167-6296(02)00126-1.

[192] C.M. Song, S.J. Lim, J.C. Tong, Recent advances in computer-aided drug design, Brief. Bioinform. 10 (2009) 579-591. doi: 10.1093/bib/bbp023.

[193] A.C. Anderson, The process of structure-based drug design, Chem. Biol. 10 (2003) 787-797. doi: 10.1016/j.chembiol.2003.09.002.

[194] Y.P. Chen, F. Chen, Identifying targets for drug discovery using bioinformatics, Expert. Opin. Ther. Targets 12 (2008) 383-389. doi: 10.1517/14728222.12.4.383.

[195] S. Kalyaanamoorthy, Y.P. Chen, Structure-based drug design to augment hit discovery, Drug Discov. Today 16 (2011) 831-839. doi: 10.1016/j.drudis.2011.07.006.

[196] G.A. Showell, J.S. Mills, Chemistry challenges in lead optimization: silico isosteres in drug discovery, Drug Discov. Today, 8 (2003) 551-556. doi: 10.1016/s1359-6446(03)02726-0.

[197] S.A. amin, N. Adhikari, T. Jha, B. Ghosh, Designing potential HDAC3 inhibitors to improve memory and learning, J.B.S.D. 37 (2019) 2133-2142. doi: 10.1080/07391102.2018.1477625.

References

[198] S. Li, Y. Ding, M. Chen, Y.Chen, J. Kirchmair, Z. Zhu, S. Wu, J. Xia, HDAC3i-Finder: A machine learning-based Computational Tool to Screen for HDAC3 inhibitors, Mol. Inf. 40 (2021) 2000105. doi: 10.1002/minf.202000105.

[199] E. f Bülbül, D. Robaa, P. Sun, F. Mahmoudi, J. Melesina, M. Zessin, M. Schutkowski, W. Sippl, Application of Ligand-and Structure-Based Prediction Models for the Design of Alkylhydrazide-Based HDAC3 Inhibitors as Novel Anti-cancer Compounds, 2023. doi: 10.20944/preprints202305.1124.v1.

[200] H. Hu, J. Xia, D. Wang, X.S. Wang, S. Wu, A Throughly validated Virtual Screening Strategy for Discovery of Novel HDAC3 Inhibitors, Int. J. Mol. Sci. 18 (2017) 137. doi: 10.3390/ijms18010137.

[201] J. Xia, H. Hu, W. Xue, X.S. Wang, S. Wu, The discovery of novel HDAC3 inhibitors via virtual screening and in vitro bioassay. J. Enzyme Inhib. Med. Chem. 33 (2018) 525-535. doi: 10.1080/14756366.2018.1437156.

[202] J. Minami, R. Suzuki, R. Mazitschek, G. Gorgun, B. Ghosh, D. Cirstea, Y. Hu, N. Mimura, H. Ohguchi, F. Cottini, J. Jakubikova, Histone deacetylase 3 as a novel therapeutic target in multiple myeloma, Leukemia 28 (2014) 680-689. doi: 10.1038/leu.2013.231.

[203] P. Karagianni, J. Wong, HDAC3: taking the SMRT-N-CoRrect road to repression, Oncogene 26 (2007) 5439-5449. doi: 10.1038/sj.onc.1210612.

[204] P. Dsilva, P. Pai, M.G. Shetty, K.S. Babitha, The role of histone deacetylases in embryonic development, Mol. Reprod. Dev. 90 (2023) 14-26. doi: 10.1002/mrd.23659.

[205] Discovery Studio 3.0 (DS 3.0), Accelrys Inc., USA, CA, 2015.

[206] The simple, user-friendly, and reliable online standalone tools freely, https://teqip.jdvu.ac.in/QSAR_Tools, (Accessed on 30 Dec 2022).

[207] L. Chen, Y. Li, Q. Zhao, H. Peng, T. Hou, ADME evaluation in drug discovery. 10. Predictions of P-glycoprotein inhibitors using recursive partitioning and naive Bayesian classification techniques, Mol. Pharm. 8 (2011) 889-900. doi: 10.1021/mp100465q.

[208] L.L. Liu, J. Lu, Y. Lu, M.Y. Zheng, X.M. Luo, W.L. Zhu, H.L. Jiang, K.X. Chen, Novel Bayesian classification models for predicting compounds blocking hERG potassium channels, Acta Pharmacol. Sininca 35 (2014) 1093-1102. doi: 10.1038/aps.2014.35.

References

[209] S.A. Amin, N. Adhikari, S. Bhargava, S. Gayen, T. Jha, An integrated QSAR modeling approach to explore the structure–property and selectivity relationships of N-benzoyl-l-biphenylalanines as integrin antagonists, Mol. Diver. 22 (2018) 129-158. doi: 10.1007/s11030-017-9789-9.

[210] S.A. Amin, S. Nandi, S.K. Kashaw, T. Jha, S. Gayen, A critical analysis of urea transporter B inhibitors: molecular fingerprints, pharmacophore features for the development of next-generation diuretics, Mol. Diver. (2011) 1-11. doi: 10.1007/s11030-021-10353-w.

[211] H. Zhang, Y.L. Kang, Y.Y. Zhu, K.X. Zhao, J.Y. Liang, L. Ding, T.G. Zhang, J. Zhang, Novel naïve Bayes classification models for predicting the chemical Ames mutagenicity, Toxicol. 41 (2017) 56-63. doi: 10.1016/j.tiv.2017.02.016.

[212] S. Banerjee, S.A. Amin, T. Jha, A fragment-based structural analysis of MMP-2 inhibitors in search of meaningful structural fragments, Comput. Biol. Med. 144 (2022) 105360. doi: 10.1016/j.compbiomed.2022.105360.

[213] M. Moinul, S.A. Amin, P. Kumar, U.K. patil, A. Gajbhiye, T. Jha, S. Gayen, Exploring sodium glucose cotransporter (SGLT2) inhibitors with Machine Learning Approach: A novel hope in anti-diabetes drug discovery, J. Mol. Graph. Model. 111 (2022) 108106. doi: 10.1016/j.jmgm.2021.108106.

[214] T. Hou, J. Wang, Y. Li, ADME evaluation in drug discovery. 8.The prediction of human intestinal absorption by a support vector machine, J. Chem. Inf. Model. 47 (2007) 2408-2415. doi: 10.1021/ci7002076.

[215] E. Mombelli, G. Raitano, E. Benfenati, In silico prediction of chemically induced mutagenicity: how to use QSAR models and interpret their results, In silico methods for predicting drug toxicity, (2016) 87-105. doi: 10.1007/978-1-4939-3609-0_5.

[216] T. Ferrari, D. Cattaneo, G. Gini, N. Golbamaki Bakhtyari, A. manganaro, E. Benfenati, Automatic knowledge extraction from chemical structures: the case of mutagenicity prediction, SAR QSAR Environ. Res. 24 (2013) 365-383. doi: 10.1080/1062936X.2013.773376.

[217] H. Yang, J. Li, Z. Wu, W. Li, G. Liu, Y. Tang, Evaluation of different methods for identification of structural alerts using chemical ames mutagenicity data set as a benchmark, Chem. Res. Toxicol. 30 (2017) 1355-1364. doi: 10.1021/acs.chemrestox.7b00083.

[218] K. Roy, S. Kar, R.N. Das, A primer on QSAR/QSPR modeling: fundamental concepts, 2015, Springer.

[219] Statistica 7.1, Statsoft lnc. 2300 East 14th Street Tulsa, OK 74104, United States.

[220] S.S. Wilks, Certain generalizations in the analysis of variance, Biometrica (1932) 471-494. doi: 10.2307/2331979.

[221] B.W. Matthews, Comparison of the predicted and observed secondary structure of T4 phage lysozyme, BBA Prot. St. 405 (1975) 442-451. doi: 10.1016/0005-2795(75)90109-9.

[222] F.J. Prado-Prado, E. Uriatre, F. Borges, H. González-Díaz, Multi-target spectral moments for QSAR and complex networks study of antibacterial drugs, Eur. J. Med. Chem. 44 (2009) 4516-4521. doi: 10.1016/j.ejmech.2009.06.018.

[223] T. Fawcett, An introduction to ROC analysis. Pattern recognition letters, Pattern Recognit. Lett. 27 (2006) 861-874. doi: 10.1016/j.patrec.2005.10.010.

[224] A. Speck-Planche, V.V. Kleandrova, F. Luan, M.N.D. Cordeiro, Fragment-based QSAR model toward the selection of versatile anti-sarcoma leads, Eur. J. Med. Chem. 46 (2011) 5910-5916. doi: 10.1016/j.ejmech.2011.09.055.

[225] A. Pérez-Garrido, A.M. Helguera, F. Borges, M.N.D. Cordeiro, V. Rivero, A.G. Escudero, Two new parameters based on distances in a receiver operating characteristic chart for the selection of classification models, J. Chem. Inf. Model. 51 (2011) 2746-2759. doi: 10.1021/ci2003076.

[226] S. Pramanik, K. Roy, Modeling bioconcentration factor (BCF) using mechanistically interpretable descriptors computed from open-source tool "PaDEL-Descriptor", Environ. Sci. Pollut. Res. 21 (2014) 2955-2965. doi: 10.1007/s11356-013-2247-z.

[227] S. Gayen, B. Debnath, S. Samanta, T. Jha, QSAR study on some anti-HIV HEPT analogues using physicochemical and topological parameters, Bioorg. Med. Chem. 12 (2004) 1493-1503. doi: 10.1016/j.bmc.2003.12.031.

[228] A. Golbraikh, A. Tropsha, Beware of q2!. Journal of molecular graphics and modelling, J. Mol. Graph. Model. 20 (2002) 269-276. doi: 10.1016/S1093-3263(01)00123-1.

[229] S.A. Amin, K. Ghosh, D. Mondal, T. Jha, S. Gayen, Exploring indole derivatives as myeloid cell leukaemia-1 (Mcl-1) inhibitors with multi-QSAR approach: a novel hope in anti-cancer drug discovery, New J. Chem. 44 (2020) 17494-17506. doi: 10.1039/D0NJ03863F.

[230] RCSB Protein Data Bank, https://www.rcsb.org, (Accessed 02 November 2022).

[231] Schrodinger Suite, Schrodinger, LLC, New York, USA, 2019. http://www.Schrodinger.com/Glide.

[232] S. Nandi, P. Kumar, S.A. Amin, T. Jha, S. Gayen, First molecular modelling report on tri-substituted pyrazolines as phosphodiesterase 5 (PDE5) inhibitors through classical and machine learning based multi-QSAR analysis, SAR QSAR Environ. Res. 32 (2021) 917-939. doi: 10.1080/1062936X.2021.1989721.

[233] S.A. Amin, S. Banerjee, N. Adhikari, T. Jha, Discriminations of active from inactive HDAC8 inhibitors Part II: Bayesian classification study to find molecular fingerprints, SAR QSAR Environ. Res. 31 (2020) 245-260. doi: 10.1080/1062936X.2020.1723136.

[234] V. Đorđević, S. Pešić, J. Živković, G.M. Nikolić, A.M. Veselinović, Development of novel antipsychotic agents by inhibiting dopamine transporter–in silico approach, New J. Chem. 46 (2022) 2687-2696. doi: 10.1080/1062936X.2020.1723136.

[235] S.E. Adeniji, S. Uba, A. Uzairu, Multi-linear regression model, molecular binding interactions and ligand-based design of some prominent compounds against Mycobacterium tuberculosis, Netw. Model. Anal. Health Inform. Bioinform. 9 (2020) 1-18. doi: 10.1007/s13721-019-0212-6.

[236] H.L. Lin, Y.W. Chiu, C.C. Wang, C.W. Tung, Computational prediction of Calu-3-based in vitro pulmonary permeability of chemicals, Regul. Toxicol. Pharmacol. 135 (2022) 105265. doi: 10.1016/j.yrtph.2022.105265.

[237] E. Papa, L. van der Wal, J.A. Arnot, P. Gramatica, Metabolic biotransformation half-lives in fish: QSAR modeling and consensus analysis, Sci. Total Environ. 470 (2014) 1040-1046. doi: 10.1016/j.scitotenv.2013.10.068.

[238] G.J. Lavado, D. Baderna, E. Carnesecchi, A.P. Toropova, A.A. Toropov, J.L.C. Dorne, E. Benfenati, QSAR models for soil ecotoxicity: Development and validation of models to predict reproductive toxicity of organic chemicals in the collembola Folsomia candida, J. Hazard. Mater. 423 (2022) 127236. doi: 10.1016/j.jhazmat.2021.127236.

[239] D.E. Arthur, A. Uzairu, P. Mamza, E. Abechi, G. Shallangwa, QSAR modelling of some anticancer PGI50 activity on HL-60 cell lines, Albanian J. Pharm. Sci. 3 (2016) 4-9.

[240] PubChem Substructure Fingerprint, https://web.cse.ohio-state.edu/~zhang.10631/bak/drugreposition/list_fingerprints.pdf (accessed on 26 Dec 2022).

[241] M. Hassam, J.A. Shamsi, A. Khan, A. Ai-Harrasi, R. Uddin, Prediction of inhibitory activities of small molecules against Pantothenate synthetase from Mycobacterium

tuberculosis using Machine Learning models, Comput. Biol. Med. 145 (105453). doi: 10.1016/j.compbiomed.2022.105453.

[242] A.K. Debnath, Pharmacophore mapping of a series of 2, 4-diamino-5-deazapteridine inhibitors of Mycobacterium avium complex dihydrofolate reductase, J. Med. Chem. 45 (2002) 41-43. doi: 10.1021/jm010360c.

[243] H.J. Kim, M.R. Doddareddy, H. Choo, Y.S. Cho, K.T. No, W. K. Park, A.N. Pae, New serotonin 5-HT6 ligands from common feature pharmacophore hypotheses. Journal of chemical information and modeling, J. Chem. Inf. Model. 48 (2008) 197-206. doi: 10.1021/ci700160t.

[244] A.K. Gupta, S. Chakroborty, K. Srivastava, S.K. Puri, A.K. Saxena, Pharmacophore modeling of substituted 1, 2, 4-Trioxanes for quantitative prediction of their antimalarial activity, J. Chem. Model. 50 (2010) 1510-1520. doi: 10.1021/ci100180e.

Appendix

Appendix

Appendix A1: SMILES notation of the dataset used for QSAR modeling studies.

Cmpd. No.	SMILES	HDAC3 inhibitory activity IC_{50}(nM)
001	C[C@H](\C=C(/C)\C=C\C(=O)NO)C(=O)c1ccc(cc1)N(C)C	20
002	CC(C)[C@@H]1NC(=O)[C@]2(C)CSC(=N2)c3ccc(CNC(=O)C[C@H](OC1=O)\C=C\CCSC(=O)C)cc3	470
003	Nc1ccccc1NC(=O)c2ccc(CNC(=O)OCc3cccnc3)cc2	790
004	CCCCCCCC(=O)SCC\C=C\[C@@H]1CC(=O)NCc2nc(cs2)C3=N[C@@](C)(CS3)C(=O)N[C@@H](C(C)C)C(=O)O1	1,360
005	Nc1ccccc1NC(=O)c2ccc(cc2)c3cn(CCc4ccsc4)nn3	3,940
006	CC(C)[C@@H]1NC(=O)[C@@H]2CCCN2C(=O)[C@H]3CCCN3C(=O)C[C@H](NC1=O)C(=O)NCCCC(=O)NO	13,700
007	ONC(=O)CCCCCCC(=O)Nc1ccccc1	1.4
008	Cc1[nH]c2ccccc2c1CCNCc3ccc(\C=C\C(=O)NO)cc3	60
009	ONC(=O)CCCCN1C(=O)[C@@H](CS)N=C(c2ccccc2)c3ccccc13	180
010	NC(=N)NCCC[C@@H]1N=C(c2ccccc2)c3ccccc3N(CCCCC(=O)NO)C1=O	220
011	CSCC[C@@H]1N=C(c2ccccc2)c3ccccc3N(CCCCC(=O)NO)C1=O	430
012	ONC(=O)CCCCN1C(=O)[C@H](Cc2ccccc2)N=C(c3ccccc3)c4ccccc14	490
013	CC(C)C[C@@H]1N=C(c2ccccc2)c3ccccc3N(CCCCC(=O)NO)C1=O	570
014	CC(C)(C)OC(=O)NCCCC[C@@H]1N=C(c2ccccc2)c3ccccc3N(CCCCC(=O)NO)C1=O	590
015	CC(C)[C@@H]1N=C(c2ccccc2)c3ccccc3N(CCCCC(=O)NO)C1=O	600
016	ONC(=O)CCCCN1C(=O)CN=C(c2ccccc2)c3ccccc13	660
017	CC(C)(C)SC[C@H]1N=C(c2ccccc2)c3ccccc3N(CCCCC(=O)NO)C1=O	750
018	ONC(=O)CCCCN1C(=O)[C@H](CCC(=O)NC(c2ccccc2)(c3ccccc3)c4ccccc4)N=C(c5ccccc5)c6ccccc16	830
019	CC(C)(C)Oc1ccc(C[C@@H]2N=C(c3ccccc3)c4ccccc4N(CCCCC(=O)NO)C2=O)cc1	850
020	C[C@@H](OCc1ccccc1)[C@@H]2N=C(c3ccccc3)c4ccccc4N(CCCCC(=O)NO)C2=O	910
021	NCCCC[C@@H]1N=C(c2ccccc2)c3ccccc3N(CCCCC(=O)NO)C1=O	950
022	ONC(=O)CCCCN1C(=O)[C@H](Cc2cc3ccccc3[nH]2)N=C(c4ccccc4)c5ccccc15	1,010
023	CC(C)(C)OC(=O)CC[C@@H]1N=C(c2ccccc2)c3ccccc3N(CCCCC(=O)NO)C1=O	1,030
024	CC[C@@H](C)[C@@H]1N=C(c2ccccc2)c3ccccc3N(CCCCC(=O)NO)C1=O	1,030
025	CC(C)(C)OC[C@@H]1N=C(c2ccccc2)c3ccccc3N(CCCCC(=O)NO)C1=O	1,210
026	ONC(=O)CCCCN1C(=O)[C@H](Cc2c[nH]cn2)N=C(c3ccccc3)c4ccccc14	1,320
027	C[C@@H](O)[C@@H]1N=C(c2ccccc2)c3ccccc3N(CCCCC(=O)NO)C1=O	1,800
028	C[C@@H]1N=C(c2ccccc2)c3ccccc3N(CCCCC(=O)NO)C1=O	1,800
029	NC(=O)CC[C@@H]1N=C(c2ccccc2)c3ccccc3N(CCCCC(=O)NO)C1=O	1,940
030	ONC(=O)CCCCN1C(=O)[C@H](Cc2cncn2C(c3ccccc3)(c4ccccc4)c5ccccc5)N=C(c6ccccc6)c7ccccc17	2,550
031	ONC(=O)CCCCN1C(=O)[C@H](CCC(=O)NO)N=C(c2ccccc2)c3ccccc13	2,570
032	ONC(=O)CCCNC(=O)C[C@@H]1N=C(c2ccccc2)c3ccccc3NC1=O	3,210
033	CC(C)(C)OC(=O)C[C@@H]1N=C(c2ccccc2)c3ccccc3N(CCCCC(=O)NO)C1=O	4,150
034	Cc1c(C)c(c(C)c2CC(C)(C)Oc12)S(=O)(=O)NC(=N)NCCC[C@@H]3N=C(c4ccccc4)c5ccccc5N(CCCCC(=O)NO)C3=O	4,290
035	ONC(=O)CCCCN1C(=O)[C@H](CC(=O)NC(c2ccccc2)(c3ccccc3)c4ccccc4)N=C(c5ccccc5)c6ccccc16	4,310
036	OC[C@@H]1N=C(c2ccccc2)c3ccccc3N(CCCCC(=O)NO)C1=O	4,940
037	ONC(=O)CCCNC(=O)CC[C@@H]1N=C(c2ccccc2)c3ccccc3NC1=O	5,170

038	CC(C)(C)OC(=O)n1c(C[C@@H]2N=C(c3ccccc3)c4ccccc4N(CCCCC(=O)NO)C2=O)cc5ccccc15	5,210
039	ONC(=O)CCCCN1C(=O)[C@H](Cc2ccc(O)cc2)N=C(c3ccccc3)c4ccccc14	5,290
040	ONC(=O)CCCCN1C(=O)[C@H](CCC(=O)O)N=C(c2ccccc2)c3ccccc13	8,710
041	ONC(=O)CCCCN1C(=O)[C@H](CC(=O)NO)N=C(c2ccccc2)c3ccccc13	10,390
042	ONC(=O)CCCCN1C(=O)[C@H](CC(=O)O)N=C(c2ccccc2)c3ccccc13	12,600
043	N[C@H](Cc1ccc(Cl)cc1Cl)C(=O)N2Cc3ccccc3C2	20,000
044	NC(=O)C[C@@H]1N=C(c2ccccc2)c3ccccc3N(CCCCC(=O)NO)C1=O	3,100
045	ONC(=O)CC[C@@H]1N=C(c2ccccc2)c3ccccc3NC1=O	>30000
046	COc1ccc(Cn2ccc3ccc(cc23)C(=O)NO)cc1	>30000
047	CC(C)[C@@H]1NC(=O)[C@H]2CCCN2C(=O)[C@@H]3CCCN3C(=O)C[C@@H](NC1=O)C(=O)NCCCC(=O)NO	>30000
048	COC(=O)CCCCN1C(=O)C(CCCNC(=N)NS(=O)(=O)c2c(C)c(C)c3OC(C)(C)Cc3c2C)N=C(c4ccccc4)c5ccccc15	>30000
049	CC(C)C[C@@H]1N=C(c2ccccc2)c3ccccc3N(CCCCC(=O)O)C1=O	>30000
050	Cc1c(C)c(c(C)c2CC(C)(C)Oc12)S(=O)(=O)NC(=N)NCCC[C@@H]3N=C(c4ccccc4)c5ccccc5N(CCCCC(=O)O)C3=O	>30000
051	O=C(C[C@@H]1N=C(c2ccccc2)c3ccccc3NC1=O)NC(c4ccccc4)(c5ccccc5)c6ccccc6	>30000
052	CC(C)(C)OC(=O)C[C@@H]1N=C(c2ccccc2)c3ccccc3N(CCCCC(=O)O)C1=O	>30000
053	CC(C)(C)OC(=O)NCCCC[C@@H]1N=C(c2ccccc2)c3ccccc3N(CCCCC(=O)O)C1=O	>30000
054	O=C1Nc2ccccc2C(=N[C@H]1Cc3cn(cn3)C(c4ccccc4)(c5ccccc5)c6ccccc6)c7ccccc7	>30000
055	CC[C@H](C)[C@@H]1N=C(c2ccccc2)c3ccccc3NC1=O	>30000
056	OC(=O)CCCCN1C(=O)[C@H](CCC(=O)O)N=C(c2ccccc2)c3ccccc13	>30000
057	CC(C)(C)OC(=O)NCCCC[C@@H]1N=C(c2ccccc2)c3ccccc3NC1=O	>30000
058	COC(=O)CCCCN1C(=O)[C@H](CC(=O)NC(c2ccccc2)(c3ccccc3)c4ccccc4)N=C(c5ccccc5)c6ccccc16	>30000
059	OC(=O)CCCCN1C(=O)CN=C(c2ccccc2)c3ccccc13	>30000
060	CC(C)(C)Oc1ccc(C[C@@H]2N=C(c3ccccc3)c4ccccc4NC2=O)cc1	>30000
061	OC(=O)C[C@@H]1N=C(c2ccccc2)c3ccccc3NC1=O	>30000
062	COC(=O)CCCCN1C(=O)[C@H](Cc2ccccc2)N=C(c3ccccc3)c4ccccc14	>30000
063	CC[C@H](C)[C@@H]1N=C(c2ccccc2)c3ccccc3N(CCCCC(=O)O)C1=O	>30000
064	CC[C@H](C)[C@@H]1N=C(c2ccccc2)c3ccccc3N(CCCCC(=O)OC)C1=O	>30000
065	CC(C)(C)OC(=O)C[C@H]1N=C(c2ccccc2)c3ccccc3NC1=O	>30000
066	CC(C)(C)SC[C@H]1N=C(c2ccccc2)c3ccccc3N(CCCCC(=O)O)C1=O	>30000
067	OC(=O)CCCCN1C(=O)[C@H](CC(=O)NC(c2ccccc2)(c3ccccc3)c4ccccc4)N=C(c5ccccc5)c6ccccc16	>30000
068	CC(C)(C)OC[C@@H]1N=C(c2ccccc2)c3ccccc3N(CCCCC(=O)O)C1=O	>30000
069	CC(C)C[C@@H]1N=C(c2ccccc2)c3ccccc3NC1=O	>30000
070	COC(=O)CCCCN1C(=O)[C@H](CCSC)N=C(c2ccccc2)c3ccccc13	>30000
071	COC(=O)CCCCN1C(=O)[C@H](Cc2cc3ccccc3n2C(=O)OC(C)(C)C)N=C(c4ccccc4)c5ccccc15	>30000
072	COC(=O)CCCCN1C(=O)[C@H](CCC(=O)OC(C)(C)C)N=C(c2ccccc2)c3ccccc13	>30000
073	COC(=O)CCCCN1C(=O)[C@@H](CSC(C)(C)C)N=C(c2ccccc2)c3ccccc13	>30000
074	C[C@H](OCc1ccccc1)[C@@H]2N=C(c3ccccc3)c4ccccc4NC2=O	>30000
075	COC(=O)CCCCN1C(=O)CN=C(c2ccccc2)c3ccccc13	>30000
076	C[C@@H]1N=C(c2ccccc2)c3ccccc3N(CCCCC(=O)O)C1=O	>30000
077	CSCC[C@@H]1N=C(c2ccccc2)c3ccccc3NC1=O	>30000
078	ONC(=O)CC[C@H]1N=C(c2ccccc2)c3ccccc3NC1=O	>30000
079	OC(=O)CCCCN1C(=O)[C@H](Cc2cncn2C(c3ccccc3)(c4ccccc4)c5ccccc5)N=C(c6ccccc6)c7ccccc17	>30000
080	COC(=O)CCCCN1C(=O)[C@H](COC(C)(C)C)N=C(c2ccccc2)c3ccccc13	>30000

081	COC(=O)CCCCN1C(=O)[C@H](CC(C)C)N=C(c2ccccc2)c3ccccc13	>30000
082	CC(C)(C)OC[C@@H]1N=C(c2ccccc2)c3ccccc3NC1=O	>30000
083	O=C1CN=C(c2ccccc2)c3ccccc3N1	>30000
084	COC(=O)CCCCN1C(=O)[C@@H](N=C(c2ccccc2)c3ccccc13)[C@@H](C)OCc4ccccc4	>30000
085	CSCC[C@@H]1N=C(c2ccccc2)c3ccccc3N(CCCCC(=O)O)C1=O	>30000
086	OC(=O)CCCCN1C(=O)[C@H](CC(=O)O)N=C(c2ccccc2)c3ccccc13	>30000
087	CC(C)(C)OC(=O)CC[C@@H]1N=C(c2ccccc2)c3ccccc3NC1=O	>30000
088	O=C(CC[C@@H]1N=C(c2ccccc2)c3ccccc3NC1=O)NC(c4ccccc4)(c5ccccc5)c6ccccc6	>30000
089	ONC(=O)C[C@H]1N=C(c2ccccc2)c3ccccc3NC1=O	>30000
090	CC(C)(C)OC(=O)n1cc(C[C@@H]2N=C(c3ccccc3)c4ccccc4NC2=O)c5ccccc15	>30000
091	OC(=O)C[C@H]1N=C(c2ccccc2)c3ccccc3NC1=O	>30000
092	CC(C)(C)OC(=O)n1c(C[C@@H]2N=C(c3ccccc3)c4ccccc4N(CCCCC(=O)O)C2=O)cc5ccccc15	>30000
093	C[C@H](OCc1ccccc1)[C@@H]2N=C(c3ccccc3)c4ccccc4N(CCCCC(=O)O)C2=O	>30000
094	COC(=O)CCCCN1C(=O)[C@H](Cc2cncn2C(c3ccccc3)(c4ccccc4)c5ccccc5)N=C(c6ccccc6)c7ccccc17	>30000
095	OC(=O)CCCCN1C(=O)[C@H](Cc2ccccc2)N=C(c3ccccc3)c4ccccc14	>30000
096	CC(C)(C)OC(=O)C[C@@H]1N=C(c2ccccc2)c3ccccc3NC1=O	>30000
097	OC(=O)CCCCN1C(=O)[C@H](CCC(=O)NC(c2ccccc2)(c3ccccc3)c4ccccc4)N=C(c5ccccc5)c6ccccc16	>30000
098	CC(C)(C)SC[C@H]1N=C(c2ccccc2)c3ccccc3NC1=O	>30000
099	COC(=O)CCCCN1C(=O)[C@H](CCC(=O)NC(c2ccccc2)(c3ccccc3)c4ccccc4)N=C(c5ccccc5)c6ccccc16	>30000
100	CC(C)(C)Oc1ccc(C[C@@H]2N=C(c3ccccc3)c4ccccc4N(CCCCC(=O)O)C2=O)cc1	>30000
101	COC(=O)CCCCN1C(=O)[C@H](CCCCNC(=O)OC(C)(C)C)N=C(c2ccccc2)c3ccccc13	>30000
102	COC(=O)CCCCN1C(=O)[C@@H](N=C(c2ccccc2)c3ccccc13)C(C)C	>30000
103	CC(C)[C@@H]1N=C(c2ccccc2)c3ccccc3NC1=O	>30000
104	COC(=O)CCCCN1C(=O)[C@H](Cc2ccc(OC(C)(C)C)cc2)N=C(c3ccccc3)c4ccccc14	>30000
105	O=C1Nc2ccccc2C(=N[C@H]1Cc3ccccc3)c4ccccc4	>30000
106	ONC(=O)C[C@@H]1N=C(c2ccccc2)c3ccccc3NC1=O	>30000
107	CC(C)[C@@H]1N=C(c2ccccc2)c3ccccc3N(CCCCC(=O)O)C1=O	>30000
108	OC(=O)CC[C@H]1N=C(c2ccccc2)c3ccccc3NC1=O	>30000
109	COC(=O)CCCCN1C(=O)[C@H](CC(=O)OC(C)(C)C)N=C(c2ccccc2)c3ccccc13	>30000
110	OC(=O)CC[C@@H]1N=C(c2ccccc2)c3ccccc3NC1=O	>30000
111	COC(=O)CCCCN1C(=O)[C@H](C)N=C(c2ccccc2)c3ccccc13	>30000
112	C[C@@H]1N=C(c2ccccc2)c3ccccc3NC1=O	>30000
113	CC(C)(C)OC(=O)CC[C@H]1N=C(c2ccccc2)c3ccccc3NC1=O	>30000
114	Cc1c(C)c(c(C)c2CC(C)(C)Oc12)S(=O)(=O)NC(=N)NCCC[C@@H]3N=C(c4ccccc4)c5ccccc5NC3=O	>30000
115	CC(C)(C)OC(=O)CC[C@@H]1N=C(c2ccccc2)c3ccccc3N(CCCCC(=O)O)C1=O	>30000

Appendix A2: SARpy training set prediction

SMILES	*Prediction*	*Training LR*	*SMARTS*
O=S(=O)(NC(=N)NCCCC1N=C(c2c(N(CCCCC(=O)NO)C1=O)cccc2)c1ccccc1)c1c(c2CC(Oc2c(c1C)C)(C)C)C	ACTIVE	7.73	C(=O)(CCCC)NO

CCCCCCCC(=O)SCCC=CC1CC(=O)NCc2scc(n2)C2=NC(CS2)(C(=O)NC(C(=O)O1)C(C)C)C	ACTIVE	inf	CC(C(=O))C
C(=O)(CCCCN1C(=O)C(N=C(c2c1cccc2)c1ccccc1)CO)NO	ACTIVE	7.73	C(=O)(CCCC)NO
ONC(=O)C=CC(=CC(C(=O)c1ccc(N(C)C)cc1)C)C	ACTIVE	inf	CC(C(=O))C
C(=O)(CCCCN1C(=O)C(N=C(c2c1cccc2)c1ccccc1)CCCNC(=N)N)NO	ACTIVE	7.73	C(=O)(CCCC)NO
c12ccc(cc1)C1=NC(CS1)(C(=O)NC(C(=O)OC(CC(=O)NC2)C=CCCSC(=O)C)C(C)C)C	ACTIVE	inf	CC(C(=O))C
N(Cc1ccc(cc1)C(=O)Nc1ccccc1N)C(=O)OCc1cccnc1	None	--	--
c1c(ccc(c1)C(=O)Nc1c(cccc1)N)c1cn(nn1)CCc1cscc1	None	--	--
C(=O)(CCCCN1C(=O)C(N=C(c2c1cccc2)c1ccccc1)CCSC)NO	ACTIVE	7.73	C(=O)(CCCC)NO
C(=O)(CCCCN1C(=O)C(N=C(c2c1cccc2)c1ccccc1)Cc1ccccc1)NO	ACTIVE	7.73	C(=O)(CCCC)NO
C(=O)(CCCCN1C(=O)C(N=C(c2c1cccc2)c1ccccc1)CCC(=O)OC(C)(C)C)OC	None	--	--
C(=O)(NCCCCC1N=C(c2c(N(C1=O)CCCCC(=O)NO)cccc2)c1ccccc1)OC(C)(C)C	ACTIVE	7.73	C(=O)(CCCC)NO
C(=O)(CCC1N=C(c2c(NC1=O)cccc2)c1ccccc1)OC(C)(C)C	None	--	--
C(=O)(CCCCN1C(=O)CN=C(c2c1cccc2)c1ccccc1)NO	ACTIVE	7.73	C(=O)(CCCC)NO
C(=O)(CCC1N=C(c2c(NC1=O)cccc2)c1ccccc1)OC(C)(C)C	None	--	--
c1ccccc1NC(=O)CCCCCCC(=O)NO	ACTIVE	7.73	C(=O)(CCCC)NO
C(=O)(CCCCN1C(=O)C(N=C(c2c1cccc2)c1ccccc1)COC(C)(C)C)OC	None	--	--
C(=O)(CCCCN1C(=O)C(N=C(c2c1cccc2)c1ccccc1)CSC(C)(C)C)NO	ACTIVE	7.73	C(=O)(CCCC)NO
C(=O)(CCCCN1C(=O)C(N=C(c2c1cccc2)c1ccccc1)CCC(=O)OC(C)(C)C)O	None	--	--
C(=O)(CCCCN1C(=O)C(N=C(c2c1cccc2)c1ccccc1)CCC(=O)NC(c1ccccc1)(c1ccccc1)c1ccccc1)NO	ACTIVE	7.73	C(=O)(CCCC)NO
c1c(cc2c(c1)ccn2Cc1ccc(cc1)OC)C(=O)NO	None	--	--
N1=C(c2c(NC(=O)C1COC(C)(C)C)cccc2)c1ccccc1	None	--	--
n1(cc(c2ccccc12)CC1N=C(c2c(NC1=O)cccc2)c1ccccc1)C(=O)OC(C)(C)C	None	--	--
C(=O)(CCCCN1C(=O)C(N=C(c2c1cccc2)c1ccccc1)Cc1ccc(cc1)OC(C)(C)C)NO	ACTIVE	7.73	C(=O)(CCCC)NO
C(=O)(CCCCN1C(=O)C(N=C(c2c1cccc2)c1ccccc1)CC(=O)OC(C)(C)C)O	None	--	--
C(=O)(CCCCN1C(=O)C(N=C(c2c1cccc2)c1ccccc1)CCCCN)NO	ACTIVE	7.73	C(=O)(CCCC)NO
C(=O)(CCCCN1C(=O)C(N=C(c2c1cccc2)c1ccccc1)COC(C)(C)C)O	None	--	--
C(=O)(CCC1N=C(c2c(N(C1=O)CCCCC(=O)NO)cccc2)c1ccccc1)OC(C)(C)C	ACTIVE	7.73	C(=O)(CCCC)NO

C(=O)(CCCCN1C(=O)C(N=C(c2c1cccc2)c1ccccc1)COC(C)(C)C)NO	ACTIVE	7.73	C(=O)(CCCC)NO
C(=O)(CCCCN1C(=O)C(N=C(c2c1cccc2)c1ccccc1)Cc1c[nH]cn1)NO	ACTIVE	7.73	C(=O)(CCCC)NO
c1cccc(C2=NC(C(=O)N(CCCCC(=O)NO)c3c2cccc3)C(C)O)c1	ACTIVE	7.73	C(=O)(CCCC)NO
C(=O)(CCCCN1C(=O)C(N=C(c2c1cccc2)c1ccccc1)CCC(=O)N)NO	ACTIVE	7.73	C(=O)(CCCC)NO
C(=O)(CCCCN1C(=O)C(N=C(c2c1cccc2)c1ccccc1)Cc1cncn1C(c1ccccc1)(c1ccccc1)c1ccccc1)NO	ACTIVE	7.73	C(=O)(CCCC)NO
C(=O)(CCCCN1C(=O)C(N=C(c2c1cccc2)c1ccccc1)CCC(=O)NO)NO	ACTIVE	7.73	C(=O)(CCCC)NO
C(CCCC(=O)NO)N1C(=O)C(N=C(c2c1cccc2)c1ccccc1)CC(=O)N	ACTIVE	7.73	C(=O)(CCCC)NO
C(=O)(CC1N=C(c2c(N(C1=O)CCCCC(=O)NO)cccc2)c1ccccc1)OC(C)(C)C	ACTIVE	7.73	C(=O)(CCCC)NO
C(=O)(CCCCN1C(=O)C(N=C(c2c1cccc2)c1ccccc1)CS)NO	ACTIVE	7.73	C(=O)(CCCC)NO
C(=O)(CCCNC(=O)CC1N=C(c2c(NC1=O)cccc2)c1ccccc1)NO	None	--	--
C(=O)(CCC1N=C(c2c(NC1=O)cccc2)c1ccccc1)NO	ACTIVE	7.73	C(=O)(CCCC)NO
C(=O)(CC1N=C(c2c(N(C1=O)CCCCC(=O)NO)cccc2)c1ccccc1)O	ACTIVE	7.73	C(=O)(CCCC)NO
N(C(=O)CC1N=C(c2c(NC1=O)cccc2)c1ccccc1)O	None	--	--
C(=O)(CCC1N=C(c2c(NC1=O)cccc2)c1ccccc1)NO	ACTIVE	7.73	C(=O)(CCCC)NO
C(=O)(CCCCN1C(=O)C(N=C(c2c1cccc2)c1ccccc1)C(C)C)OC	None	--	--
n1(c(cc2ccccc12)CC1N=C(c2c(N(C1=O)CCCCC(=O)NO)cccc2)c1ccccc1)C(=O)OC(C)(C)C	ACTIVE	7.73	C(=O)(CCCC)NO
C(=O)(CCCCN1C(=O)C(N=C(c2c1cccc2)c1ccccc1)Cc1ccc(cc1)OC(C)(C)C)OC	None	--	--
C(=O)(NCCCC(=O)NO)CCC1C(=O)Nc2ccccc2C(=N1)c1ccccc1	None	--	--
C(=O)(CCCCN1C(=O)C(N=C(c2c1cccc2)c1ccccc1)Cc1ccc(cc1)O)NO	ACTIVE	7.73	C(=O)(CCCC)NO
N(C(=O)CC1N=C(c2c(NC1=O)cccc2)c1ccccc1)O	None	--	--
C(=O)(CCCCN1C(=O)C(N=C(c2c1cccc2)c1ccccc1)CC(=O)NO)NO	ACTIVE	7.73	C(=O)(CCCC)NO
N1C(=O)C(N=C(c2c1cccc2)c1ccccc1)Cc1ccccc1	None	--	--
C(=O)(CCC1N=C(c2c(NC1=O)cccc2)c1ccccc1)O	None	--	--
C(=O)(CCCNC(=O)C1NC(=O)C(C(C)C)NC(=O)C2N(CCC2)C(=O)C2CCCN2C(=O)C1)NO	None	--	--
O=S(=O)(c1c(c2CC(Oc2c(c1C)C)(C)C)C)NC(=N)NCCCC1N=C(c2c(NC1=O)cccc2)c1ccccc1	None	--	--
c1c(cc(c(c1)CC(C(=O)N1Cc2c(C1)cccc2)N)Cl)Cl	None	--	--
C(=O)(CCCCN1C(=O)C(N=C(c2c1cccc2)c1ccccc1)CC(C)C)O	None	--	--
O=S(=O)(NC(=N)NCCCC1N=C(c2c(N(CCCCC(=O)O)C1=O)c	None	--	--

ccc2)c1ccccc1)c1c(c2CC(Oc2c(c1C)C)(C)C)C			
C(=O)(CCCCN1C(=O)C(N=C(c2c1cccc2)c1ccccc1)CCCCNC(=O)OC(C)(C)C)O	None	--	--
c1ccc2c(c1)NC(=O)C(N=C2c1ccccc1)C	None	--	--
C(=O)(NCCCCC1N=C(c2c(NC1=O)cccc2)c1ccccc1)OC(C)(C)C	None	--	--
c1(C(NC(=O)CC2N=C(c3c(N(CCCCC(=O)OC)C2=O)cccc3)c2ccccc2)(c2ccccc2)c2ccccc2)ccccc1	None	--	--
C(=O)(CCCCN1C(=O)C(N=C(c2c1cccc2)c1ccccc1)Cc1ccccc1)OC	None	--	--
N1=C(c2c(NC(=O)C1C(CC)C)cccc2)c1ccccc1	None	--	--
C(=O)(CCCCN1C(=O)C(N=C(c2c1cccc2)c1ccccc1)C(CC)C)O	None	--	--
C(=O)(CCCCN1C(=O)C(N=C(c2c1cccc2)c1ccccc1)C(CC)C)OC	None	--	--
c1(ccccc1)C(NC(=O)CC1N=C(c2c(N(CCCCC(=O)O)C1=O)ccccc2)c1ccccc1)(c1ccccc1)c1ccccc1	None	--	--
C(=O)(CC1N=C(c2c(NC1=O)cccc2)c1ccccc1)O	None	--	--
C(=O)(CCCCN1C(=O)C(N=C(c2c1cccc2)c1ccccc1)C(C)C)O	None	--	--
N1=C(c2c(NC(=O)C1Cc1ncn(c1)C(c1ccccc1)(c1ccccc1)c1ccccc1)cccc2)c1ccccc1	None	--	--
C(=O)(CCCCN1C(=O)C(N=C(c2c1cccc2)c1ccccc1)CCSC)OC	None	--	--
C(=O)(CCCCN1C(=O)C(N=C(c2c1cccc2)c1ccccc1)CSC(C)(C)C)OC	None	--	--
N1=C(c2c(NC(=O)C1Cc1ccc(cc1)OC(C)(C)C)cccc2)c1ccccc1	None	--	--
C(=O)(CCCCN1C(=O)C(N=C(c2c1cccc2)c1ccccc1)C)O	None	--	--
N1=C(c2c(NC(=O)C1CC(C)C)cccc2)c1ccccc1	None	--	--
C(=O)(CCCCN1C(=O)C(N=C(c2c1cccc2)c1ccccc1)Cc1cncn1C(c1ccccc1)(c1ccccc1)c1ccccc1)O	None	--	--
C(=O)(CCCCN1C(=O)C(N=C(c2c1cccc2)c1ccccc1)CC(C)C)OC	None	--	--
C(=O)(CCCCN1C(=O)C(N=C(c2c1cccc2)c1ccccc1)C)OC	None	--	--
N1=C(c2c(NC(=O)C1C(C)OCc1ccccc1)cccc2)c1ccccc1	None	--	--
C(=O)(CCCCN1C(=O)C(N=C(c2c1cccc2)c1ccccc1)C(C)OCc1ccccc1)OC	None	--	--
C(=O)(CCCCN1C(=O)C(N=C(c2c1cccc2)c1ccccc1)CC(=O)O)O	None	--	--
C(=O)(CCC1N=C(c2c(NC1=O)cccc2)c1ccccc1)NC(c1ccccc1)(c1ccccc1)c1ccccc1	None	--	--
C(=O)(CCCCN1C(=O)C(N=C(c2c1cccc2)c1ccccc1)C(C)OCc1ccccc1)O	None	--	--
O(C(=O)CCCCN1C(=O)C(N=C(c2ccccc12)c1ccccc1)Cc1n(cnc1)C(c1ccccc1)(c1ccccc1)c1ccccc1)C	None	--	--
c1(ccccc1)C(NC(=O)CCC1N=C(c2c(N(CCCCC(=O)O)C1=O)ccccc2)c1ccccc1)(c1ccccc1)c1ccccc1	None	--	--
c1(ccccc1)C(NC(=O)CCC1N=C(c2c(N(CCCCC(=O)OC)C1=O)cccc2)c1ccccc1)(c1ccccc1)c1ccccc1	None	--	--

C(=O)(CCCCN1C(=O)C(N=C(c2c1cccc2)c1ccccc1)Cc1ccc(cc1)OC(C)(C)C)O	None	--	--
C(=O)(CCCCN1C(=O)C(N=C(c2c1cccc2)c1ccccc1)CCCCNC(=O)OC(C)(C)C)OC	None	--	--
N1=C(c2c(NC(=O)C1)cccc2)c1ccccc1	None	--	--

Appendix A3: SARpy Test set Prediction

SMILES	*Prediction*	*Test LR*	*SMARTS*
O=C(NO)C=Cc1ccc(CNCCc2c3c([nH]c2C)cccc3)cc1	None	--	--
C(=O)(CCCCN1C(=O)C(N=C(c2c1cccc2)c1ccccc1)CC(C)C)NO	ACTIVE	7.73	C(=O)(CCCC)NO
C(=O)(CCCCN1C(=O)C(N=C(c2c1cccc2)c1ccccc1)C(C)C)NO	ACTIVE	7.73	C(=O)(CCCC)NO
C(=O)(CCCCN1C(=O)C(N=C(c2c1cccc2)c1ccccc1)C(C)OCc1ccccc1)NO	ACTIVE	7.73	C(=O)(CCCC)NO
C(=O)(CCCCN1C(=O)C(N=C(c2c1cccc2)c1ccccc1)Cc1[nH]c2c(c1)cccc2)NO	ACTIVE	7.73	C(=O)(CCCC)NO
C(=O)(CCCCN1C(=O)C(N=C(c2c1cccc2)c1ccccc1)C(C)CC)NO	ACTIVE	7.73	C(=O)(CCCC)NO
C(=O)(CCCCN1C(=O)C(N=C(c2c1cccc2)c1ccccc1)C)NO	ACTIVE	7.73	C(=O)(CCCC)NO
c1cccc2c1N(C(=O)C(N=C2c1ccccc1)CC(=O)NC(c1ccccc1)(c1ccccc1)c1ccccc1)CCCCC(=O)NO	ACTIVE	7.73	C(=O)(CCCC)NO
C(=O)(CCC1N=C(c2c(N(C1=O)CCCCC(=O)NO)cccc2)c1ccccc1)O	ACTIVE	7.73	C(=O)(CCCC)NO
O=S(=O)(NC(=N)NCCCC1N=C(c2c(N(CCCCC(=O)OC)C1=O)cccc2)c1ccccc1)c1c(c2CC(Oc2c(c1C)C)(C)C)C	None	--	--
c1(ccccc1)C(NC(=O)CC1N=C(c2c(NC1=O)cccc2)c1ccccc1)(c1ccccc1)c1ccccc1	None	--	--
C(=O)(CCCCN1C(=O)C(N=C(c2c1cccc2)c1ccccc1)CCC(=O)O)O	None	--	--
C(=O)(CCCCN1C(=O)CN=C(c2c1cccc2)c1ccccc1)O	None	--	--
C(=O)(CC1N=C(c2c(NC1=O)cccc2)c1ccccc1)OC(C)(C)C	None	--	--
C(=O)(CCCCN1C(=O)C(N=C(c2c1cccc2)c1ccccc1)CSC(C)(C)C)O	None	--	--
C12CCCN2C(=O)CC(C(=O)NCCCC(=O)NO)NC(=O)C(C(C)C)NC(=O)C2N(C1=O)CCC2	None	--	--
n1(c(cc2ccccc12)CC1N=C(c2c(N(C1=O)CCCCC(=O)OC)cccc2)c1ccccc1)C(=O)OC(C)(C)C	None	--	--
C(=O)(CCCCN1C(=O)CN=C(c2c1cccc2)c1ccccc1)OC	None	--	--
N1=C(c2c(NC(=O)C1CCSC)cccc2)c1ccccc1	None	--	--
C(=O)(CCCCN1C(=O)C(N=C(c2c1cccc2)c1ccccc1)CCSC)O	None	--	--

C(=O)(CC1N=C(c2c(NC1=O)cccc2)c1ccccc1)O	None	--	--
C(=O)(CCCCN1C(=O)C(N=C(c2c1cccc2)c1ccccc1)Cc1n(c2c(c1)cccc2)C(=O)OC(C)(C)C)O	None	--	--
C(=O)(CCCCN1C(=O)C(N=C(c2c1cccc2)c1ccccc1)Cc1ccccc1)O	None	--	--
C(=O)(CC1N=C(c2c(NC1=O)cccc2)c1ccccc1)OC(C)(C)C	None	--	--
N1=C(c2c(NC(=O)C1CSC(C)(C)C)cccc2)c1ccccc1	None	--	--
N1C(=O)C(N=C(c2c1cccc2)c1ccccc1)C(C)C	None	--	--
C(=O)(CCCCN1C(=O)C(N=C(c2c1cccc2)c1ccccc1)CC(=O)OC(C)(C)C)OC	None	--	--
C(=O)(CCC1N=C(c2c(NC1=O)cccc2)c1ccccc1)O	None	--	--